

博 士 論 文

Research for Tsunami Measurement Based on 3D Image

Measurement Technique

福岡工業大学大学院工学研究科

知能情報システム工学専攻

伊 浩

2018年5月

要旨

津波被害を減らすためには、津波の早期発見が必要である。本研究の目的は、陸上に設置したカメラから 5km~20km 先の海面の変化を監視することである。

本論文では、津波計測のための 3 次元画像計測技術を用いた遠距離海面高度計測システムの構築について紹介する。まず、広範囲の海面を計測するために、パン・チルト・ステージを用いてカメラの角度を制御する。また、計測精度を向上するために、特徴が既知のスケールポールを使用して、カメラの固有パラメータおよび計測システムの外部パラメータを較正する手法を提案した。また、海波を抽出するために、領域分割法と動的閾値法を用いた波自動抽出手法を提案した。最後に、海波の平均高さに基づく海面の高さを算出する手法を提案した。

本論文は 5 つの章で構成されている。第 1 章では、本論文の背景と既存の津波計測手法について説明し、3 次元画像処理技術を用いた津波計測の考え方を提案する。その後、本研究の目的と本論文の構成を述べる。

第 2 章では、遠方海面計測のためのカメラシステムのキャリブレーション方法について述べる。まず、両眼立体視の理論とカメラキャリブレーション方法を説明し、遠距離のキャリブレーションの困難性を述べる。その後、提案したキャリブレーション手法を述べる。

第 3 章では、海波の抽出方法について述べる。まず、遠距離の海波抽出の困難性を説明し、提案した領域分割法と動的閾値法を用いた波の自動抽出法を述べる。その後、ステレオ画像上の海波のマッチング方法について述べる。まず、対応点をそれぞれマッチングすることの困難性を説明し、この問題に対する解決策を述べる。

第 4 章では、検証実験の方法、実験結果及び考察を述べる。まず、実験条件と実験方法を紹介し、その後実験結果について説明し、考察を述べる。

第 5 章では、本論文のまとめと今後の課題について述べる。

Abstract

In order to reduce the loss of life in disasters, it is necessary to construct a tsunami measurement system. Our purpose is to monitor the change of sea levels of 20 km using by two cameras installed on the seashore.

In this paper, we construct the measurement system of long distance sea-level height based on 3-D image measurement technique. First, in order to measure a wide range of the sea surface, we can use the pan and tilt stage to rotate cameras in this system. In order to improve the accuracy of the tsunami measurement system, we propose a long distance calibration method of camera measurement system that uses the standard scale pole to calibrate intrinsic and extrinsic parameters of cameras system. Then, we proposed a dynamic threshold method in blocks to extract the sea waves automatically. Finally, we propose a sea level calculation method based on average value of wave heights.

This paper consist of five chapters. In the Chapter 1, we explain the background of this paper and tsunami measurement methods, In addition, we proposed our approach of tsunami measurement system with 3-D image measurement technique. Then, we introduce the system and explain the purpose of this research.

In the chapter 2, we propose the calibration method of long distance 3-D image measurement system. First, we illustrate the theory of binocular stereoscopic vision and camera calibration. Then we explain the method of camera calibration.

In the chapter 3, we introduce the extraction method of sea wave. First, we illustrate the difficulties of long distance sea wave extraction and then we proposed a dynamic threshold extraction method for long distance image. Then, we introduce the difficulties of corresponding point matching. Finally, based on feature matrix, we propose a method of matching point and show the results of this method.

In the chapter 4, we describe the experimental conditions, the experimental results and consideration.

In the chapter 5, we summary the work in this paper and give an outlook of the future work.

Contents

Chapter 1 Introduction.....	1
1.1 Analysis of tsunami characteristics and tsunami disaster	2
1.2 The meaning of wave height measurement and the existing measurement methods	6
1.3 3-D image measurement technology	11
1.4 The purpose of our research and structure of this paper	15
Chapter 2 Calibration of long distance 3-D image measurement system	16
2.1 The theory of binocular stereoscopic vision.....	17
2.2 The existing calibration method	25
2.3 The improved calibration method	27
2.4 Calibration experiments.....	30
2.5 Summary.....	38
Chapter 3 Image processing	39
3.1 Difficult of sea wave extraction	40
3.2 Sea wave extraction	45
3.4 Experiments and results.....	53
3.5 Summary.....	57
Chapter 4 Experimental results and consideration.....	58
4.1 Proposed sea wave height measurement system.....	59
4.2 Experimental conditions	61
4.3 Measurement of the height of sea level	62
4.4 Experiments and results.....	64
4.5 Summary.....	92
Chapter 5 Conclusions.....	93
References.....	95
Research Published	100
Acknowledgement	101

Figure 1 .1 Tsunami propagation.....	3
Figure 1 .2 Wind-generated waves	4
Figure 1 .3 Tsunami in Miyako	5
Figure 1 .4 Measurements along coast.....	7
Figure 1 .5 Measurements in open sea area	7
Figure 1 .6 Dart system	9
Figure 1 .7 TOF system.....	12
Figure 1 .8 The system of pattern projection method.....	12
Figure 1 .9 Stereo vision method.....	13
Figure 1 .10 Ideal stereo vision system	14
Figure 2 .1 Images coordinate and the image plane coordinate	18
Figure 2 .2 Theory of pinhole model	19
Figure 2 .3 Binocular stereo vision system in the ideal model.....	22
Figure 2 .4 The measurement theory of x and y axis	23
Figure 2 .5 The usual model of binocular stereo vision system	24
Figure 2 .6 Calibration block of DLT method	25
Figure 2 .7 Mapping relations between the images coordinate with the world coordinate.....	26
Figure 2 .8 Calibration model	27
Figure 2 .9 The sea area in Shikashima.....	30
Figure 2 .10 Image at 12:00.....	31
Figure 2 .11 Images at 12:30	31
Figure 2 .12 Images at 13:15	31
Figure 2 .13 The images of calibration in Shikashima.....	32
Figure 2 .14 Sea area in Shigu	33
Figure 2 .15 Hollow plastic bar for calibration	34
Figure 2 .16 Calibration image in Shigu	34
Figure 2 .17 Verification images in Shigu	35
Figure 2 .18 Sea area in Tsuyazaki	36
Figure 2 .19 Calibration Images in Tsuyazaki.....	37
Figure 3 .1 Extract image with Otsu threshold.....	41
Figure 3 .2 Extract image with adaptive threshold	43
Figure 3 .3 The sawteeth in image.....	44
Figure 3 .4 Divide blocks	45
Figure 3 .5 Optimum block threshold method	47
Figure 3 .6 Comparison of the results	47
Figure 3 .7 The flow chart of extraction sea waves	48

Figure 3.8 Select sea wave.....	49
Figure 3.9 Template Matching	50
Figure 3.10 SIFT matching.....	51
Figure 3.11 The feature of sea wave.....	52
Figure 3.12 Extraction result (1)	54
Figure 3.13 Matching result (1).....	55
Figure 3.14 Extraction and matching result (2).....	56
Figure 4.1 Measurement System	59
Figure 4.2 Flow chart of sea-level height measurement.....	60
Figure 4.3 Measurement system.....	61
Figure 4.4 The change of sea-level height	62
Figure 4.5 Experiment places.....	64
Figure 4.6 Images in Shigu at 6:48	65
Figure 4.7 Calculation of the height of sea level at 6:48	66
Figure 4.8 Image in Shigu at 7:49.....	67
Figure 4.9 Calculation of the height of sea level at 7:49	68
Figure 4.10 Image in Singu at 8:50.....	69
Figure 4.11 Calculation of the height of sea level at 8:50	70
Figure 4.12 Image in Singu at 9:51.....	71
Figure 4.13 Calculation of the height of sea level at 9:51	72
Figure 4.14 Image in Singu at 10:52.....	73
Figure 4.15 Calculation of the height of sea level at 10:52	74
Figure 4.16 Image In Singu at 11:53.....	75
Figure 4.17 Calculation of the height of sea level at 11:53	76
Figure 4.18 Image in Singu at 12:53.....	77
Figure 4.19 Calculation of the height of sea level at 12:53	78
Figure 4.20 Image in Singu at 13:54.....	79
Figure 4.21 Calculation of the height of sea level at 13:54	80
Figure 4.22 Image In Singu 14:55	81
Figure 4.23 Calculation of the height of sea level at 14:55	82
Figure 4.24 Image in Singu at 15:56.....	83
Figure 4.25 Calculation of the height of sea level at 15:56	84
Figure 4.26 Image in Singu at 16:57.....	85
Figure 4.27 Calculation of the height of sea level at 16:57	86
Figure 4.28 Image in Singu at 17:58.....	87
Figure 4.29 Calculation of the height of sea level at 17:58	88

Figure 4 .30 Experiment result in Singu on March 8.....	89
Figure 4 .31 Experiment result in Singu on March 9.....	90
Figure 4 .32 Experiment result in Singu on March 10.....	90
Figure 4 .33 Experiment result in Singu on March 14.....	91
Figure 4 .34 Experiment result in Singu on March 15.....	91
Table 2 .1 Camera parameters.....	21
Table 2 .2 The result of calibration in Shikashima	32
Table 2 .3 The error of calibration in Shikashima	33
Table 2 .4 The result of calibration in Shigu.....	35
Table 2 .5 The error of calibration in Shigu.....	36
Table 2 .6 The result of calibration in Tsuyazaki.....	37
Table 2 .7 The error of calibration in Tsuyazaki.....	37
Table 3 .1 Gaussian convolution kernel	42
Table 3 .2 Result of matching image (1)	55
Table 3 .3 Result of matching image (2)	56

Appendices-Sign in paper

- A : The sum of all the pixels of sea wave.
- AS_{ij} : The similarity of the area.
- b : The length of base line.
- C : The ratio of perimeter to area.
- $C_{(i,j)}$: The cross-correlation constraint at the point(i, j).
- $C_0(t), C_1(t)$: The two classes separated by a threshold t .
- CS_{ij} : The similarity of the curvature.
- d_x, d_y : The physical dimensions of one pixel in the X-axis and Y-axis.
- $Dist_{ij}$: The similarity of the feature vector.
- f : The local length of camera.
- $f(i, j)$: The gray value at the point(i, j) in the input image.
- g : The standard acceleration due to gravity.
- h : The height from the sea surface to the seafloor.
- $H_{(i,j)}$: The Gaussian convolution kernel in point(i, j).
- i : Image coordinate in x direction.
- $I_{(m,n)}, R_{(m,n)}$: The gray value at the point (m, n).
- \bar{I}, \bar{R} : The average gray value with block size $M \times N$.
- j : Image coordinate in y direction.
- L_i : The length from the point P_1 to point Q_i .
- M_1 : The internal parameter matrix of the camera.
- M_2 : The external parameter matrix for the camera.
- n_i : The number of the gray value i .
- $O(i, j)$: The gray value at the point(i, j) in the output image.
- P : The sum of all the pixels of the perimeter of sea wave.
- p : The ratio of left-(x, y) width per block width.
- p_i : The probability of each gray value.
- PM : The 3×4 projection matrix.
- PS_{ij} : The similarity of the perimeter.
- q : The ratio of bottom-(x, y) width per block width.
- r : The distance from each pixel to center point.
- R : The rotation matrix.
- $T_{(m,n)}$: The threshold in block (m, n).
- $t_{(i,j)}$: The threshold of point(i, j).
- T : The translation matrix.

T_x, T_y, T_z : The element of translation matrix
 (u, v) : The point position in pixel coordinates.
 (u_0, v_0) : The principal point of camera.
 v : The speed of Tsunami.
 V : The feature vector.
 VL : The left feature matrix.
 VR : The right feature matrix
 (x_0, y_0) : The center point of image.
 (x_i, y_i) : The point coordinate in the image.
 X_w, Y_w, Z_w : The coordinate in 3-D world coordinates.
 X_c, Y_c, Z_c : The coordinates in the 3-D camera coordinates
 Y_i : The height value of sea wave.
 YS_{ij} : The similarity of the position.
 α : The angle of rotating toward the z_axis.
 β : The angle of rotating toward the y_axis.
 γ : The angle of rotating toward the x_axis.
 $\delta^2(t)$: The variance of threshold t .
 $\omega_0(t), \omega_1(t)$: The probabilities of the two classes separated by a threshold t .
 $\mu_0(t), \mu_1(t)$: The average gray of $C_0(t)$ class, $C_1(t)$ class.

Chapter 1 Introduction

Tsunami, one of the most dangerous natural disasters, damages the coastal countries. Tsunami occurs frequently in recent years. Thus, it is necessary to detect the tsunami before it reaches the shore in 15 to 20 minutes. Comparing with typical tsunami prediction methods, our lab has proposed a method based on 3-D image measurement technique to detect the long distance sea surface. In order to achieve the purpose of the tsunami forecast eventually, we must overcome all kinds of problems of long distance. This system monitors the range of sea waves which are more than 20km.

In this chapter, first, we will introduce the purpose of our research, the characteristics of the tsunami and the existing methods of tsunami forecast. Then, we introduce the 3-D image measurement technique. Finally, we introduce the research significance of this research and the structure of the system.

1.1 Analysis of tsunami characteristics and tsunami disaster

Tsunami is a series of huge waves that can cause great devastation and loss of life when reaching coasts. Tsunami is caused by the underwater earthquake, a volcanic eruption, a sub-marine rockslide, or, more rarely, by an asteroid or meteoroid crashing into in the water from space. Most tsunamis are caused by underwater earthquake, but not all underwater earthquakes cause tsunamis - an earthquake is over about magnitude 6.75 on the Richter scale to cause the tsunami ^[1]. About 90 percent of all tsunamis occur in the Pacific Ocean.

Many tsunamis are detected before they hit the land, and the loss of life can be minimized. With the use of modern technology, including seismographs (which detect earthquakes), we can computerized offshore buoys that can measure changes in wave height, and a system of sirens on the beach to alert people of the potential danger of tsunami.

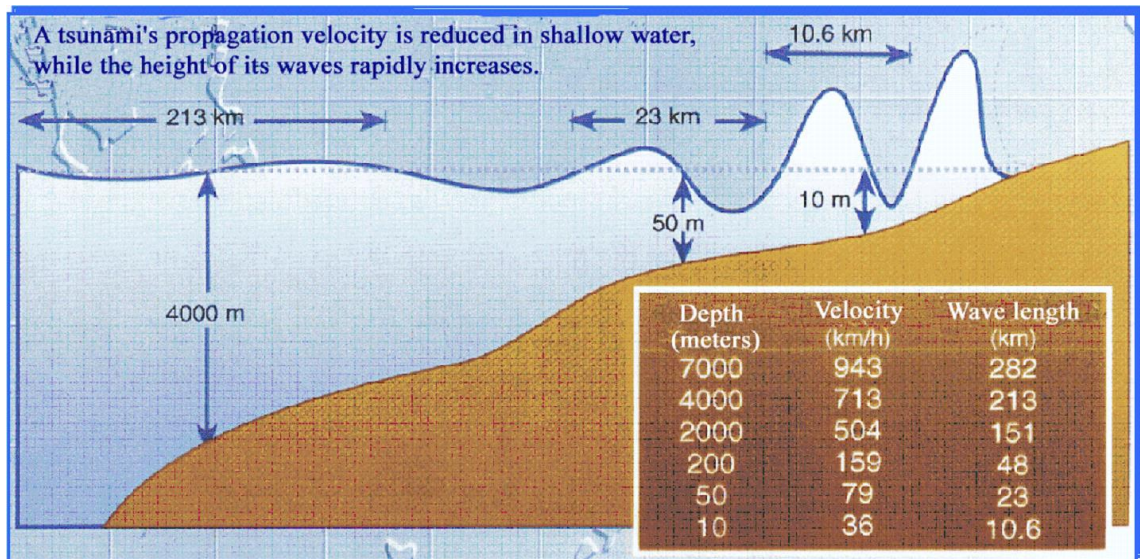
When considering how tsunami waves propagate, or travel across the ocean, it is important to understand wave behavior. Before discussing tsunami waves, we know the definition and characteristics of the wave. Comparing wind-generated waves, tsunami waves are useful for understanding the force, scope and potential danger of large tsunamis.

Using data from past tsunami events and known wave characteristics, scientists have developed models for calculating tsunami travel times to deliver warnings to communities that may be impacted by the tsunami. These models make use of complex data based on the size and location of an earthquake, the depth of the ocean determined by bathymetric measurements, the distance to a given location, the shape of the coastline in impacted zones, and past run-up heights.

Scientists of the tsunami warning center have developed some models to predict the arrival times of tsunami for the certain high-risk locations. When an earthquake of magnitude 6.75 or higher magnitude generates along a coastal area, warning centers may be able to warn communities of an impending tsunami and estimate when the first wave will arrive.

In the early stage, huge waves cannot be observed when the tsunami is far from coast and the propagation speed can be very fast. With the tsunami coming to near shore areas, obvious huge waves can be noticed and tsunami propagation velocity will slow down. Figure 1.1 shows the relations between depth, velocity and the wave length. This phenomenon stems from the relationship of tsunami propagation velocity and sea depth in the equation (1.1) ^[2].

$$v = \sqrt{gh} \quad (1.1)$$



(https://www.senat.fr/opecst/english_report_tsunami/english_report_tsunami2.html)

Figure 1.1 Tsunami propagation

Where, v is the propagation velocity of tsunami, g is the gravitational acceleration, and h is the depth of the sea. It is difficult to detect the tsunami when the height of the sea waves is low and the propagation velocity is high in the early stage^[3].

Waves are a disturbance that propagates, or travels, through space and time transferring energy from one point to another. Waves can be electromagnetic or mechanical. The basic parts of any type of waves are same, although waves differ in their characteristics.

The state of equilibrium is the state when the system is in balance. The disturbance makes the system out of equilibrium. All systems try to return to equilibrium after the disturbance.

Gravity is the force that attempts to restore water molecules to equilibrium when they are disturbed by the wave energy.

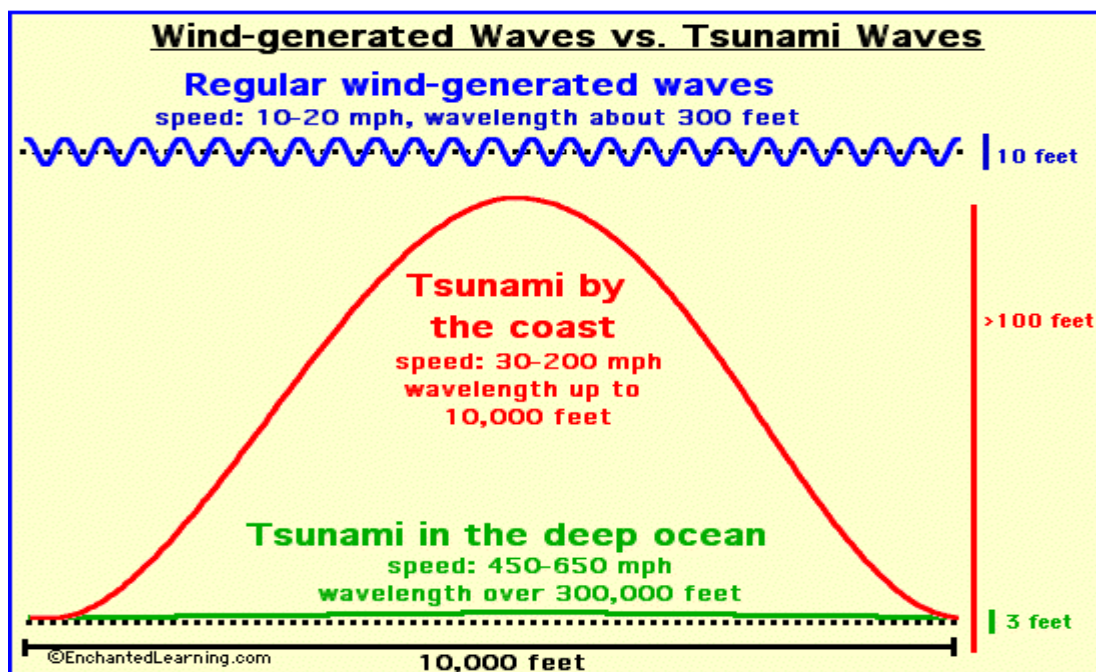
The equilibrium of ocean water is disturbed by the gravity of the moon and the sun, which produce the tides. Other disturbances include tsunami triggers, wind and human and animal activity.

There are four basic types of water waves: tides, seiches, wind-generated waves, and tsunamis waves.

Tides are the sea level rise and fall caused by the combined gravity of the moon and the sun. The seiche is a standing or stationary wave oscillating in an enclosed body of water such as a bay, lake or reservoir often caused by an earthquake, wind or tsunami. A

seiche looks like waves that slosh back and forth from one end of a bay to another. Two propagating waves traveling in opposite directions combine to form the standing wave.

Most ocean waves are generated by wind. As the wind blows across the surface of the water, it pushes on the surface of the water forming waves. Wind can create waves of different sizes, from small capillary or ripple waves, to large swells. Strong winds and storms can produce chops and swells. Wavelengths vary from centimeters to 90 meters high (300 feet) as follow in the Figure 1.2 [4].



(<https://trestlessurfcrowd.wordpress.com/tag/capistrano-beach/>)

Figure 1.2 Wind-generated waves

As the wind blows on the surface, the energy of the wave reaches a certain known depth into the water and the depth of influence, which is equal to one half of the wavelength. The motion of the water particles decreases as depth increases, until the depth of influence is reached.

In deep water, wind waves cause water particles to move in a circular motion. There is a common misconception is that wind waves propel a boat or an object forward on the surface of the water. Because water particles return to the same position approximately as the energy passes through, an object on a wave does not move forward with the wave energy, but it returns to the same general area.

As wind-generated waves approach a shoreline, and the depth of the water decreases, the height and amplitude of the wave increases until the wave breaks due to gravity, which is popular for surfers [5].

Tsunami waves differ from wind-generated waves which shouldn't be surfed. When tsunamis produce, the water is displaced by an earthquake, landslide, or volcanic activity, they can generate waves that travel in all directions through the entire water column from the bottom of the ocean to the top. The energy of tsunami waves is much greater than most wind-generated waves'. Some tsunamis may be barely noticeable in size, while others generate powerful waves that can devastate coastal areas.

Tsunamis are characterized by very long wavelengths that travel across the open ocean very quickly. The speed of tsunami waves depends on the depth of the ocean and the gravity: the deeper the ocean is, the faster the waves travel, sometimes as fast as 890 kilometers per hour or the same speed as a jet airplane's.

Tsunami waves are also characterized by small amplitudes so that on the open ocean the tsunami might be unnoticed by a ship that experiences nothing more than a gentle rise and fall [6].

According to the history, tsunamis have frequently brought tremendous damage to the countries. We can take the recent one--East Japan Earthquake and Tsunami in 2011 as an example. By November 2, 2011, deaths from the Great East Japan Earthquake and Tsunami reached 15,829, with 3,679 missing and 5,943 injured in the event. The initial economic outlook of the earthquake was severe: it brought the enormous direct loss for Japanese industry. Japan's early loss estimated at 20-25 trillion yen, or about 4% to 6% of Japan's GDP. Although the loss estimate has dropped to 10-12 trillion yen in the next five years, the loss was still huge. Figure 1.3 shows the disastrous part of this tsunami [7].



(<http://news.163.com/photoview/6R2E0001/2241820.html#p=CFALO34D6R2E0001>)

Figure 1.3 Tsunami in Miyako

1.2 The meaning of wave height measurement and the existing measurement methods

1.2.1 Measurement methods in short distance

Due to the serious tsunami, the tsunami forecast research has made considerable progress. According to different criteria, the existing forecasting methods are divided into two categories ^[8]: the change of water pressure and the reflection of wave. Figure 1.4 shows some typical predictions based on changes of water pressure. In this category, predictive judgment is made by measuring changes of water pressure. This method of prediction is easy to set up and costs low relatively. However, when a real tsunami comes, pressure sensors are easily damaged and it is often difficult to predict the tsunami. Figure 1.4 lists three installations for tsunami measurements along the coast.

(a) A tide gauge (also known as a mareograph or, sea level recorder) is a device that used to measure changes of sea level relative to a vertical datum ^[9]. The sensor continuously records the height of the water level relative to the height reference surface near the geoid. Water enters the device through the bottom pipe. The device measures the height of water and sends the data to the computer.

Historical data is available for approximately 1,450 stations worldwide, of which about 950 have provided updates to global data centers since January 2010. Some places have recorded historical data for centuries, such as Amsterdam dating back to 1700. Used by satellite data, new modern tide gauge can often be improved.

Based on measuring the average sea level, tide gauge is used to measure tides and quantify the size of the tsunami. In this way, sea level slopes up to several 0.1m/1000km and more tsunamis can be detected. Tsunami can be detected when sea level starts to rise, although warnings from seismic activity may be more useful.

(b) The tsunami meter measures the height of sea level by transmitting the ultrasonic wave ^[10]. It is known as acoustic tsunami observation meter, which is usually placed above the water surface. First, the transmitter emits ultrasonic waves to the sea surface. Then, the height information of the water surface is measured by the time taken for transmission and reception of the ultrasonic waves. This method has the same advantages as the tide gauge station's, such as simple structure, high precision and low cost. However, it also has the disadvantages of limited measurement range, easy damage and inability to be used for tsunami prediction.

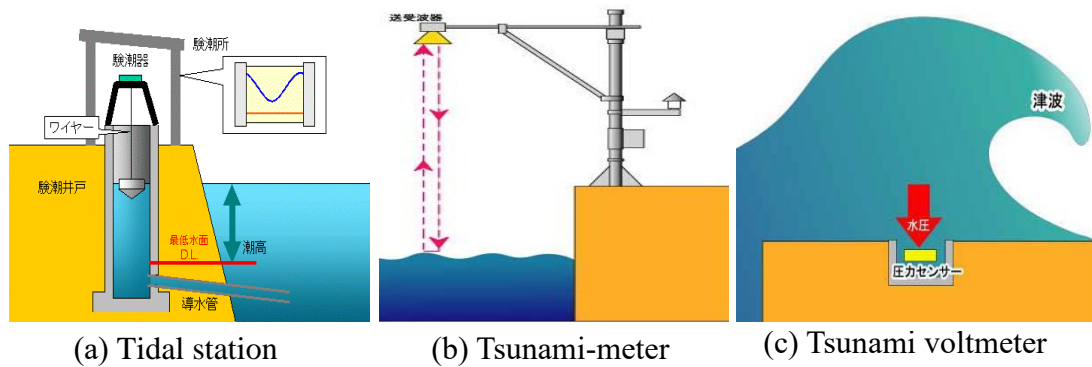


Figure 1.4 Measurements along coast

(c) The Tsunami voltmeter consists of a pressure sensor. When the tsunami comes, the height of sea wave is measured by the voltmeter^[10]. This system is simple and accurate. However, due to be installed on the coast, it cannot be used for tsunami prediction. In addition, the system is easy to be destroyed by the tsunami.

1.2.2 Measurement methods in long distance

Several common methods of measuring offshore altitude have been described above. Although these methods have different forms and principles, they all have the advantages of simple equipment and low cost. However, at the same time, there is a defect that the measurement range is small and it cannot be used for tsunami prediction. Therefore, if you want to predict the tsunami, you need to establish a method in the open-sea area or non-contact to measure tsunami.

Three types of long-range tsunami measurements are listed in Figure 1.5. Figure 1.5 (a) and Figure 1.5 (c) show the measurement system in the open-sea area. Figure 1.5 (b) shows a non-contact measurement.

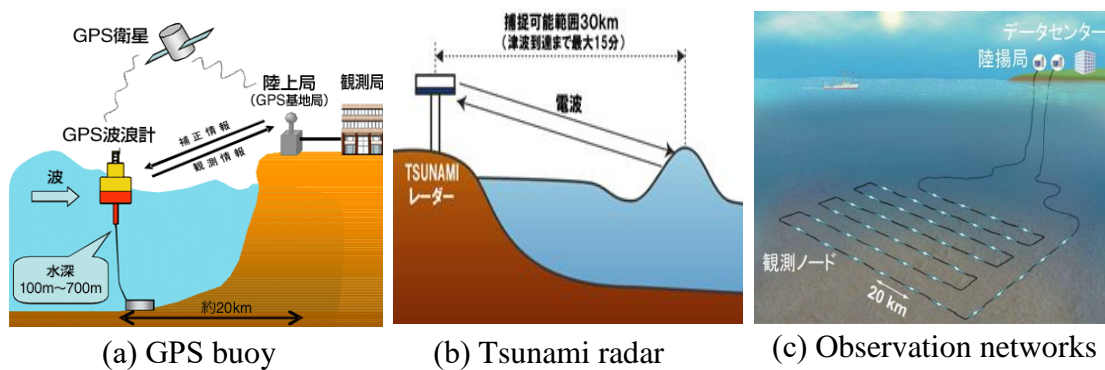


Figure 1.5 Measurements in open sea area

(a) The GPS Buoy (GB) system can be classified as an inverted long baseline (LBL) acoustic positioning device where the transducers is installed GPS-equipped sonobuoys that are either drifting or moored ^[11]. The GB can be used in conjunction with an active underwater equipment (such as a pinger-equipped torpedo) or with a passive acoustic source (such as inert bombs that strike the surface of the water). Time of arrival (TOA) techniques are commonly used to track or locate the sound source or impact event. Several GBs are often deployed in a given operating area; the total number is determined by the size of the test area and the accuracy of the desired result. You can use different GPS positioning methods to locate the array of GBs, with accuracies of the cm to meter level in real-time possibly.

(b) The tsunami radar can capture the tsunami in a distance of 30km from the sea surface and about 15 minutes before the tsunami arrives. Through transmitting and receiving radar waves, the observation frequency can reach once every two seconds ^[12-13]. However, it is difficult to measure the shape of the sea waves by this method. Especially for long-period and low-amplitude sea waves, the device is difficult to receive the returned waves after emitted by them. In addition, this device is also quite difficult to measure the distance of tsunami more than 30km.

(c) The Submarine Earthquake Tsunami Observing Network has set up a number of pressure sensor nodes on the seafloor ^[14]. The distance between node and node is about 20km and the coverage area is wide so that earthquakes and tsunamis can be observed as well as the tsunami arrival time can be predicted. However, the single node of the device has a limited measuring range and many disadvantages such as high installation cost, difficult maintenance, etc.

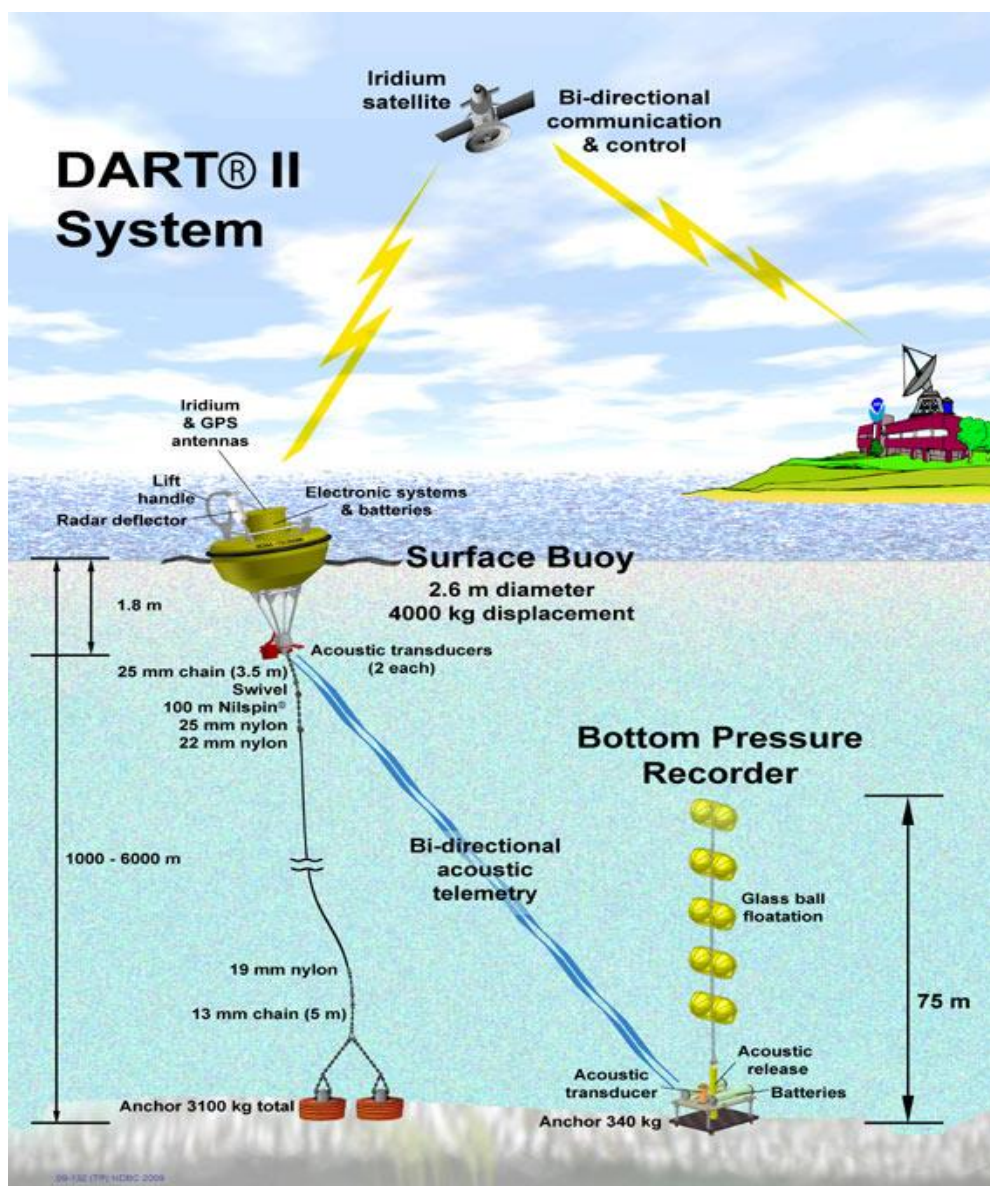
Although these two types of measurement methods do not have the ideal performance, the combination of the two type methods do some improvements. One of the famous combination methods is the DART (Deep-ocean Assessment and Report of Tsunami) ^[15]. Each DART station consists of a surface buoy and a seafloor bottom pressure recording (BPR) package that detects pressure changes caused by tsunamis. The surface buoy receives transmitted information from the BPR via an acoustic link and then transmits data to a satellite, which retransmits the data to ground stations for immediate dissemination to NOAA's Tsunami Warning Centers, NOAA's National Data Buoy Center, and NOAA's pacific marine environmental laboratory (PMEL) ^[16]. The Iridium commercial satellite phone network is used for communication between 31 of the buoys.

When on-board software identifies a possible tsunami, the station will leave standard mode and start transmitting in event mode. In standard mode, the station reports water temperature and pressure (converted to sea level height) every 15 minutes. At the

beginning of the event mode, the buoys report the measurement every 15 seconds in several minutes.

The first generation DART I stations have one-way communication capabilities, and rely solely on software's ability to detect tsunamis to trigger event mode so that data transfers fast. In order to avoid false positives, the detection threshold is set relatively high, which may cause the low-amplitude tsunami not to trigger the station.

The second generation DART II is equipped with a two-way communication system that allows tsunami forecasters to change the station in event mode in anticipation of a tsunami's arrival.



(https://nctr.pmel.noaa.gov/Dart/dart_ms1.html)

Figure 1.6 Dart system

The above describes three tsunami technologies with large-distance measurement methods. Compared with near-distance tsunami measurements, long-distance measurements can detect from the coast to the ocean so that they can be applied to the tsunami prediction. Tsunami information can be obtained before the tsunami arrives. In particular, the GPS buoys and the DART, they are now relatively mature technologies and they are widely used in early warning systems for tsunamis. However, obviously, the existing problems are the high cost. They cannot monitor the large sea area. They can just detect the place where the buoy is near. There are still major problems to be solved.

For the task of monitoring tsunami, we need to obtain 3-D information such as the sea level height and the arrival time. Therefore, in view of the shortcomings of the existing sea level measurement methods and the advantages of the image measurement technology, this paper proposes a method of measuring the height of the sea level by using the 3-D image measurement technology to predict the tsunami.

1.3 3-D image measurement technology

The development of 3-D image measurement is rapid during recent years. They can be used widely for large range of wave heights measurement. 3-D image measurement methods also have the good performance in many fields. There are mainly three kinds of 3-D image measurement methods, which have been widely applied.

1.3.1 TOF method

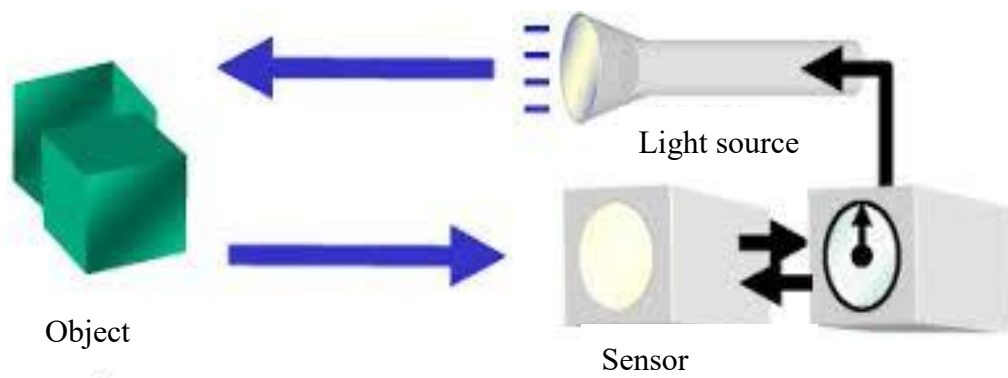
The TOF (time of flight) method is similar to a radar that measures 3-D information by measuring the round time of the signal. System as shown in the Figure 1.7. For radar, the signal is microwave. For the TOF method, the signal is visible light. Figure 1.7 shows the structure diagram of the TOF method. The TOF method has the advantages of low cost. It is easy to use, and it has high precision. It has been widely applied in the fields of machine vision and 3-D scanning printing ^[17].

In TOF method, cameras, sensor and active light sources are necessary. It works by emitting the modulated light to the object and receiving the reflected light. It measures the circular time or phases shift between emission and reflection as well as converts it to distance. The light is usually near infrared. It is invisible to the human eye. The sensor should be designed to respond to the same spectrum.

Time-of-flight cameras for civil applications began to emerge around 2000, as the semiconductor processes became fast enough for such devices. The systems cover ranges of a few centimeters up to several kilometers. The distance resolution is about 1 cm. Compared to standard 2D video cameras, the lateral resolution of time-of-flight cameras is generally low and most commercially available devices at 320×240 pixels or less as of 2011. Compared to 3D laser scanning methods for capturing 3D images, TOF cameras operate very quickly, providing up to 160 images per second.

For the TOF sensor, an experiment was conducted to verify the measurement range. OPTEX's ZC-1050's TOF 3-D distance camera captures images of people at four different distances. For different distances, people's colors are different. The results show that the TOF sensor can only measure a distance of about 7 meters.

TOF sensors are not suitable for tsunami monitoring due to the measurement distance limitations. Just like radars, it consumes a lot of energy when the active measurement method is used for large area detection, which makes the cost too high to be realized.



(http://www.idl.rie.shizuoka.ac.jp/study/project/tof/index_e.html)

Figure 1.7 TOF system

1.3.2 Pattern projection method

This method is a 3-D scanning device for measuring the 3-D shape of an object using projected light patterns and a camera system. A typical system is shown in the Figure 1.8, including projector and regular camera ^[18]. First, the projector sends the pattern light to the object, and the camera takes image of the reflected projection. By using the correspondence between the projection pattern and the reflection pattern, 3-D space information can be extracted. A faster and more versatile method is the projection of patterns consisting of many stripes at once, or of arbitrary fringes, as this allows the acquisition of a multitude of samples simultaneously. Seen from different viewpoints, the pattern appears geometrically distorted due to the surface shape of the object.

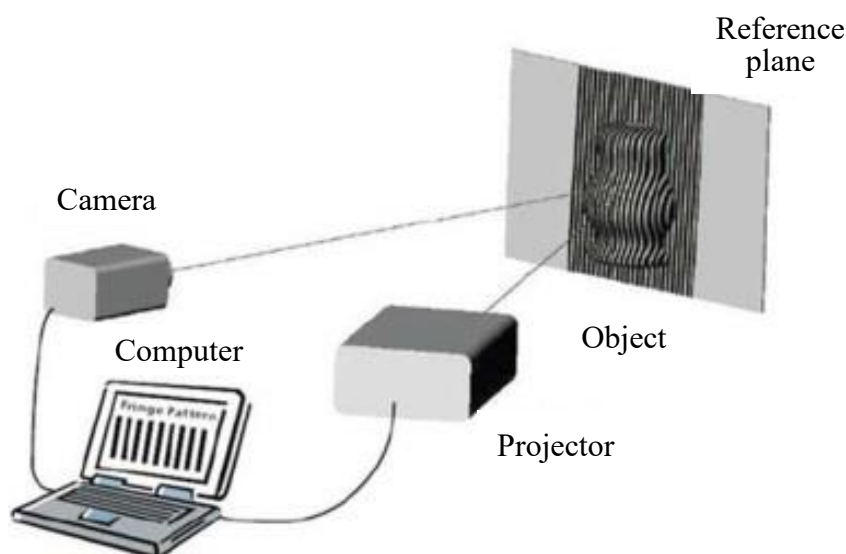


Figure 1.8 The system of pattern projection method

Projection patterns can be divided into two types: binary patterns and non-binary patterns. Binary patterns include such as spot pattern, slit pattern or special coded pattern. Multi-projection is necessary and this procedure takes much time and slows down the whole measurement speed. Non-binary patterns include intensity gradient pattern, color modulation pattern. They simplify the multi-projecting into single or twice projecting, which are widely used nowadays.

1.3.3 Stereo vision method

Stereo vision is another popular 3-D measurement method which uses two separated cameras at the same scene or objects ^[19-20]. Figure 1.9 shows the basic components of the stereo vision method. The focal lengths of the two cameras are all f , the distance between the two cameras named as base line is b ; and the corresponding projection points of target point P in the two images are represented as $p_1(x_1, y_1)$ and $p_2(x_2, y_2)$.

This method is based on a triangulation theory and recovers scene depth from the parallax of the images. The ideal structure is shown as Figure 1.10 which consists of two parallel camera images. O_1 and O_2 are the centers of camera images; the projection points of the target point P are $p_1(x_1, y_1)$ and $p_2(x_2, y_2)$., equations (1.1) and (1.2) show how to calculate the distance Z by using the principle of similar triangles.

$$f/Z_w = x1/L \tag{1.1}$$

$$f/Z_w = (-x2)/R \tag{1.2}$$

$$b = L + R \tag{1.3}$$

$$Z = bf/(x1 - x2) \tag{1.4}$$

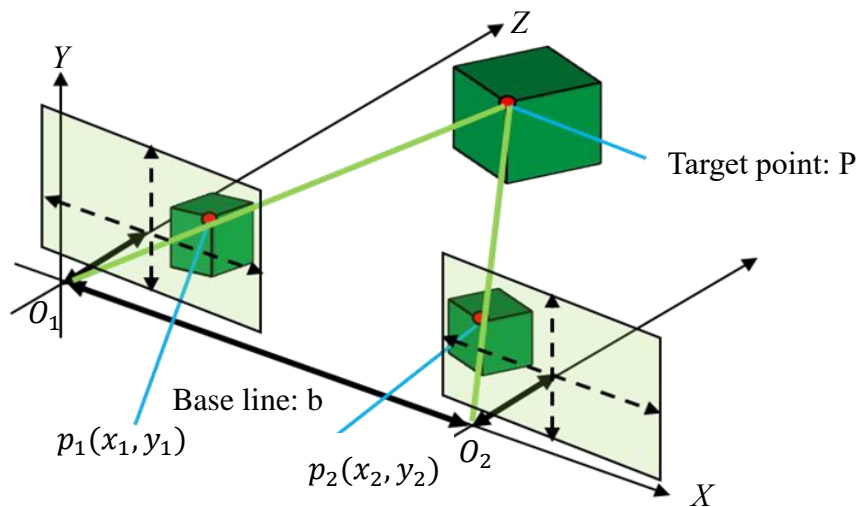


Figure 1.9 Stereo vision method

In order to find out the parallax, corresponding points matching is very important. Through stereo image rectification, images are projected onto a common plane which results in it that the corresponding points have the same row coordinates. This process helps reduce the 2-D stereo correspondence problem to a 1-D problem.

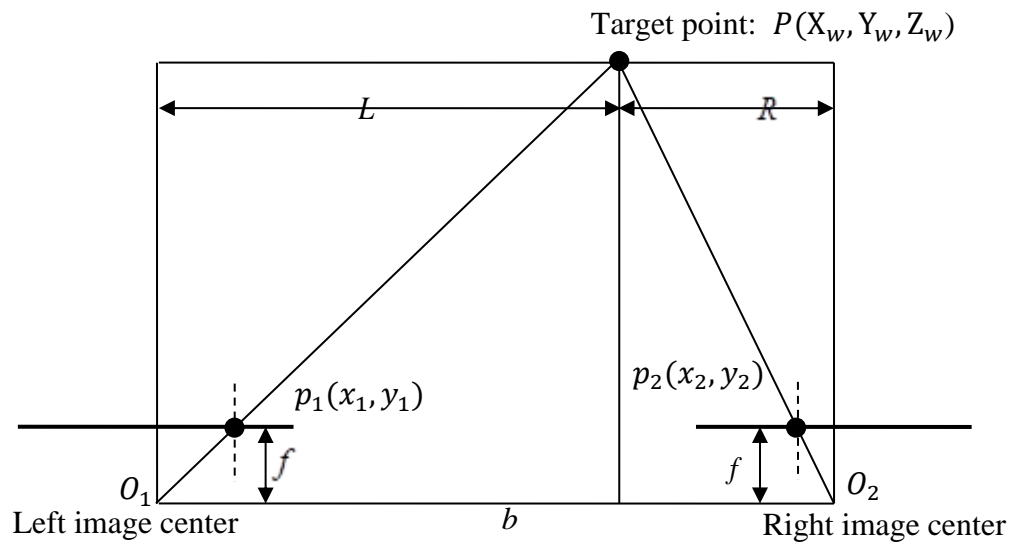


Figure 1.10 Ideal stereo vision system

1.4 The purpose of our research and structure of this paper

In the last section, we mention some progress achieved in short distance experiment. To realize the purpose of tsunami forecast finally, long distance measurement is a necessary process. This paper focuses on the long distance and we attempt to solve the problems occurring during the distance extension. The structure of this paper is as followed:

Chapter 1 explains the background of this paper and the existing forecast methods. In addition, it also proposes the conceive of forecast tsunami with 3-D image processing technology. This part introduces the system and finally gives the purpose as well as structure of this paper.

Chapter 2 introduces the calibration of binocular stereoscopic vision technology. First, we illustrate the theory of binocular stereoscopic vision.

Chapter 3 introduces the extraction methods of sea wave. First, we illustrate the difficulties in long distance sea wave extraction and then propose a partial analyze of pre-processing, double-threshold extraction method for different situations at long distance. This part explains the sea wave matching method. First, we introduce the difficulties of direct point matching and then explain the solution to this problem. Therefore, we propose the matching sea wave base on the feature matrix and show the results of this method.

In the chapter 4, we do some experiments. First, we introduce experimental conditions, and we propose to calculate the sea level through the average of many sea wave. Then, compare the calculated date with the data from the Meteorological Agency.

Chapter 5 summaries the work in this paper and gives an outlook of the future work.

Chapter 2 Calibration of long distance 3-D image measurement system

Camera system calibration is an essential part in 3-D image measurement. The principle of ideal binocular stereo vision system is convenient. However, the two cameras in the measuring system are usually not parallel configurations in the actual measurement. In this case, the simple triangulation method cannot meet the requirements of calculation. We must configure the usual pin model of the binocular stereo vision.

Though many existing methods can calibrate cameras, but those methods are just effective to the close range, and they usually use a calibration target to calibrate the cameras. Since the distance of monitoring sea is very far, those methods are very difficult to apply the long-distance measurement, especially more than 20 kilometers. We construct a measurement system of long distance sea-level height for disaster prevention based on a 3-D image measurement technique. First, in order to monitor a wide range of the sea surface, this system utilizes the pan and tilt stages and angle sensors to rotate the cameras. In order to improve the accuracy of calibration, we use the standard scale pole to calibrate intrinsic and extrinsic parameters of cameras and angle sensors. In addition, all the equipment can be set in one place so it is convenient to maintain.

This chapter explains the principles of binocular stereo vision. Contrast with the exiting calibration, we propose the improved calibration method. Finally, experiments verify the calibration accuracy and it can meet the requirements of the system.

2.1 The theory of binocular stereoscopic vision

The camera model determines the geometric relationship of optical imaging of the camera. The simplest and most commonly used camera model is called the pinhole model, which is a linear model. The pinhole camera model is not a universal, wide-angle lens or some special lens, such as fish-eye lens, whose imaging rules are non-linear and cannot be solved with a pinhole model^[21]. The camera used in this paper is the camera that meets the pinhole model.

The imaging relationship of the pinhole model is shown in Figure 2.2. For any measurement point of space, its coordinates in the camera coordinate system can be represented $P(X_c, Y_c, Z_c)$. The position $p(x, y)$ of the image on the image plane satisfies the linear imaging rule, i.e. the projection position of the point P is the intersection of the line O_cP of optical center O_c and the point P of the camera to the plane of the image. This projection is also known as perspective projection.

To make it easier to understand the imaging process and geometry of points in the perspective projection model of the camera, it is necessary to understand the four coordinate systems associated with them, namely the image coordinate system, the image plane coordinate system^[22], the camera coordinate system and the world coordinate system.

First, the image coordinate system is a coordinate system that describes the position of the pixel in the image. The digital image is stored in a computer in pixels. The computer divides the image into $M \times N$ small squares. each square is one pixel. As shown in Figure 2.1, the purple part of the image plane, the Cartesian coordinate system, is known as the image coordinate system. In general, the origin O_0 of the image coordinate system is located in the upper left corner of the image. The coordinates (u, v) in the coordinate system represent the number of rows and columns of a pixel in the digital image. However, only the image coordinate system cannot show the physical location of the pixel, so another coordinate system with a physical unit is needed. Such coordinate system is called the image plane coordinate system. In general, the origin O_1 of a plane-like coordinate system is defined at the intersection of the optical axis of the camera and the image plane, which is generally at the center of the image. The horizontal x axis and the vertical y axis are respectively parallel to the u axis and the v axis of the image coordinate system. We can assume that the origin of a plane coordinate system is expressed as u_0, v_0 , and the physical dimensions of one pixel in the x -axis and y -axis directions are expressed as d_x and d_y . Then, the coordinates of any pixel in the image in both coordinate systems are a conversion between (2.1) and (2.2).

$$u = \frac{x}{d_x} + u_0 \quad (2.1)$$

$$v = \frac{y}{d_y} + v_0 \quad (2.2)$$

(2.1) and (2.2) can be expressed as (2.3) in the form of homogeneous coordinates and matrix:

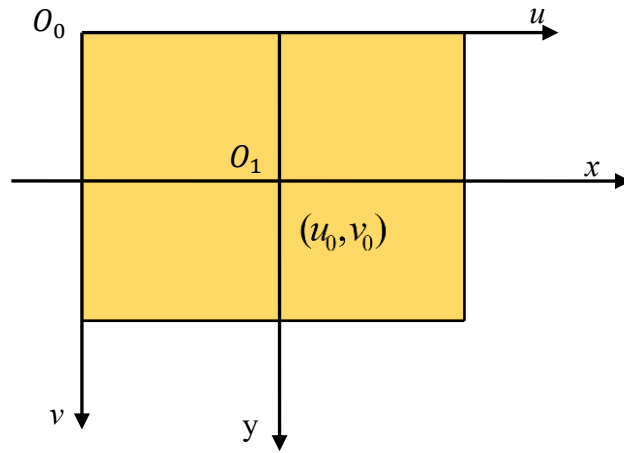


Figure 2.1 Images coordinate and the image plane coordinate

$$\begin{bmatrix} u \\ v \\ 1 \end{bmatrix} = \begin{bmatrix} \frac{1}{d_x} & 0 & u_0 \\ 0 & \frac{1}{d_y} & v_0 \\ 0 & 0 & 1 \end{bmatrix} \begin{bmatrix} x \\ y \\ 1 \end{bmatrix} \quad (2.3)$$

The other two coordinate systems are the camera coordinate system and the world coordinate system, which can be shown in Figure 2.2. The origin O_c of the camera coordinate system is the lens center of the camera. The X_c axis and Y_c axis of the camera coordinate system are parallel to the x axis and y axis of the image plane coordinate system, and the Z_c axis is perpendicular to the image plane, that is, the optical axis direction of the camera [23]. The intersection of the camera's optical axis and the image plane is the origin (u_0, v_0) of the plane coordinate system, and the length of the connection $O_c O_1$ is the so-called focal length of the camera. The world coordinate system is a coordinate system used to describe the position of any object in the space including the camera. It is composed of X_w, Y_w, Z_w axes. The conversion relation between the camera

coordinate system and the world coordinate system can be expressed by a rotation matrix R and a translation vector T . Let the homogeneous coordinates of the measurement points P in the world coordinate system be $(X_w, Y_w, Z_w, 1)^T$, and the homogeneous coordinate in the camera coordinate system is $(X_c, Y_c, Z_c, 1)^T$. There is a conversion between the two coordinates as shown in (2.4).

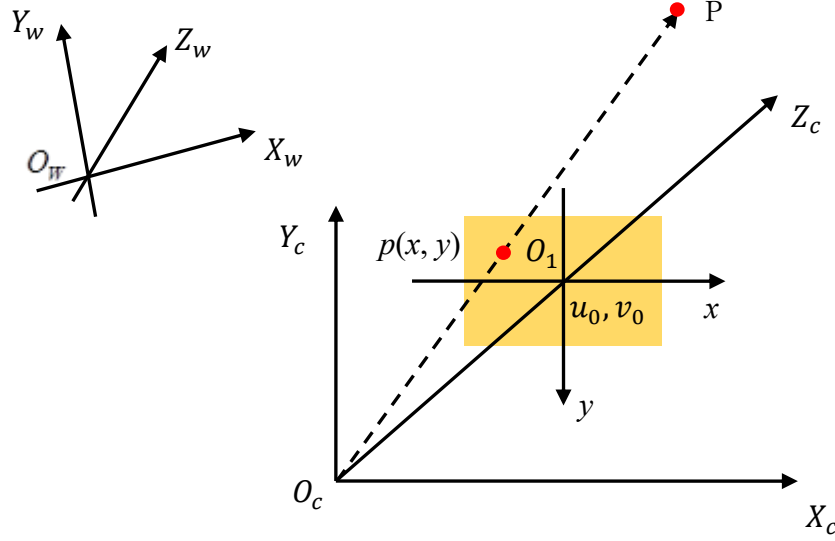


Figure 2.2 Theory of pinhole model

$$\begin{bmatrix} X_c \\ Y_c \\ Z_c \\ 1 \end{bmatrix} = \begin{bmatrix} R & T \\ 0 & 1 \end{bmatrix} \begin{bmatrix} X_w \\ Y_w \\ Z_w \\ 1 \end{bmatrix} \quad (2.4)$$

Where, R is the rotation matrix, is a 3×3 orthogonal unit matrix; T is the three-dimensional translation vector.

In general, the rotation matrix can be expressed by equation (2.5). Where, γ, β, α are the rotation angles based on the X -axis, Y -axis and Z -axis, the translation vector T can be expressed by (2.6), t_x, t_y, t_z is the parallel movement based on the X -axis, Y -axis and Z -axis.

$$R = \begin{bmatrix} \cos\alpha & -\sin\alpha & 0 \\ \sin\alpha & \cos\alpha & 0 \\ 0 & 0 & 1 \end{bmatrix} \begin{bmatrix} \cos\beta & 0 & \sin\beta \\ 0 & 1 & 0 \\ -\sin\beta & 0 & \cos\beta \end{bmatrix} \begin{bmatrix} 1 & 0 & 0 \\ 0 & \cos\gamma & -\sin\gamma \\ 0 & \sin\gamma & \cos\gamma \end{bmatrix} = \begin{bmatrix} r_1 & r_2 & r_3 \\ r_4 & r_5 & r_6 \\ r_7 & r_8 & r_9 \end{bmatrix} \quad (2.5)$$

$$T = \begin{bmatrix} t_x \\ t_y \\ t_z \end{bmatrix} \quad (2.6)$$

These are four coordinate systems associated with the camera perspective projection model^[24]. After understanding the relationship between the various coordinate systems, you can understand and apply the camera imaging geometry better. The relationship between the equation (2.7) and the equation (2.8) can be obtained according to the proportional relation of its coordinates.

$$x = \frac{fX_c}{z_c} \quad (2.7)$$

$$y = \frac{fY_c}{z_c} \quad (2.8)$$

The relationship between the above perspective projection relationships (2.9) can be transformed by the homogeneous coordinate and matrix.

$$Z_c \begin{bmatrix} x \\ y \\ 1 \end{bmatrix} = \begin{bmatrix} f & 0 & 0 & 0 \\ 0 & f & 0 & 0 \\ 0 & 0 & 1 & 0 \end{bmatrix} \begin{bmatrix} X_c \\ Y_c \\ Z_c \\ 1 \end{bmatrix} \quad (2.9)$$

The corresponding relation between the coordinates of the points in the world coordinate system and the coordinates of the projection points in the image coordinate system can be obtained in the equation (2.10).

$$\begin{aligned} Z_c \begin{bmatrix} u \\ v \\ 1 \end{bmatrix} &= \begin{bmatrix} \frac{1}{d_x} & 0 & u_0 \\ 0 & \frac{1}{d_y} & v_0 \\ 0 & 0 & 1 \end{bmatrix} \begin{bmatrix} f & 0 & 0 & 0 \\ 0 & f & 0 & 0 \\ 0 & 0 & 1 & 0 \end{bmatrix} \begin{bmatrix} R & T \\ 0 & 1 \end{bmatrix} \begin{bmatrix} X_w \\ Y_w \\ Z_w \\ 1 \end{bmatrix} = \\ & \begin{bmatrix} f_x & 0 & u_0 & 0 \\ 0 & f_y & v_0 & 0 \\ 0 & 0 & 1 & 0 \end{bmatrix} \begin{bmatrix} R & T \\ 0 & 1 \end{bmatrix} \begin{bmatrix} X_w \\ Y_w \\ Z_w \\ 1 \end{bmatrix} = M_1 M_2 \begin{bmatrix} X_w \\ Y_w \\ Z_w \\ 1 \end{bmatrix} = PM \begin{bmatrix} X_w \\ Y_w \\ Z_w \\ 1 \end{bmatrix} \quad (2.10) \end{aligned}$$

In the equation $f_x = \frac{f}{d_x}$, $f_y = \frac{f}{d_y}$, M_1 is the internal parameter matrix of the camera; M_2 is the external parameter matrix for the camera; PM is the 3×4 matrix,

which is called the projection matrix.

Table 2.1 describes the specific meaning of each camera parameter. Among them, the internal parameter matrix M_1 is only related to the internal structure of the camera, which represents internal parameters including of camera focal length. The external parameters M_2 are completely determined by the camera relative to the position of the world coordinate system, called the external parameters of the camera. The process of solving these two parameters is called the calibration of the camera, and the calibration precision is related to the accuracy of the measurement results, which is a crucial link in the three-dimensional measurement [25-27].

Table 2.1 Camera parameters

Intrinsic parameters	Focus	The vertical distance from the center of the camera lens to the image plane.
	The center of image	The intersection of the optical axis with the image plane.
	Pixel sizes	The actual size of the pixel in the horizontal axis and the vertical axis.
	Distortion	Distortion parameters generated by the lens.
Extrinsic parameters	Rotation matrix	Based on the orientation of the optical axis in three-dimensional space.
	Movement matrix	Coordinate of camera's optical center based on 3-D space.

This section firstly describes how to calculate the 3-D coordinates of an arbitrary point in a binocular stereo vision system under ideal conditions. The top view of the binocular stereo vision system is shown in Figure 2.3. There are two cameras on the left and right in the picture. The two cameras are identical. Light-colored oval-shaped part of the two cameras represents the lens and the focal length are f . Below the camera is the camera's imaging plane. The connection between the center of the left camera and the center of the lens of the right camera is called the baseline and the base line can be expressed in letters. If the optical axes of both cameras are strictly parallel and the camera's image plane is parallel to the baseline, such system is called the binocular vision system under ideal conditions.

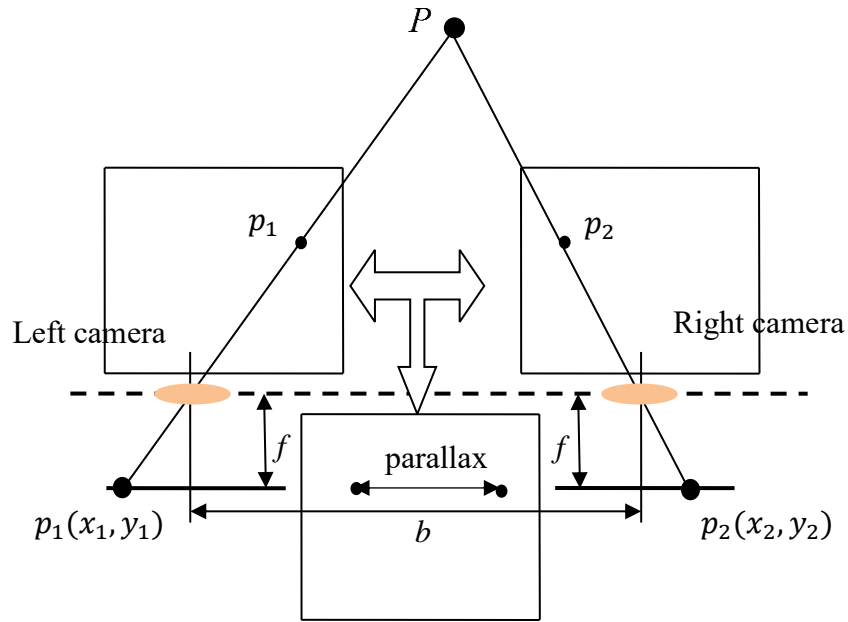


Figure 2.3 Binocular stereo vision system in the ideal model

The black object is the measured object in Figure 2.3, assuming that objects have a measurement point P . The left $p_1(x_1, y_1)$ and right $p_2(x_2, y_2)$ of two cameras shooting are left and right two projection point in the image coordinates. In addition, they are respectively according to the position of the two zero gap, which is as shown in Figure 2.4. The projection on the same point in the left view and projection on the right view on the same image contrast, the distance between them is the parallax^[28]. According to the parallax point can be calculated relative to the distance measurement system (i.e. the depth information), the depth information of the measurement point P and thus they can be used to get the measurement point which is relative to the corresponding three-dimensional coordinates measuring system. Then some simple derivation of the calculation process of the three-dimensional coordinate values is carried out.

In order to obtain the three-dimensional coordinate information of the measuring point, the relative distance between the measuring point and the measurement system is firstly needed to measure the depth information of the measuring point based on the Z-axial direction of the measurement system^[29]. Figure 1.10 is the calculation schematic diagram of the coordinates of the measuring points in the axial direction.

If you get a point in the direction of the axis, you can calculate the value of that point based on the other two dimensions. Figure 1.10 is the calculation principle of the coordinate values of the measuring points in the X-axis and Y-axis direction. As shown in Figure 2.4, it is in the direction of the horizontal axis (the X-axis) or on the vertical

axis (Y-axis) direction. Once get the coordinates Z of the Z-axis direction, we just need the distance from the image point $p_1(x_1, y_1)$ to horizontal distance and vertical distance of the center (x_0, y_0) of the image, as shown in the equation (2.11-2.14). Similarly, the measurement point P is calculated according to the principle of similar triangles On the X-axis and Y-axis coordinate values.

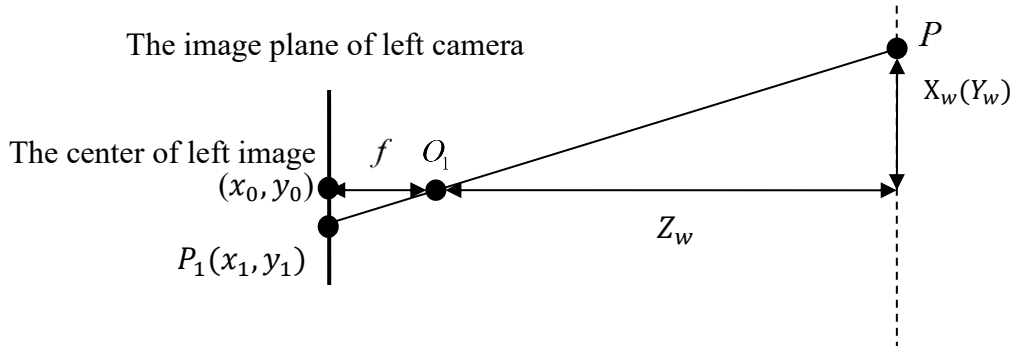


Figure 2.4 The measurement theory of x and y axis

$$\frac{x_1}{f} = \frac{X}{Z} \quad (2.11)$$

$$\frac{y_1}{f} = \frac{Y}{Z} \quad (2.12)$$

$$X_w = \frac{bx_1}{x_2 - x_1} \quad (2.13)$$

$$Y_w = \frac{by_1}{x_2 - x_1} \quad (2.14)$$

Finally, consolidating equations, the three-dimensional coordinate of the measuring point can be expressed by equation (2.15). Thus, the measured value of the point P calculated is the three-dimensional coordinate relative to the center of the left camera lens in the binocular stereo vision system.

$$\begin{bmatrix} X_w \\ Y_w \\ Z_w \end{bmatrix} = \frac{b}{x_1 - x_2} \begin{bmatrix} x_1 \\ y_1 \\ f \end{bmatrix} \quad (2.15)$$

The above pure ideal situation of the binocular stereo vision system computing flow.

However, the reality of binocular vision system is not able to achieve such an ideal, which the light axis of the two cameras is strictly parallel and the imaging plane is parallel to the baseline ^[30]. At the time of actual configuration camera system, the placement of the cameras unavoidably some angles such as deviation, or already need a camera optical axis angle system to correspond to a specific measurement occasions. Under the condition of the wave height measurement, in order to realize the remote measurement at the same area of the measurement requirements, or achieve the purpose of extend measurement range, it is necessary to carry out the camera rotation. This configuration of binocular stereo vision system is shown in Figure 2.5, and there is an angle between the optical axis of the left camera and the optical axis of the right camera ^[31]. The three-dimensional measurement of the non-ideal conditions has a complete set of calculations. Its calculation method is based on the projection principle of space center point in the camera. The next section focuses on the relevant knowledge of camera perspective projection model.

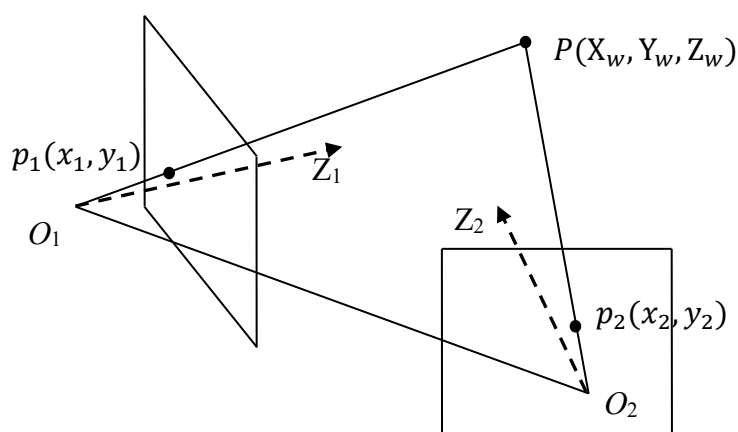


Figure 2.5 The usual model of binocular stereo vision system

2.2 The existing calibration method

Direct linear transformation (DLT) is an algorithm which solves a set of variables from a set of similarity relations ^[32-34]. The direct linear transformation solution is a solution to establish a direct linear relationship between the coordinates of the coordinates (measured coordinates) and the coordinates of the corresponding object point shown as in Figure 2.6.

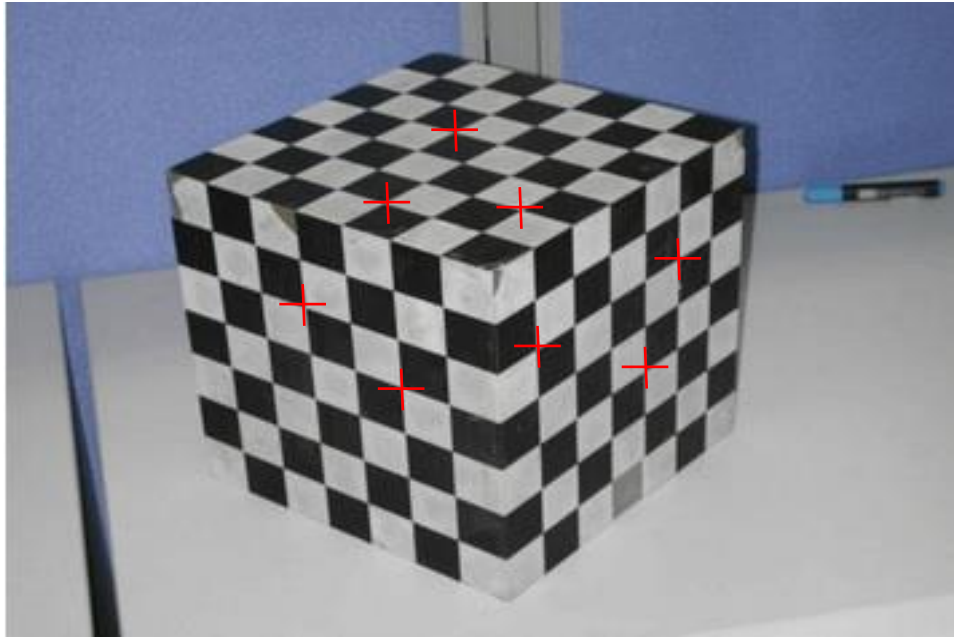


Figure 2.6 Calibration block of DLT method

There are many characteristics on the DLT. First, they don't require the inner elements, without the orientation, which is suitable for a variety of non-measurement camera. Second, we do not need the initial value of the outer position, which is suitable for large angle close-up photogrammetry. Third, object space must be arranged a certain number of control points. Forth, in essence, it is a space rear intersection and front intersection solution.

In principle, the solution to the direct linear change is deduced from the collinearity equation. It is shown as in equation (2.16).

$$\begin{cases} x - x_0 = -f \frac{a_1(X_W - X_C) + b_1(Y_W - Y_C) + c_1(Z_W - Z_C)}{a_3(X_W - X_C) + b_3(Y_W - Y_C) + c_3(Z_W - Z_C)} \\ y - y_0 = -f \frac{a_2(X_W - X_C) + b_2(Y_W - Y_C) + c_2(Z_W - Z_C)}{a_3(X_W - X_C) + b_3(Y_W - Y_C) + c_3(Z_W - Z_C)} \end{cases} \quad (2.16)$$

Where (x, y) is the image point in the image plate coordinate system. (x_0, y_0) is the center point of the image in the image plate coordinate system. (X_w, Y_w, Z_w) is the coordinate of the object in the world coordinate system. (X_c, Y_c, Z_c) is the coordinate of the object in the camera coordinate system. (a_i, b_i, c_i) is the parameter of the rotation matrix.

Thus, the direct linear transformation has the remarkable characteristic that firstly the coordinates of the object space are directly transformed into the object space coordinates, so the initial values of the interior and exterior orientation elements are not needed. Secondly, the direct use of the original observation - image point coordinates, which can be effective system error compensation, especially for CCD camera calibration. Compared with the conventional camera calibration, there are two main aspects: the influence of the electrical error on the calibration; the algorithm requires fast real-time and it is stable and reliable.

Therefore, the CCD camera calibration often use the additional parameters of the direct linear transform method. When we consider the nonlinear distortion (radial optical distortion), the direct linear transformation method in the image space coordinates and the corresponding coordinates of the object are shown as follows:

$$\begin{cases} x - x_0 + \Delta x = -f \frac{a_1(X_w - X_c) + b_1(Y_w - Y_c) + c_1(Z_w - Z_c)}{a_3(X_w - X_c) + b_3(Y_w - Y_c) + c_3(Z_w - Z_c)} \\ y - y_0 + \Delta y = -f \frac{a_2(X_w - X_c) + b_2(Y_w - Y_c) + c_2(Z_w - Z_c)}{a_3(X_w - X_c) + b_3(Y_w - Y_c) + c_3(Z_w - Z_c)} \end{cases} \quad (2.17)$$

Where $(\Delta x, \Delta y)$ is correction number of the Linear error.

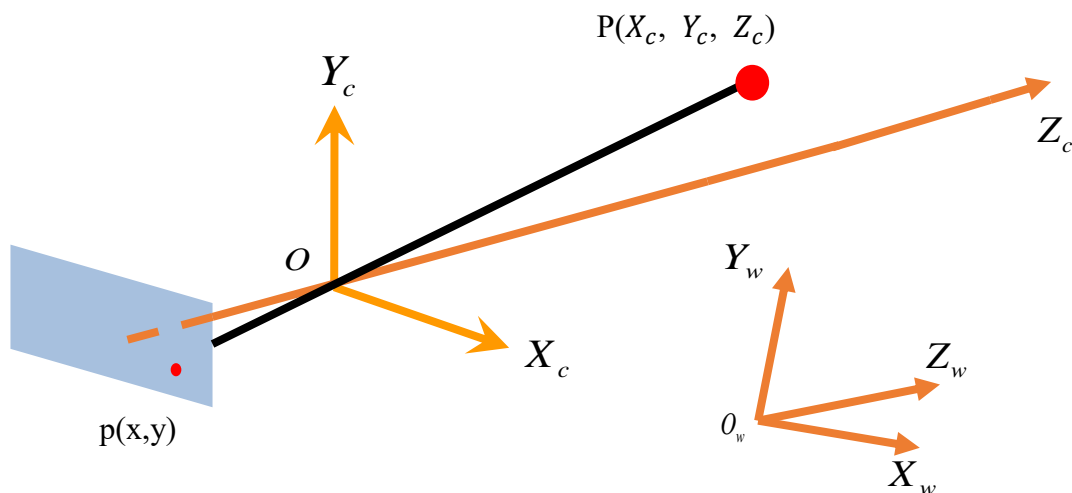


Figure 2.7 Mapping relations between the images coordinate with the world coordinate

2.3 The improved calibration method

Though existing calibration method is effective for close range 3-D measurement, which is difficult for this technique. Those methods usually use a known plate to calibrate camera, but the distance is very long, it is difficult to make the plate. A calibration method to calibrate camera with long distance is proposed [35]. With this method, we calibrate the intrinsic parameters and extrinsic parameters of cameras, and calibrate the position relationship between the centers of pan and tilt head as well as camera center. Then, we can use the parameters of camera and the camera's rotation angle to calculate the sea wave from long distance. The model is shown as in Figure 2.8.

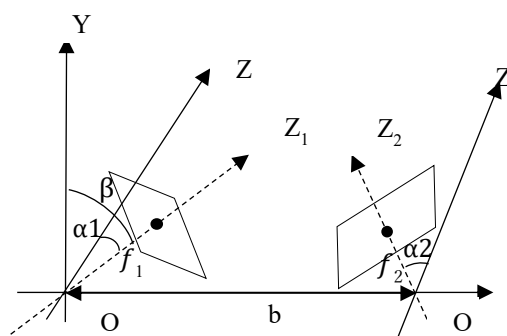


Figure 2.8 Calibration model

To solve the problem of increasing deviation along with distance extension, a sequence of images are taken to calculate the parameters. We can use one known constraint to calculate parameters and obtain an optimal result.

By considering the leveling device of camera and fix the focal length of the camera, we simplify the process of calibration. Only the focal length of camera, rotation angle of Y-axis and baseline are considered in this method.

We use α, β, γ to represent the angle of X-axis, Y-axis, and Z-axis respectively. We suppose that γ equals to 0 and the original point is the center of the image. First, calculating the wave height roughly to test whether this method is feasible. The precise problem is considered later, and we can constrain the assumption while conducting experiment. We can just consider the degree of α . The degree of β doesn't have influence on the parallax, and simplifies the perspective projection matrix as equation (2.18).

$$Z_c \cdot \begin{bmatrix} x \\ y \\ 1 \end{bmatrix} = \begin{bmatrix} f & 0 & 0 & 0 \\ 0 & f & 0 & 0 \\ 0 & 0 & 1 & 0 \end{bmatrix}.$$

$$\begin{bmatrix} \cos\alpha & 0 & -\sin\alpha & \cos\alpha t_x - \sin\alpha t_z \\ 0 & 1 & 0 & t_y \\ \sin\alpha & 0 & \cos\alpha & \sin\alpha t_x + \cos\alpha t_z \\ 0 & 0 & 0 & 1 \end{bmatrix} \cdot \begin{bmatrix} X_w \\ Y_w \\ Z_w \\ 1 \end{bmatrix} \quad (2.18)$$

$$t_x = d \quad (2.19)$$

$$t_z = 0 \quad (2.20)$$

Where, Z_c is the distance from the world point to the parallax. The t_x, t_y, t_z are the elements of the translation vector. The f is the local length of camera. $[x, y, 1]^T$ is the homogeneous coordinate of camera coordinate system, $[X_w, Y_w, Z_w, 1]^T$ is the homogeneous coordinate of the world coordinate system, L is the distance between the center of pan and tilt head and the camera center. α is the angle between the horizontal line of the center of pan and tilt head with the camera center. We can get equation (2.21) from the equation (2.18-20).

$$\begin{cases} f\cos\alpha X_w - f\sin\alpha Z_w + f(\cos\alpha t_x - \sin\alpha t_z) = Z_c X \\ fY_w + ft_y = Z_c Y \\ \sin\alpha X_w + \cos\alpha Z_w + \sin\alpha t_x + \cos\alpha t_z = Z_c \end{cases} \quad (2.21)$$

Simplify the equation (2.21) to equation (2.22)

$$(f - X\tan\alpha)X_w - (f\tan\alpha + X)Z_w + (f - X\tan\alpha)t_x - (f\tan\alpha + X)t_z = 0 \quad (2.22)$$

Set the original point of the left camera as the original point of the world coordinate system. The Z-axis of the world coordinate system is vertical to the base line, the X-axis of the world coordinate system is parallel to the base line, the Y-axis of the world coordinate system is parallel to the Y-axis of the camera coordinate system, we can obtain (2.23) from the equation (2.22).

$$\begin{cases} Z_w = b/(\tan(\alpha_1 + x_1/f) + \tan(\alpha_2 + x_2/f)) \\ X_w = x_1 \times Z_w / (f \times \tan(\alpha_1 + x_1/f)) \\ Y_w = y_1 \times Z_w / f \end{cases} \quad (2.23)$$

Where, b is the length of base line, x_1, x_2 are the camera coordinate and α_1, α_2 are the degree with the Z-axis. Then the length of fence equation is followed.

$$L = \sqrt{(Z_{w1} - Z_{w2})^2 + (X_{w1} - X_{w2})^2 + (Y_{w1} - Y_{w2})^2} \quad (2.24)$$

Where, L is the length of grid in every images. $X_{w1}, X_{w2}, Y_{w1}, Y_{w2}, Z_{w1}, Z_{w2}$ are the X-axis, Y-axis, and Z-axis world coordinate of the two different point in one image.

$$\min = \sum_{i=1}^n (L_i - L) \quad (2.25)$$

Where, the known length of grid and this equation is optimized with the Levenberg-Marquardt method to obtain the unknown parameters. Equation (2.25) has four unknown parameters, b, α_1, α_2 and f .

2.4 Calibration experiments

2.4.1 Sea area in Shikashima

This experiment happened in Shikashima sea area as in Figure 2.9 shown. The distance is 5km. The accuracy of the wave height is affected by many factors. There are two main aspects, one is the measurement accuracy of the photographic system and the other is the correctness of the wave extraction. In order to verify the accuracy of the wave height measurement in the experiment, we use the ship marked with different colors to complete the experiment of measuring for the accuracy of the experimental camera.

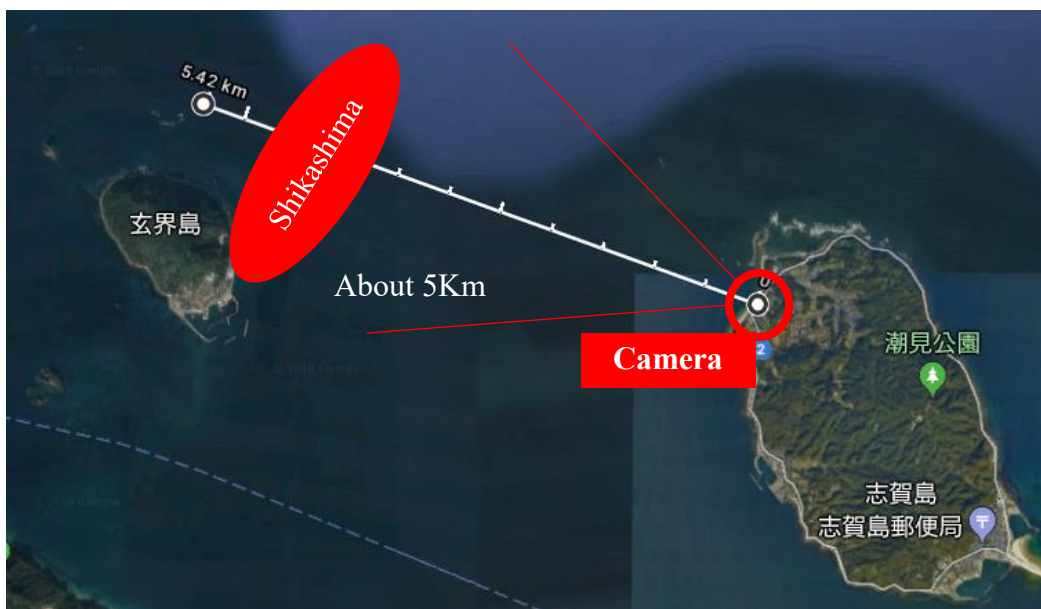


Figure 2.9 The sea area in Shikashima

We put massive tags on the boat to obtain the length of boat from each image and four lengths of known boat can obtain the one set unknown parameters of the camera. We can obtain optimal set of parameter from massive solutions.

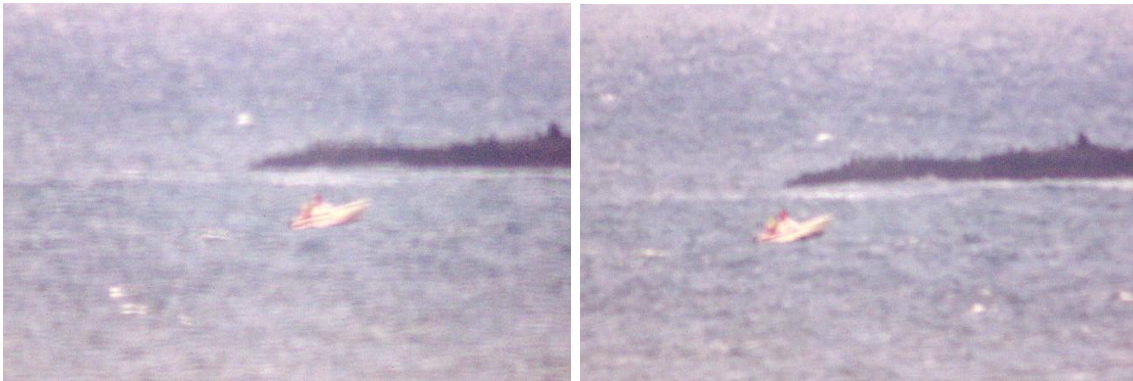
The ship's appearance is shown in Figure 2.10-12, with a length of 5.38 meters and the boat traveling on the sea. We take pictures of the ship in different locations. The camera take pictures at the same time and 10 sets of photos are taken for calibration.



a. Left camera

b. Right camera

Figure 2.10 Image at 12:00



a. Left camera

b. Right camera

Figure 2.11 Images at 12:30



a. Left camera

b. Right camera

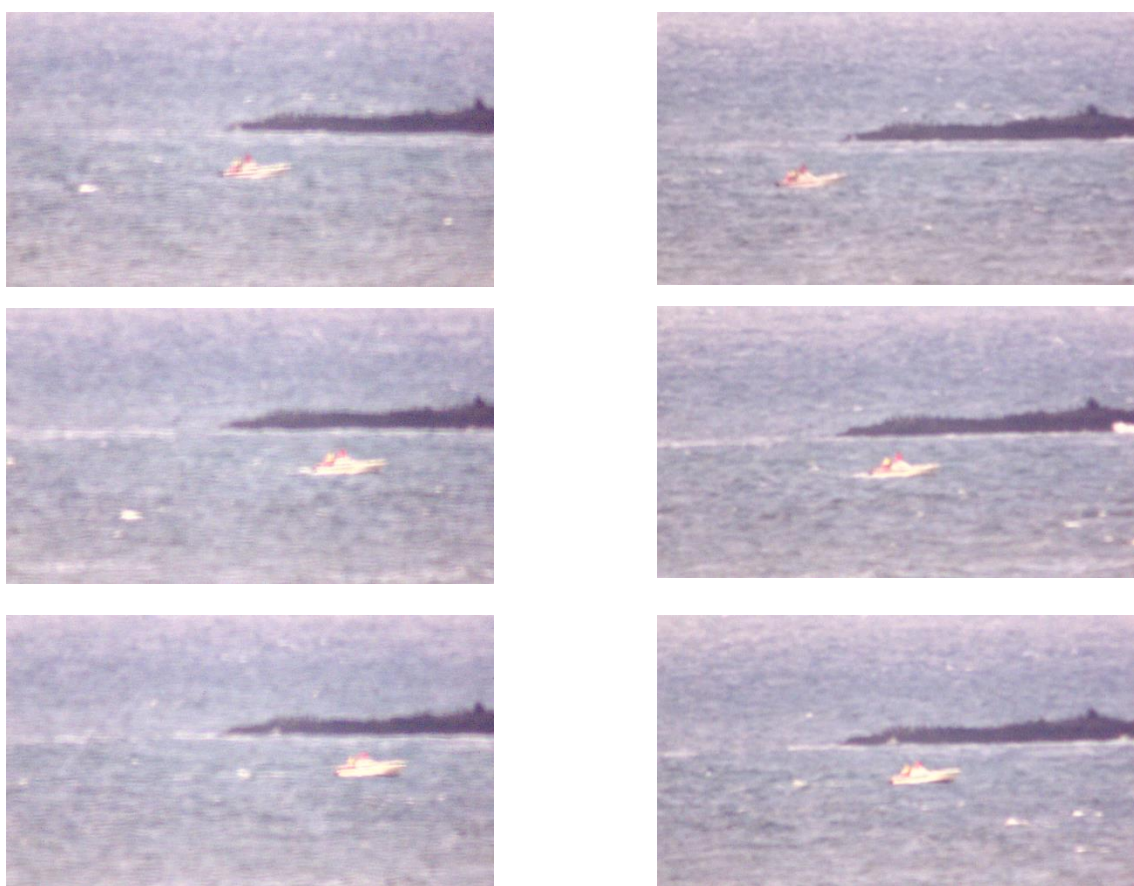
Figure 2.12 Images at 13:15

Finally, followed by the coordinate of the boat, Table 2.2 shows the calibration results.

Table 2.2 The result of calibration in Shikashima

Parameters	Values
$f(\text{pixel})$	244620
$\alpha_1(^{\circ})$	-0.03
$\alpha_z(^{\circ})$	-0.42
$b(\text{m})$	40.91

Then we verify the calibration accuracy by measuring the length of the other photographs of the ship. The verification pictures are shown in Figure 2.13.



a. Left camera

b. Right camera

Figure 2.13 The images of calibration in Shikashima

The results of measuring the length of the ship are summarized in Table 2.3

Table 2.3 The error of calibration in Shikashima

No	Real Values(m)	Calculate Values(m)	Error(%)
1	5.38	5.45	1.3
2	5.38	6.03	12.1
3	5.38	4.96	7.8
4	5.38	5.05	6.1
5	5.38	5.96	10.8

Table 2.3 is the result of distance between every person in the first calibration in which we can see that the max error is 12.1%, the min error is 1.3%, the average error is 7.6%, and the standard deviation is 3.79%.

2.4.2 Sea area in Shigu

The location of the experiment is on the shores of the Shigu as shown in Figure 2.14. The distance is about 5km. The calibration bar is shown in Figure 2.15. The shaft is red and white. The standard length of each small segment (red or white) is 0.5 m and the diameter is 0.65 cm. We choose a hollow plastic bar as a target and select the red and white boundary points on the central axis as feature points.



Figure 2.14 Sea area in Shigu

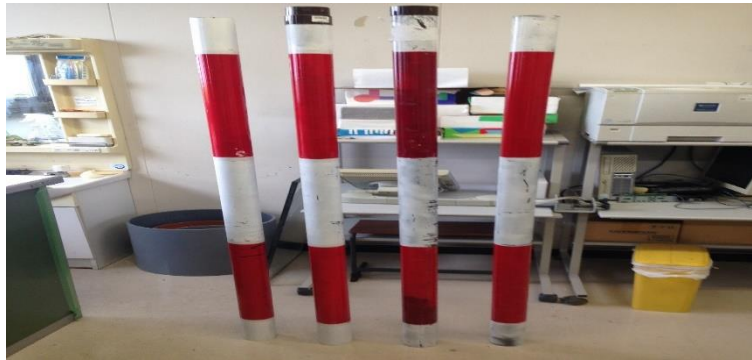


Figure 2.16 Hollow plastic bar for calibration

In this experiment, everyone lifts the pole vertically in the designated place. The total number is four poles. In the first set of photos, the distance between the markers is 9m and 7m from left to right. In the second set of photos, the distances between the markers



a. Left camera (1)



b. Right camera (1)



a. Left camera (2)



b. Right camera (2)



a. Left camera (3)



b. Right camera (3)

Figure 2.15 Calibration image in Shigu

are 11m and 10m from left to right, and the distance between the two markers in the third group is 6m, which is shown in Figure 2.16. Finally, followed by the coordinate of the feature points, Table 2.4 shows the calibration result.

Table 2.4 The result of calibration in Shigu

Parameters	Values
$f(\text{pixel})$	125620
$\alpha_1(^{\circ})$	5
$\alpha_z(^{\circ})$	5.55
$b(\text{m})$	29.95

Then we verify the calibration accuracy by measuring the length of the person. The

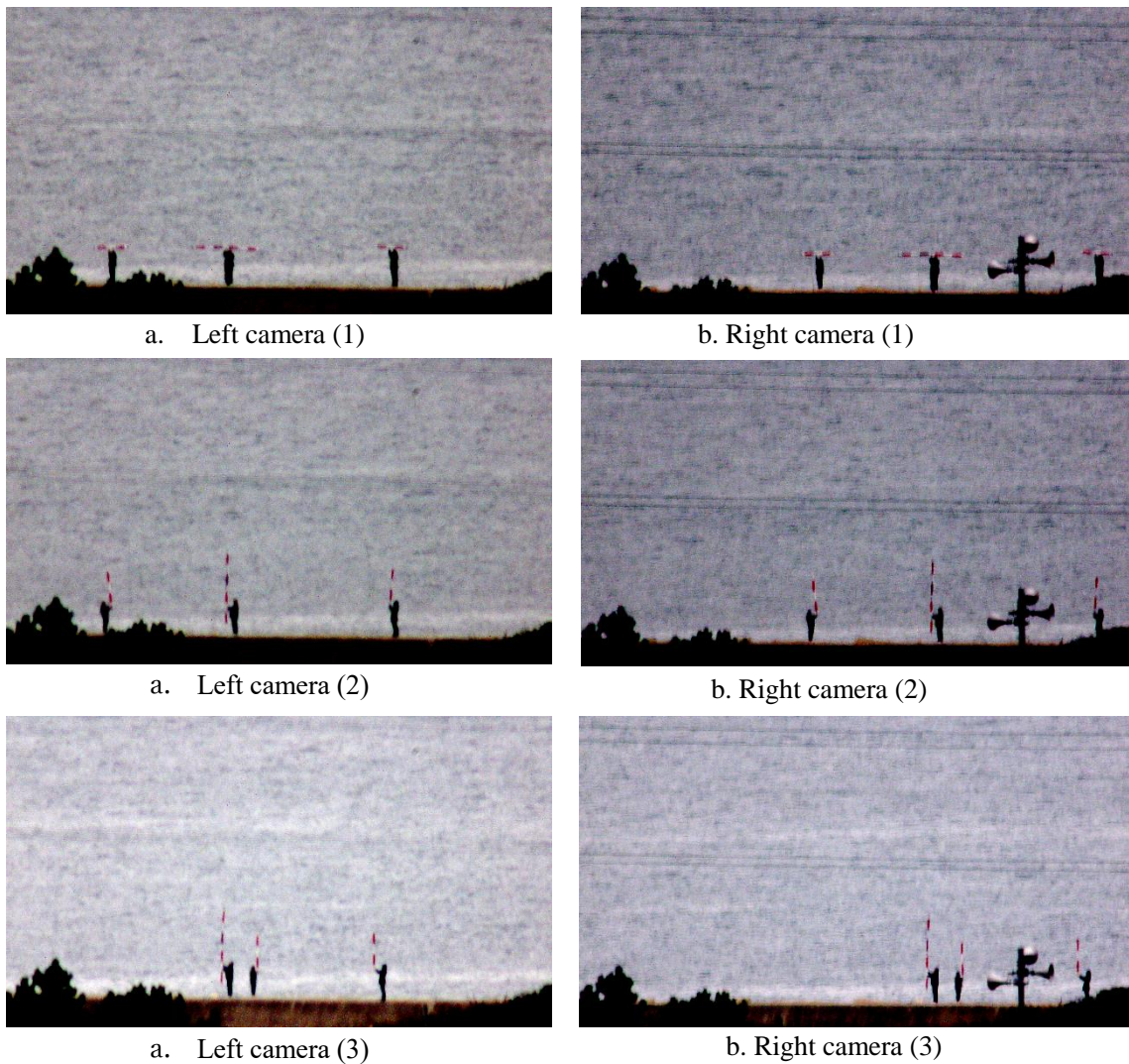


Figure 2.17 Verification images in Shigu

verification images are shown as in Figure 2.17.

The result of measuring the length between the bars is summarized in Table 2.5

Table 2.5 The error of calibration in Shigu

No	Calculated values(m)	Real values(m)	Error(%)
1	11.4	12.03	5.52
2	5.8	6.41	10.5
3	14.3	14.03	1.88
4	22	21.4	2.72
5	8.5	7.66	9.88
6	16.3	15.1	7.36
7	7.7	7.5	2.6

Table 2.5 is the result of distance between every person in the verification images in which we can see that the max error is 10.5%, the min error is 1.78%, the average error is 5.79%, and the standard deviation is 3.3%.

2.4.3 Sea area in Tsuyazaki

As the Figure 2.18 shown, the location of the experiment is on the shores of the Tsuyazaki. The distance is about 10km.



Figure 2.18 Sea area in Tsuyazaki

In this experiment, we firstly take a pair of images which include the red lighthouse and the iron shelves as shown in Figure 2.19.

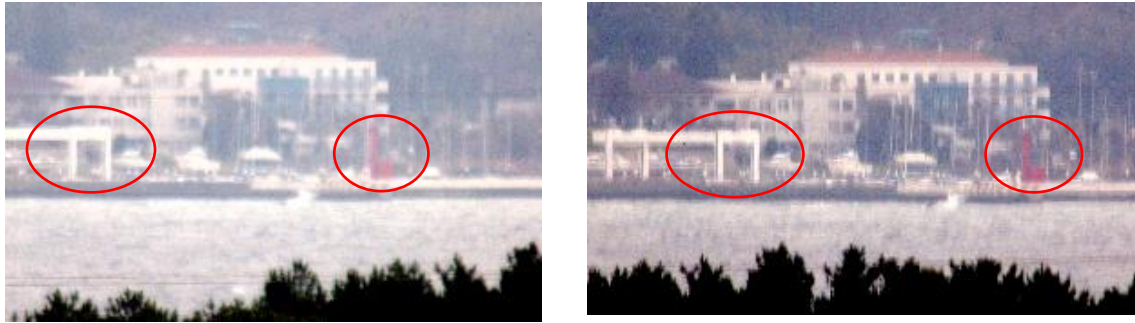


Figure 2.19 Calibration Images in Tsuyazaki

Finally, followed by the coordinate of red lighthouse and iron shelves, Table 2.6 shows the calibration result.

Table 2.6 The result of calibration in Tsuyazaki

Parameters	Values
$f(\text{pixel})$	244620
$\alpha_1(^{\circ})$	20.42
$\alpha_z(^{\circ})$	20.22
$b(\text{m})$	29.95

Then we verify the calibration accuracy by measuring the length of the other building. We extract five known lengths on the calibration object.

Table 2.7 The error of calibration in Tsuyazaki

No	Calculated values(m)	Real values(m)	Error(%)
1	0.91	0.80	13.8
2	0.95	0.80	18.6
3	1.24	1.00	24
4	2.17	2.30	5.7
5	6.14	5.50	11.57

Table 2.7 is the result of the red lighthouse and iron shelves in the third calibration in which we can see that the max error is 24%, the min error is 5.7%, the average error is 14.36%, and the variance error is 3.7%.

2.5 Summary

Through the basic binocular stereo vision calibration described further, this section proposes an improved calibration method. Finally, the algorithm is verified by three experiments. In the three experiments, the error is the largest 12.8%, the smallest error is 1.06%, the standard deviation of error is 6.79. Through the experimental verification, the calibration method can meet the tsunami measurement and plays a key role in the future tsunami prediction.

Chapter 3 Image processing

Image processing is to deal with the image of the waves. This is also a very important part of this experiment. This part of the work is mainly divided into pre-processing, the extraction of the waves and the matching of the corresponding points of the waves. Due to the distance, it brings a lot of problems to the processing of waves

This chapter, we firstly explain the image pre-processing, which is mainly to reduce image noise to make the image as clear as possible. This step is very important, and even affects the effect of wave extraction. Next, the sea waves are extracted. The last step is to match the sea waves.

3.1 Difficult of sea wave extraction

In order to study the state of the waves, whether it is the wave height, the speed or the direction of the wave, the first step is to extract the waves from the picture. When a person observes a photograph with his eyes, the difference between the waves and other objects can be distinguished mainly through the difference of the color of the waves and the surrounding scenery. In general, the part of the waves in the photograph will be brighter than the other part. Therefore, the difference of color concentration has become the first method to extract waves.

Image segmentation is an important method of image analysis and processing. Its purpose is to separate the target area and the background area from the image. There are many ways to divide an image. The simplest and most effective method is the threshold method. Threshold processing is a method of selecting one or more appropriate grayscale values to segment the image. How to select the appropriate threshold is the key to the threshold processing.

3.1.1 Single threshold method

Otsu method was proposed by Otsu in 1979 and it is a classic algorithm, also known as discriminant analysis ^[36]. For an image, t is recorded as the segmentation threshold of the foreground and the background, the number of the former points of interest accounts for the proportion of the image is ω_0 , and the average gray is μ_0 ; the number of background points in the image is ω_1 , and the average gray is μ_1 . The total average gray level of the image is μ .

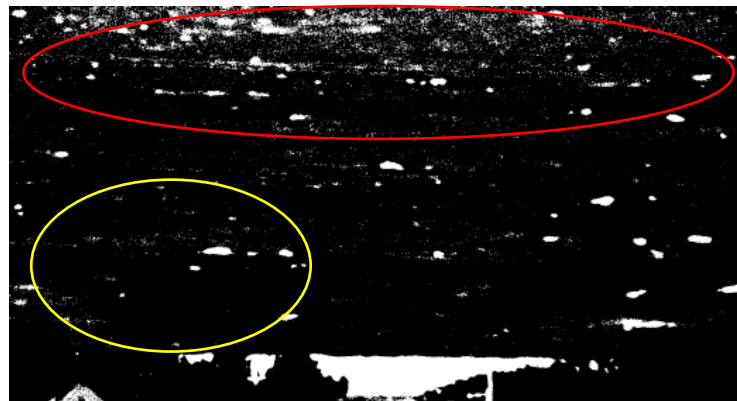
We traverse from the minimum gray value to the maximum gray value when t makes the value maximum

$$\delta^2(t) = \omega_0(t)(\mu_0(t) - \mu)^2 + \omega_1(t)(\mu_1(t) - \mu)^2 \quad (3.1)$$

$\delta^2(t)$ is the optimal threshold for segmentation. The Otsu method can be said to be an adaptively-calculated single threshold and that is a simple and efficient method to convert a grayscale image into a binary image. The result of extraction sea wave is shown as in Figure 3.1.



a. Original image



b. The Otsu threshold

Figure 3.1 Extract image with Otsu threshold

Figure 3.1 shows the processing results based on the Otsu method. From the results, the single-threshold methods do not give very good results for wave images. The sea waves can't be extracted on the top of the image. Due to the uneven brightness from the top to the bottom in the image, it is difficult to extract them with a single threshold. Therefore, we try to use the local threshold method to extract the sea waves.

3.1.2 Adaptive threshold method

The local adaptive threshold is determined by the pixel value in the local block. The advantage is that the threshold of each pixel is not fixed and it is determined by the distribution of neighboring pixels around it. The threshold of the image area with higher brightness is generally higher, and the threshold of the image area with lower brightness is correspondingly smaller. Local image regions of different brightness will be corresponding to local thresholds. Frequently-used local adaptive threshold is the

Gaussian weighted sum of the local neighborhood block.

When it comes to adaptive threshold method, one of the typical algorithms is the Gaussian gray value method. This method take the Gaussian of the grayscale values of all the pixels in the image as a threshold. The threshold can be calculated from the equation in (3.2)

$$H_{(i,j)} = \frac{1}{2\pi\delta^2} e^{-\frac{(i-k-1)^2+(j-k-1)^2}{2\sigma^2}} \quad (3.2)$$

Where, (i, j) is the coordinate of the image. δ is the variance. $H_{(i,j)}$ is the Gaussian convolution kernel at the point (i, j) . $(2k+1) \times (2k+1)$ is the Dimension of Gaussian kernel matrix.

Suppose that $k = 1$, $\delta = 1$. so we use this equation to calculate the Gaussian convolution kernel around the (i, j) and normalize them to get the results as the Table 3.1 shown.

Table 3.1 Gaussian convolution kernel

0.0751	01238	0.0751
0.1238	0.2042	0.1238
0.0751	0.1238	0.0751

(i,j)

When we want to obtain the threshold of the point (i, j) , we calculate the weighted Gaussian mean of the $(2k+1) \times (2k+1)$ size block around the point. The equation shows as in the equation (3.3).

$$t_{(i,j)} = 0.0751 \times (f_{(1,1)} + f_{(1,3)} + f_{(3,1)} + f_{(3,3)}) + 0.1238 \times (f_{(1,2)} + f_{(2,1)} + f_{(2,3)} + f_{(3,2)}) + 0.2042 \times f_{(2,2)} \quad (3.3)$$

Where, $t_{(i,j)}$ is the threshold in point (i, j) and $f_{(i,j)}$ is the gray value of the corresponding position of the Gaussian kernel.

This method is necessary to calculate a Gaussian convolution kernel for a local block when calculating the threshold of each point, which requires a large amount of time. As the Gaussian kernel increased, the amount of computer will increase greatly.



a. Original image



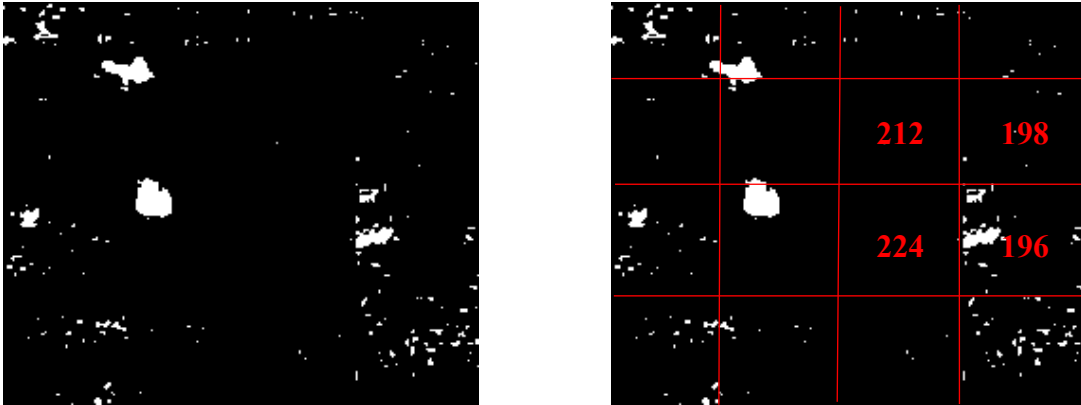
b. The adaptive threshold

Figure 3.2 Extract image with adaptive threshold

3.1.3 Block threshold method

Block threshold method is to divide the image into many small blocks as the Figure 3.3 shown. This makes sure that the brightness is almost same in every small block. However, it is inevitable that a sea wave may be divided into multiple blocks, which brings to be discontinuous between the blocks. Due to the different threshold in each block, a sea wave will be separated between blocks.

In this method, we still use the Otsu algorithm to calculate the threshold of each small blocks. Then extract the sea wave with the threshold of block.



(a) Extracted image

(b) Blocks threshold

Figure 3.3 The sawteeth in image

According to the Figure 3.3 shown, there are many sawteeth when using the block threshold to extract the sea waves directly.

Look at the above pictures. Obviously, a part of the sea wave was cut off. That is because this sea wave was divided into different blocks, and different blocks have different thresholds. The threshold of left block is big (224), thus, the left part of sea wave was cut off. The threshold of right block is small (196), so the right part of sea wave was remained. To solve this problem, we proposed the optimum threshold method to extract the sea waves.

3.2 Sea wave extraction

As for the long distance sea wave extraction, we proposed an algorithm based on the optimum block threshold method. First, this method divided image into many small blocks to solve the problem of the uneven brightness. According to different blocks, the thresholds are varied. Then, associate with the thresholds of the surrounding four blocks to extract the complete sea waves. This method can extract sea waves from long distance images. Our purpose is to extract the sea wave 20-200 in one image.

3.2.1 Proposed optimum block threshold method

The algorithm of the optimum block threshold method presented in this paper is divided into two steps. First, use the Otsu algorithm to find the threshold for each small block. Then, calculate the threshold of the pixel corresponding to the ratio of the distance from this point to the surrounding four blocks.

First, divide the picture into many small blocks. In these experiments, the small blocks are 32×18 as the Figure 3.4 shown. For example, we want to obtain the threshold of this block and we use $T_{(m,n)}$ to represent the threshold in block (m, n) .

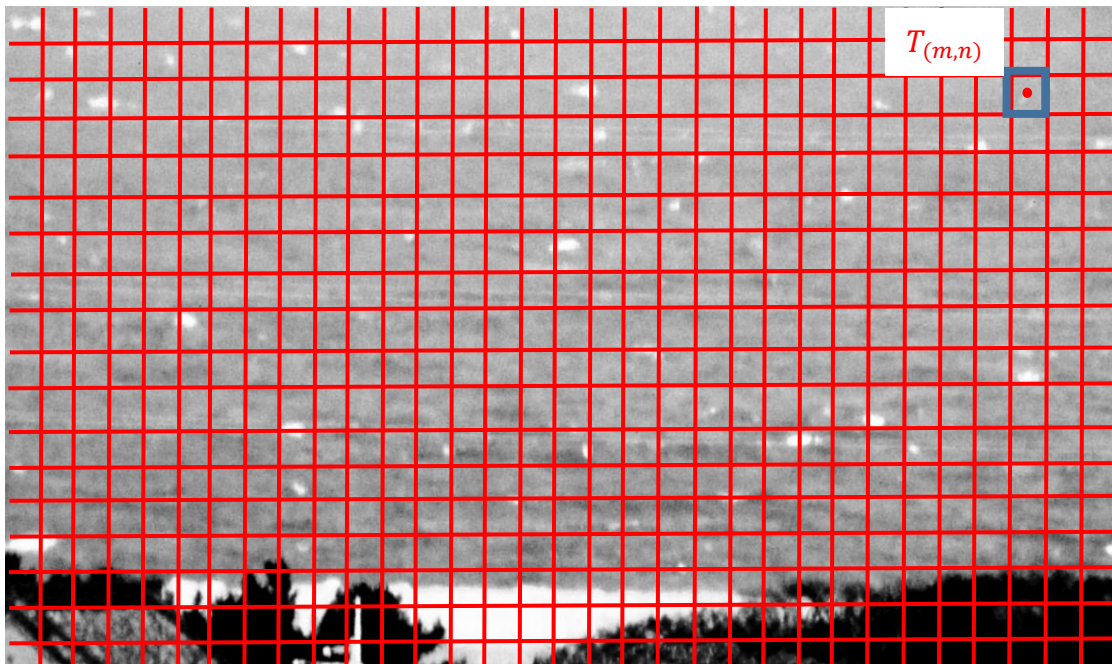


Figure 3.4 Divide blocks

Divide all gray values into three segments $C_0(t)\{0\sim t\}$ 、 $C_1(t)\{t + 1\sim 255\}$. The number of the gray value i is n_i , then the all number of pixel are N , the probability of each gray value is p_i the average gray value of the image is μ .

$$\omega_0(t) = \sum_{i=0}^t p_i \quad (3.4)$$

$$\omega_1(t) = \sum_{i=t+1}^{255} p_i \quad (3.5)$$

$$\mu_0(t) = \frac{\sum_{i=0}^t ip_i}{\omega_0(t)} \quad (3.6)$$

$$\mu_1(t) = \frac{\sum_{i=t+1}^{255} ip_i}{\omega_1(t)} \quad (3.7)$$

$$\mu = \sum_{i=0}^{255} ip_i \quad (3.8)$$

Where, $\omega_0(t)$ and $\omega_1(t)$ are the probabilities of the two classes separated by a threshold t , $\mu_0(t)$ and $\mu_1(t)$ are the mean of class $C_0(t)$ and $C_1(t)$.

Thus, the formula (3.1) of the maximum inter-class variance is $\delta^2(t)$.

Use the formula (3.1) to calculate the variance $\delta^2(t)$. Through testing t from one to 255, t is the threshold of the block when the variance value is the maximum.

Suppose we want to obtain the threshold of this point (i, j) as the Figure 3.5 shown. To solve this problem, first, in our method, take this point as a center to make a block size square. The threshold of this point is determined by the thresholds of the surrounding four blocks. Use this equation (3.9) to obtain the threshold of this point (i, j) .

$$t_{(i,j)} = q * \left((1 - p) * T_{m,n} + p * T_{m+1,n} \right) + (1 - q) * \left((1 - p) * T_{m,n+1} + p * T_{m+1,n+1} \right) \quad (3.9)$$

Where, p is the ratio of left- (i, j) width per block width. q is the ratio of bottom- (i, j) width per block width. $t_{(i,j)}$ is the threshold of the pixel (i, j) . $T_{(m,n)}$ is the threshold in block (m, n) .

When expressed by a mathematical formula, the grayscale value range of the original image is $[I_{min}, I_{max}]$. I_{min} refers to the minimum gray value, and the threshold of the

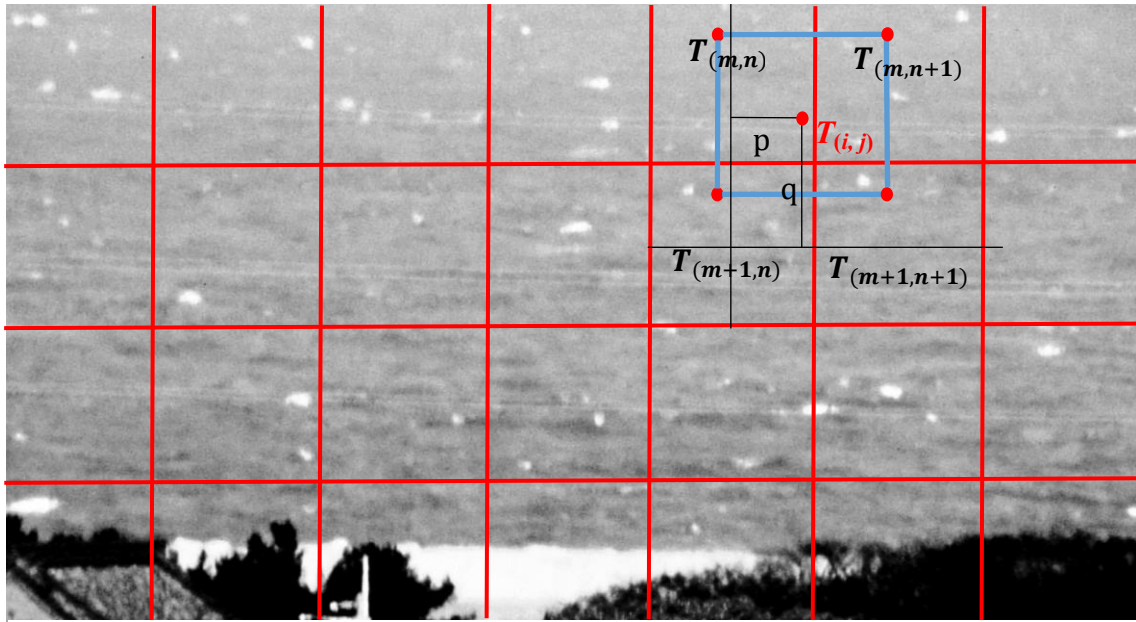


Figure 3.5 Optimum block threshold method

pixel is $t_{(i,j)}$, then the grayscale value of the pixel after processing is expressed by Equation (3.10).

$$O(i,j) = \begin{cases} 255 & t_{(i,j)} \leq f(i,j) \leq I_{max} \\ 0 & otherwise \end{cases} \quad (3.10)$$

Here I_{max} refers to the maximum gray value, $f(i,j)$ refers to the input pixel, and $O(i,j)$ refers to the output pixel.

Finally, we use this method to extract the sea waves as the Figure 3.6 shown.



(a) Block threshold



(b) Optimum block threshold

Figure 3.6 Comparison of the results

We made a comparison between the two pictures. In the left image, a part of sea wave was cut off and sawteeth could be seen. In the right image, we can extract the complete sea wave using by the optimum block threshold. Based on the result, this method can solve the problem of sawteeth.

3.2.2 Extract sea wave

The extraction sea wave has five steps. Step 1, use the mean filter to reduce the noise. Step 2, divide small blocks and calculate the threshold in each block. Step 3, extract the waves. Step 4, use erosion and dilation to reduce the salt and pepper noise. Step 5, label the waves. The flow chart shows is shown as the Figure 3.7.

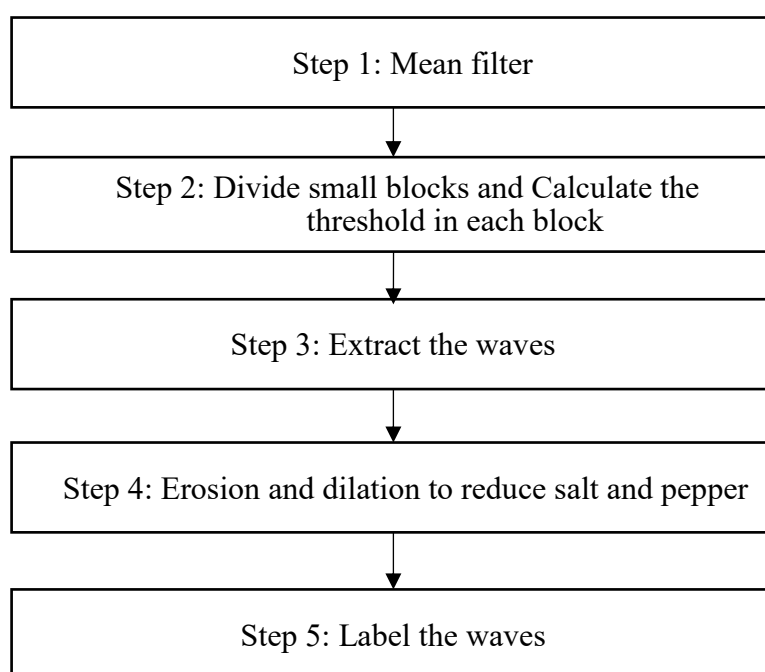


Figure 3.7 The flow chart of extraction sea waves

After the extracted wave area being obtained, each wave need to be separated from the subsequent waves. Marking connected areas in a binary image is an important image processing method. The purpose of the label is to assign the same tag value to the interconnected parts, and different interconnected areas are distinguished by different tag values. Through this step, it is possible to separate the sea waves of the image, and it also facilitates the extraction of features (area, circumference, etc.) of the sea wave.

The steps of the label algorithm are as follows:

(1) Traverse an image. If a pixel P that has not been tagged is found, a new tag value is assigned to the pixel P.

- (2) The same tag value is assigned to the pixel connected to the pixel P.
- (3) Repeat the above steps until all the pixels of interconnected pixel P are labeled with the same tag value.
- (4) Return to step 1. If a new unlabeled pixel is found, label it to the new label and repeat steps 1~3.
- (5) Traverse all the sea waves until the search for the entire image has been completed.



a. The original image



b. Extracted sea wave



c. Selected sea wave

Figure 3.8 Select sea wave

3.3 Sea wave matching

3.3.1 The problem of exiting methods

Template matching is a technique for finding an area of an image that matches a template image. It is widely used in manufacturing as a part of quality control, a way of navigating mobile robots or to detect the edges of an image. Use the equation (3.11) to calculate the cross-correlation constraint [37].

Where, (i, j) is the top left point of the matching block in the target image, $I_{(m, n)}$, $R_{(m, n)}$ is the gray value. \bar{I} , \bar{R} is the average gray value in the block $M \times N$.

$$C_{(i,j)} = \frac{\sum_{m=1}^M \sum_{n=1}^N (I_{(i+m,j+n)} - \bar{I}) \cdot (R_{(m,n)} - \bar{R})}{\sqrt{[\sum_{m=1}^M \sum_{n=1}^N (I_{(i+m,j+n)} - \bar{I})^2] \cdot [\sum_{m=1}^M \sum_{n=1}^N (R_{(m,n)} - \bar{R})^2]}} \quad (3.11)$$

When matching the template image, we need to move one pixel at a time on the patch. At each location, we can calculate the cross-correlation value followed by this equation. After moving all the location, we will get all the c value. The larger the value is, the more similar the template is. When the value $C_{(i,j)}$ is the maximum, the point (i, j) is the top left point of the matching block in target image.

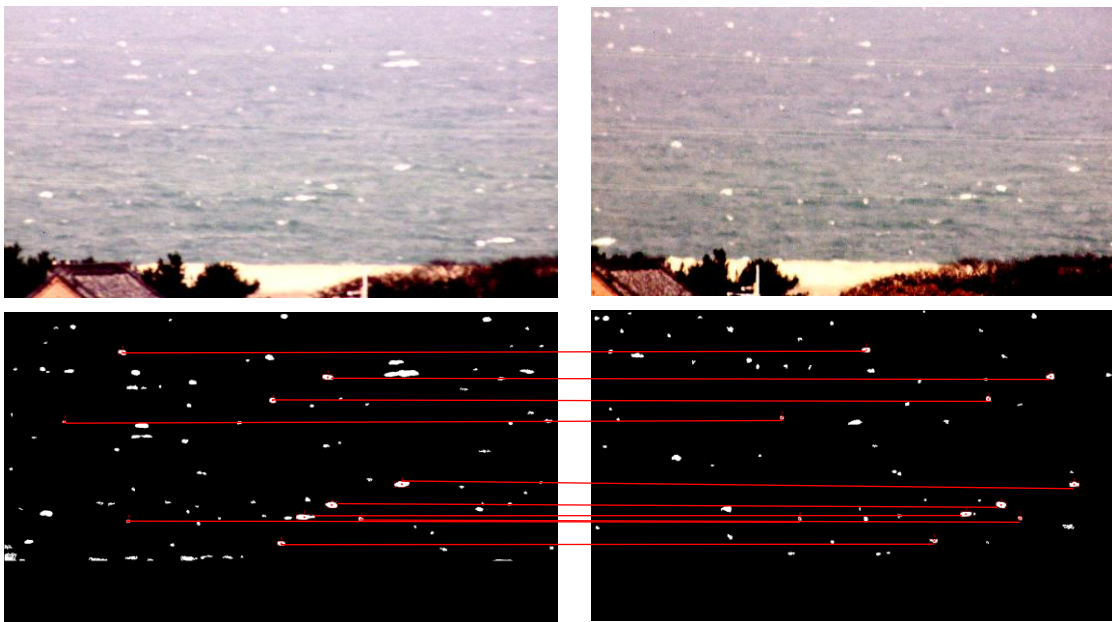


Figure 3.9 Template Matching

The number of matching sea waves is ten. Nevertheless, using this method can match the sea wave and the running time is about 10 seconds. The time is too long to meet the requirement that process the image in real time.

The other typical feature-based matching algorithm is Scale Invariant Feature Transform (SIFT). It is an algorithm in computer vision to detect and describe local features in images^[38]. However, there is no matching method that can be applied to all situations. Under normal circumstances, some image matching methods may be suitable for certain situations. All methods are subject to some adjustments according to different circumstances. The matching result is shown as the Figure 3.10.

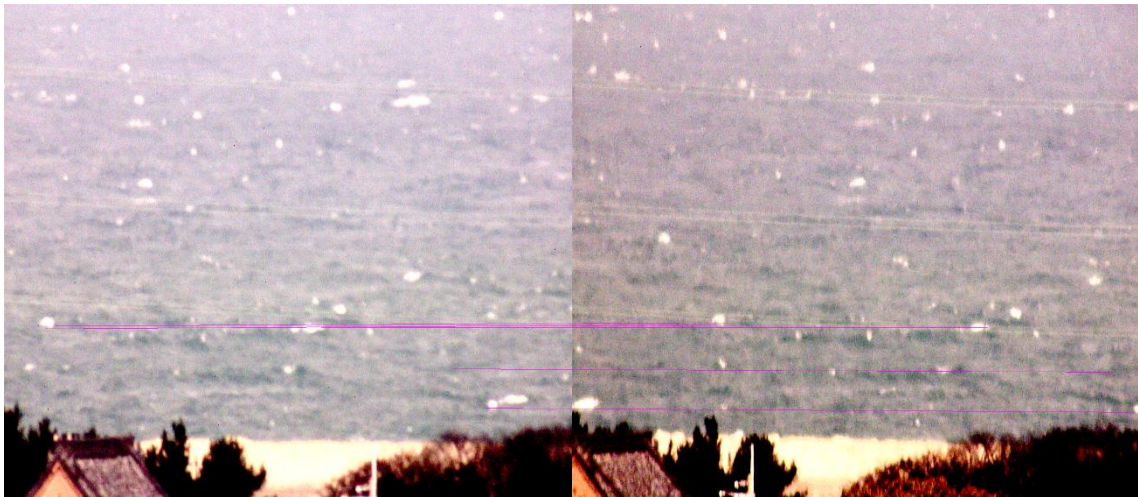


Figure 3.10 SIFT matching

The number of matching sea waves is five. The reason is the distance more than 5 km. There are no particular features of sea waves that are obvious enough to distinguish the small size sea waves from each other. It is difficult to obtain key point. The running time is about 25 seconds. It also doesn't meet the requirement.

To solve this problem, we proposed our approach: Feature-matrix method for matching the sea wave. The first, define a feature-matrix to contain all the sea waves. The second, compared with the feature vector directly, it is so fast. The third, it is high accuracy. The matching method based on the wave feature matrix is a matching method that improves template matching by combining feature-based matching. The purpose is to match the sea waves 10-100 in a pair of images.

3.3.2 Matching based feature matrix

In the last section, we extracted the ocean waves from the original image, and the result

shown in the binary image was shown in Figure 3.9, which clearly shows the waves. Template settings can be done in binary images.

Before setting the template, we need to label all the waves in the extracted image. After labeling the sea wave, we can get the location and size of the waves. Notice that the waves are irregular. So we label the location of wave with the center of gravity. For the waves in the left Figure, the template settings are shown in Figure 3.11. This template is a rectangle. Pay attention to the center of gravity (x_0, y_0) of the waves in the image. For each sea wave, we define a feature vector V , which is consisted by area A , perimeter P , curvature C and line segments $L_1 \sim L_4$ as shown in Figure 3.12. From the equation (3.12), we can obtain L_i .

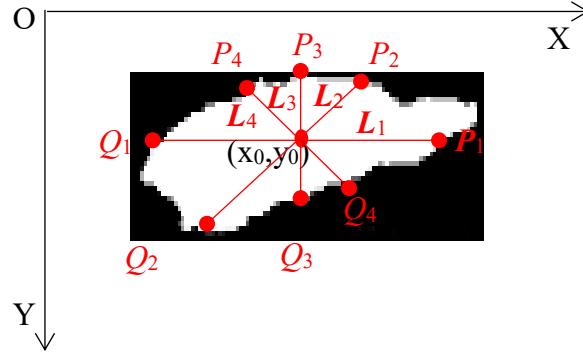


Figure 3.11 The feature of sea wave

$$L_i = \sqrt{(P_{ix} - Q_{ix})^2 + (P_{iy} - Q_{iy})^2} \quad (3.12)$$

Where L_i is the length from P_i to Q_i . Then, the feature vector V shows formula (3.13):

$$V = \{A, P, C, y_0, L_1, L_2, L_3, L_4\} \quad (3.13)$$

Next, we can obtain the feature matrix of left images VL and right image VR .

$$VL = [V_1, V_2, \dots, V_i, \dots, V_N]$$

$$VR = [V_1, V_2, \dots, V_i, \dots, V_M]$$

Then, we can calculate many parameters from formula (3.14) and (3.15).

$$AS_{ij} = \left| \frac{A_i - A_j}{A_i} \right| \quad PS_{ij} = \left| \frac{P_i - P_j}{P_i} \right| \quad CS_{ij} = \left| \frac{C_i - C_j}{C_i} \right| \quad (3.14)$$

$$YS_{ij} = |y_i - y_j| \quad (3.15)$$

$$Dist_{ij} = \sqrt{\sum(VL_i - VR_j)^2} \quad (3.16)$$

Where, AS_{ij} is the similarity of the area; PS_{ij} is the similarity of the perimeter; CS_{ij} is the similarity of the curvature; YS_{ij} is the similarity of the position; $Dist_{ij}$ is the similarity of the feature vector. VL_i is the left feature matrix, VR_j is the right feature matrix. For a pair of images with N sea waves in the left image and M sea waves in the right image.

3.3.2 Sea waves matching

In this method, we could define four restrictions and one criteria, namely area size constraint AS, curvature constraint CS, perimeter constraint PS, the center of gravity and similarity criteria Transform constraint Dist.

The process of matching is as follows:

1. Obtain the feature matrix of left image and right image
2. Calculate the area constraint between AS_i and vectors R, the larger AS indicates bigger difference of area, while the same sea wave did not change too much in area in two images. Ascend all the AS and keep those vectors with AS in the top $n_1\%$ to gather a new-matrix B1 from R;
3. Calculate the perimeter constraint between PS_i and vectors in B1. Ascend all the PS and keep those vectors with PP in the top $n_1\%$ to gather a new-matrix B2;
4. Calculate the curvature constraint between CS_i and vectors in B2. Ascend all the CS and keep those vectors with CS in the top $n_3\%$ to gather a new-matrix B3.
5. Calculate the coordinate constraint between YS_i and vectors in B3. Ascend all the YP and keep those vectors with YP in the top $n_4\%$.
6. Calculate the similarity of vectors by Euclidean distance (Dist), shown as equation (3.16). When the value of Dist is the smallest, the two vectors are considered to be the most similar.
7. Repeat the step from 2 to 6 until the sea waves of left image are finished.
8. After the 2D matching, the 3-D verification is performed to improve accuracy.

3.4 Experiments and results

In this section, we will introduce some experiments and the results of the extraction.

We have already obtained a number of long-wave images in long distance. Here we choose two experiments. As mentioned above, we used the two lenses developed by FUJIFILM to take image at the same time as much as possible. At long distance, we used two same telephoto lens and the resolution of the image is 1920 * 1080.

Experiment I

Experiment I happened in Shingu sea area. The distance is about 5km. The camera system is located on the A building. In this experiment, two telephoto lens cameras were set to take photos at the same sea. During the shooting, both cameras remain stationary and the parameters are consistent for a series of images in one day

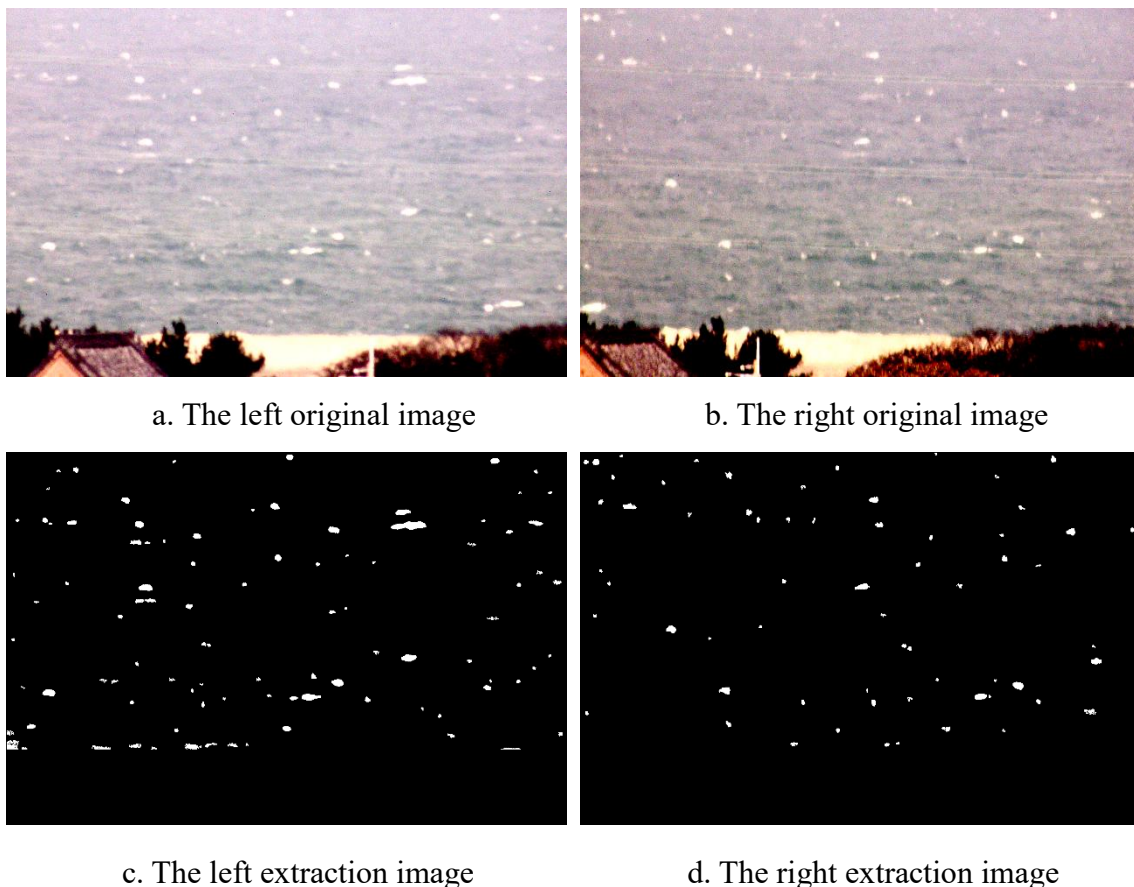


Figure 3.12 Extraction result (1)

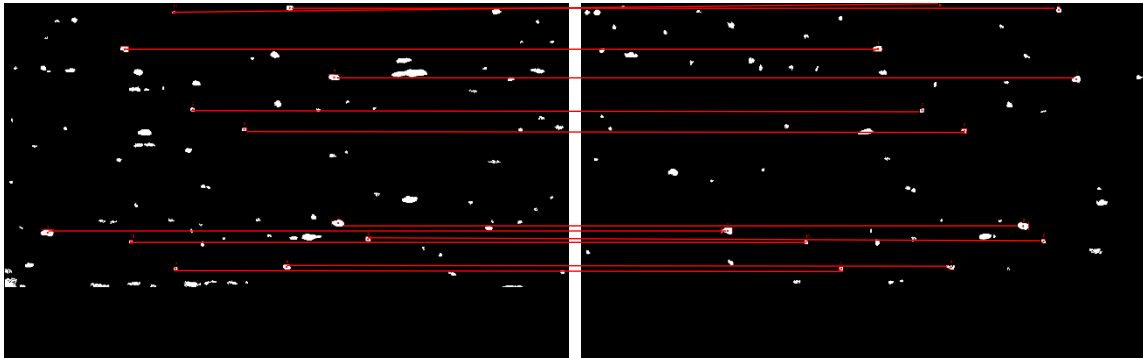


Figure 3.13 Matching result (1)

Table 3.2 Result of matching image (1)

	Extraction	Matching	Matching Percent	Correct Percent
Left image	99	12	12%	100
Right image	63		19%	

From the table 3.2, the number of matching sea wave is 12. The correct matching is also 100%.

Experiment II

Experiment II happened in Tsuyazaki sea area. The distance is about 10km. The camera system is located on the A building. In this experiment, two telephoto lens cameras were set to take photos at the same sea. During the shooting, both cameras remain stationary and the parameters are consistent for a series of images in one day



Figure 3.14 Extraction and matching result (2)

Table 3.3 Result of matching image (2)

	Extraction	Matching	Matching Percent	Correct Percent
Left image	35	5	14%	100
Right image	20		25%	

From the table 3.3, the number of matching sea wave is five. The correct matching is also 100%.

3.5 Summary

In this chapter, we introduce the complexity of long distance sea wave extraction and some of the problems of matching sea wave. In order to solve these problems, the method of sea wave extraction used by optimum block threshold is proposed. The extraction results show that this method has gotten good results in long-range wave extraction. This method can extract the sea waves 20-200 in one picture. In addition, it eliminates the sawteeth between the sea waves.

Except for sea wave extraction, we introduce some image matching methods and discuss the problems in long distance matching. Since it is difficult to obtain the feature points directly from the image, we try to extract the waves and get the corresponding points. The proposed method of sea-wave matching is based on feature matrices. Experiments show that this method can correctly match most of the waves.

Chapter 4 Experimental results and consideration

In this chapter, we first present our measurement system and then introduce our experimental environment. Next, we propose to use the average of a large number of waves as the height of the sea level. Finally, we describe the process and results of the experiment in detail. Through the final measurement results and the tidal change data provided by the government department, the results of our experiments prove that our proposed method can effectively measure the sea level height change.

4.1 Proposed sea wave height measurement system

Considering the feasibility and the expenses to be cost, we finally choose to use the stereo vision method to realize a measurement system of sea wave height [39]. This project was sponsored by Ministry of Education, Culture, Sports , Science and Technology of Japan (NO.S1311050). In this system, two cameras will be set on shore and by taking two images of the target scene, sea wave heights can be calculated. Figure 4.1 is the primary conceive of this system. It mainly contains two cameras on land photographing the sea zone.

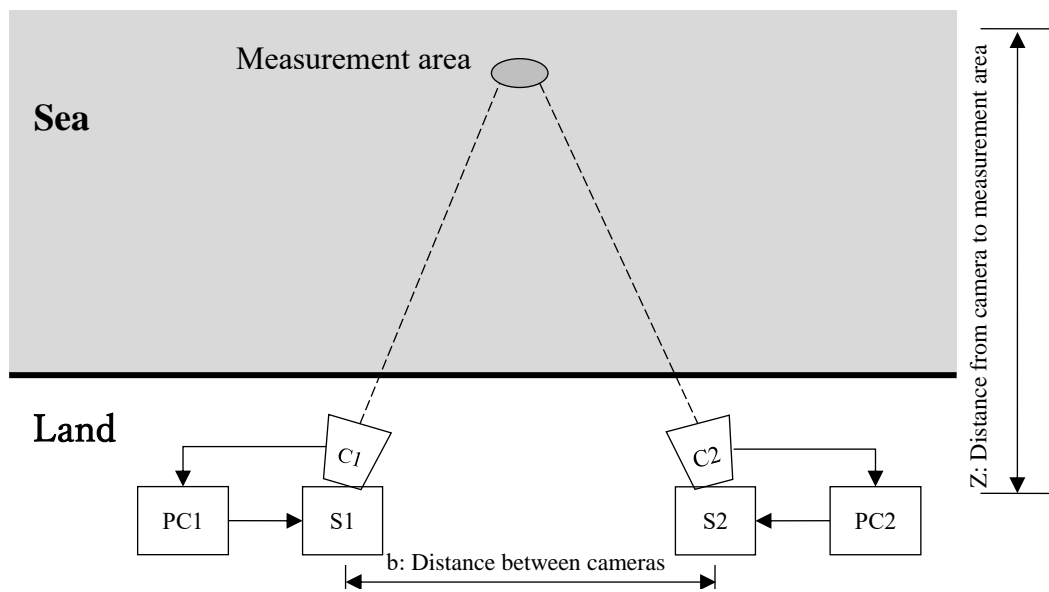


Figure 4.1 Measurement System

Figure 4.1 shows the measurement system. In this system, C1 and C2 show two cameras, S1 and S2 show two rotation stages, PC1 and PC2 show two personal computers. We controlled pan and tilt stages to take the two images in the same sea area. An angle sensor was installed in the pan and tilt stage, which was used to measure the angle of the cameras when they are rotating. That way, we could know the relative angles of the cameras that are moving to monitor the larger sea area. The computer controlled the camera and the remote controller. When we were taking images, the image data automatically transmitted to the computer, and we could use software to change the parameters of the camera through the remote controller.

Figure 4.2 was the flow chart of the proposed wave height measurement method. First, set two cameras and then controlled these two cameras to take photos of sea waves;

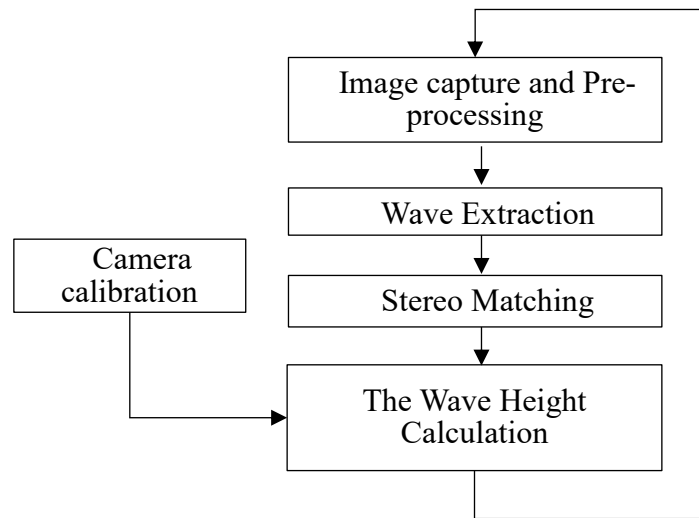


Figure 4.2 Flow chart of sea-level height measurement

through the pre-processing, we could get the clear images. Obtain 3-D information of sea waves to reconstruct sea wave; Calculate and estimate the arrival of sea waves and finally achieve the target of forecast.

Among these steps, image processing played a key role. It contained image pre-processing, sea wave extraction and sea wave matching. Image pre-processing usually aimed at obtaining more clear images despite the weather influence. Removed some non sea area such as building. This paper contained of the latter condition as well as sea wave extraction and sea wave matching.

Previous research done use a 3-D camera developed by FUJIFILM to take photos of sea waves at the same time, extract sea waves from the original images, obtain corresponding points which are the top and the bottom of sea wave in the case of long distance, finally, calculate the height of sea wave.

4.2 Experimental conditions

In this section, we will introduce some experiments conditions. We have already obtained a number of long-distance images of sea waves. Here we choose two experimental places. As mentioned above, we used the two lenses developed by FUJIFILM to take images simultaneously. The ordinary camera cannot meet the requirements of long distance. In the case of long distance, we use two same telephoto lens and the image size is 1920 * 1080.

In order to build a long-distance 3-D images measurement system, the hardware device included the two cameras with telephoto lens, computers, angle sensors, a remote camera controller and pan and tilt stages. Figure 4.3 shows the measurement system. In this system, there were two cameras, rotation stages, personal computers. We controlled pan and tilt stages to take the two images in the same sea area. An angle sensor was installed in the pan and tilt stage, which was used to measure the angle of the cameras when they were rotating. That way, we could know the relative angles of the cameras that were moving to monitor the larger sea area. The computer controlled the camera and the remote controller. When we were taking images, the image data automatically transmitted to the computer, and we could use software to change the parameters of the camera through the remote controller.

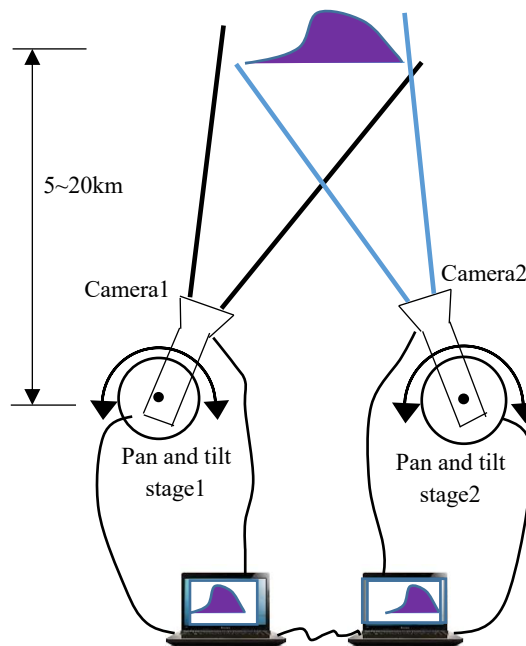


Figure 4.3 Measurement system

4.3 Measurement of the height of sea level

The height of the sea level mainly fluctuates from the tidal water, so we constructed a model [40-41]. The red wavy line represented the fluctuation of the tide. The black curve represented the fluctuation of the actual sea level. The difference between the two waveforms represented the impact of other conditions on the sea level. We used a large number of points to simulate the height of the actual sea level through the average of many points in our experiment, which meant that we extracted many points at each moment, and then calculated the average of all points as the height of the sea level at the current time.

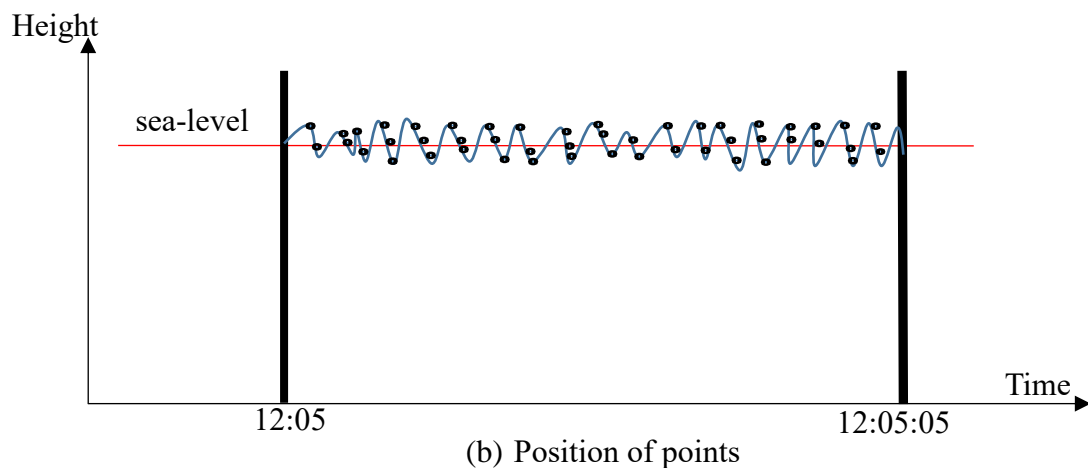
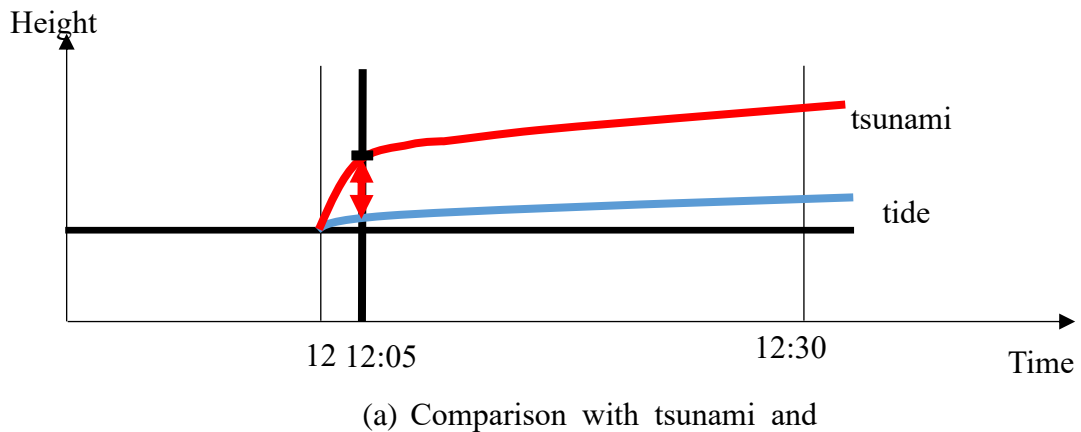


Figure 4.4 The change of sea-level height

From the Figure 4.4(a), if the tsunami happens at 12 o'clock, the sea level suddenly raises higher than the tide. The red line is the change of the sea-level height. As the tsunami moves toward the shore, the sea level is raising.

For example, when we monitor that the height of the sea level is abnormal at 12:05, we start warning if the height of the sea level is higher 20cm than the tide. How can we measure the sea-level height at this time? We can amplify this instant time as the Figure 4.4(b) shown. In this instant time, the sea surface is fluctuating.

From the Figure 4.4(b), we can see that there are many small waves on the sea surface. We can extract many points on the sea surface. As the picture shown, some points are located on the top of sea wave, some points are located on the bottom, and some points are located on the middle. We are based on the principle that the points are normal distribution. So we use this equation to calculate the average of the height of all the points as the sea-level height.

$$h = \frac{\sum_{i=1}^N Y_i}{N} \quad (4.1)$$

Where, Y_i is the height value of one point. h is the height of the sea-level. N is the number of all matching sea wave.

In our system, set the original point of the world coordinates as the original point of the left camera. Our system is located on the A building. The height of the sea wave is relative to the height of the left camera. The tidal height on the Meteorological Agency is near the sea level. Thus, before we compared the data, the height of the measurement had been subtracted from a certain height of a camera (59.65m).

4.4 Experiments and results

In this experiment, we want to monitor the sea near by Singu as shown in Figure 4.5. We did this experiment on May 9 2017. Two telephoto lens cameras were set to take photos of the same sea area, and the two cameras were conducted on the building A of Fukuodai. The data from the cameras were saved automatically.

One second saved 30 images and the data was saved continuously for 5 seconds. In other words, every time captures 150 images. In this experiment, we chose 11 hours' images in one day from AM 7:00 to PM 18:00.



Figure 4.5 Experiment places

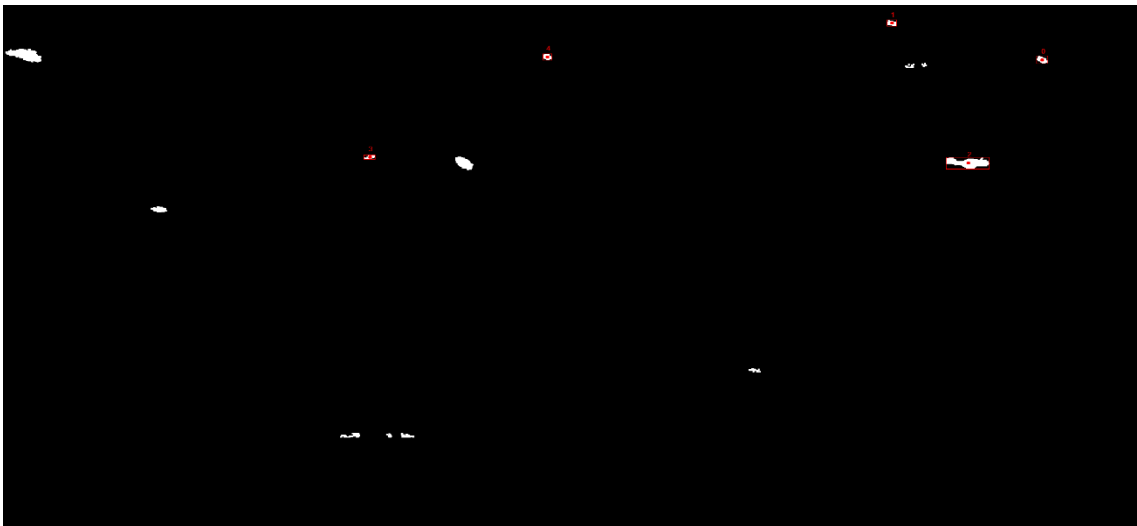


(a) Original image of left

(b) Original image of right



(c) Matching point of left



(d) Matching point of right

Figure 4.6 Images in Shigu at 6:48

In Figure 4.6, (a) is the original image of left, (b) is the original image of right, (c) is the image after extracting the sea wave used by our methods from image (a). In addition, (d) is the image after extracting the sea wave from image (b). In image (c), there are many sea waves that are encircled by a rectangle box, which means that the ocean sea waves have been matched with the image (d) in the pair of images. The matched sea waves have serial numbers, which are list by the acquaintance and the size of sea wave. The serial numbers start from zero. The red point in the rectangle box expresses that it is the center of gravity in sea wave, which is the matching point in pair of images. In image (c), we extract 20 sea waves from image (a). In image (d), we extract 14 sea waves from image (b). The number of matching points is five. The matching success rate is 25% for the left mapping and 35.7% for the right mapping.

In every time, we take 150 pairs of images, so the Figure 4.6 is just one of the pairs of images. We extract and match sea wave from 150 pairs of image and the result is shown in Figure 4.7.

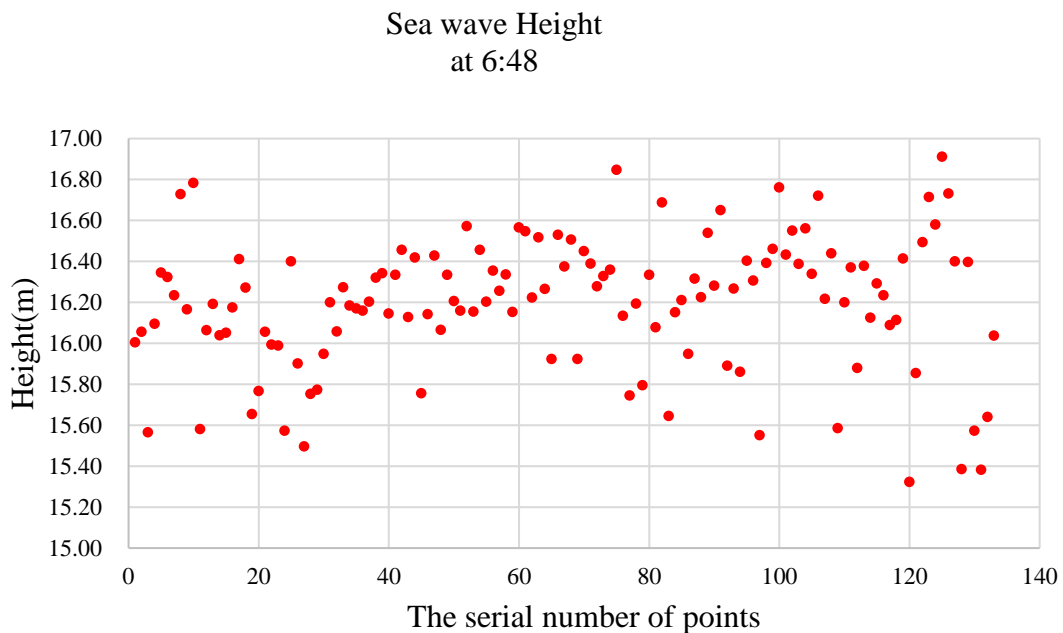


Figure 4.7 Calculation of the height of sea level at 6:48

We successfully match the 133 corresponding points from 150 pairs of images. Through calculation, we could know that the average of sea level height is 16.2(m). The max value is 16.91(m). The min value is 15.32(m). The standard deviation is 0.32.



(a) Original image of left



(b) Original image of right



(c) Matching point of left



(d) Matching point of right

Figure 4.8 Image in Shigu at 7:49

In Figure 4.8, (a) is the original image of left, (b) is the original image of right, (c) is the image after extracting the sea wave used by our methods from image (a). In addition, (d) is the image after extracting the sea wave from image (b). In image (c), there are many sea waves that are encircled by a rectangle box, which means that the ocean sea waves have been matched with the image (d) in the pair of images. The matched sea waves have serial numbers, which are list by the acquaintance and the size of sea wave. The serial numbers start from zero. The red point in the rectangle box expresses that it is the center of gravity in sea wave, which is the matching point in pair of images. In image (c), we extract 38 sea waves from image (a). In image (d), we extract 19 sea waves from image (b). The number of matching points is six. The matching success rate is 15.8% for the left mapping and 31.6% for the right mapping.

In every time, we take 150 pairs of images, so the Figure 4.8 is just one of the pairs of images. We extract and match sea wave from 150 pairs of image, then calculate the height of sea level, Figure 4.9 show the result.

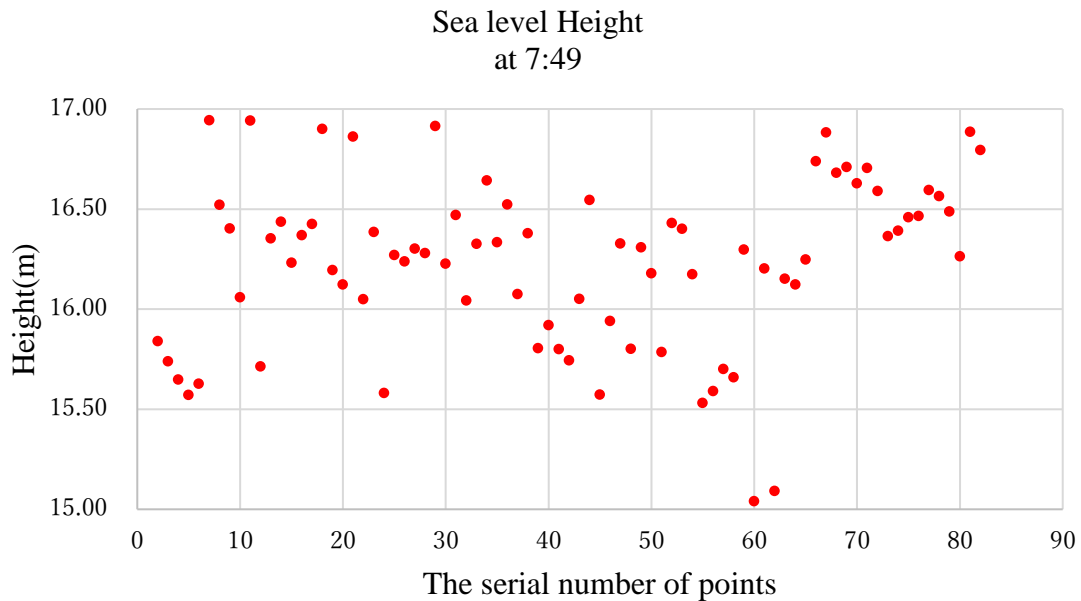
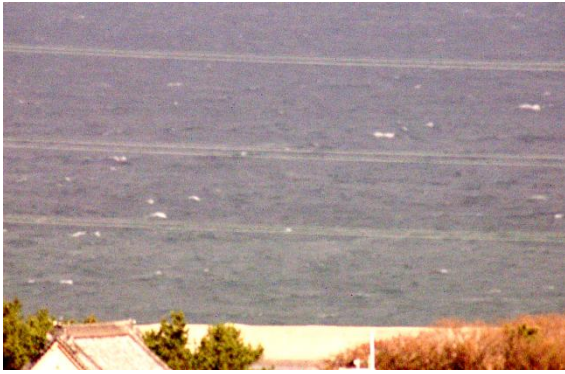


Figure 4.9 Calculation of the height of sea level at 7:49

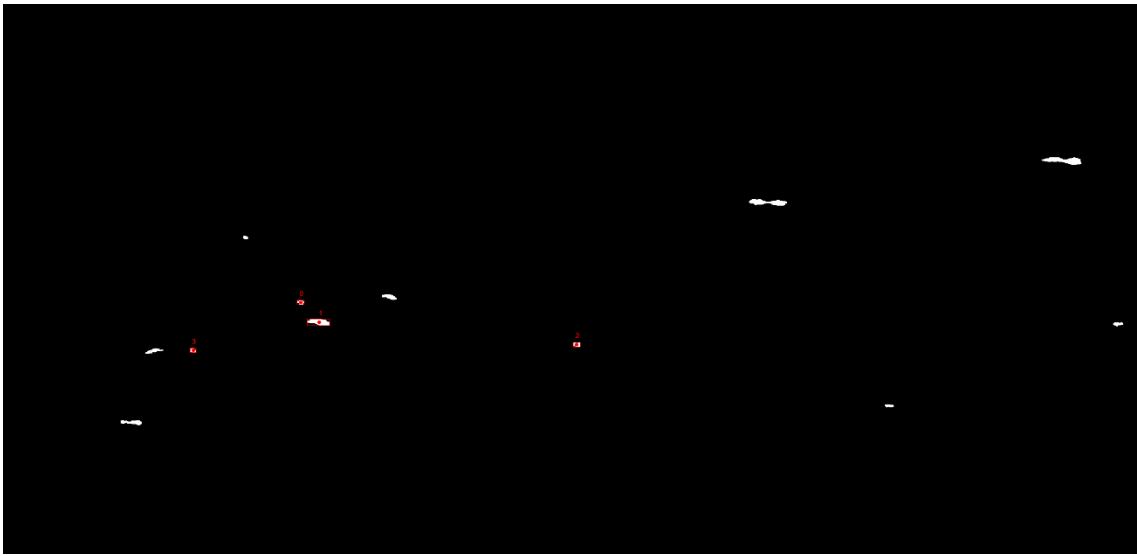
We successfully match the 81 corresponding points from 150 pairs of images. Through calculation, we could know that the average of sea level height is 16.22(m). The max value is 16.94(m). The min value is 15.04(m). The standard deviation is 0.42.



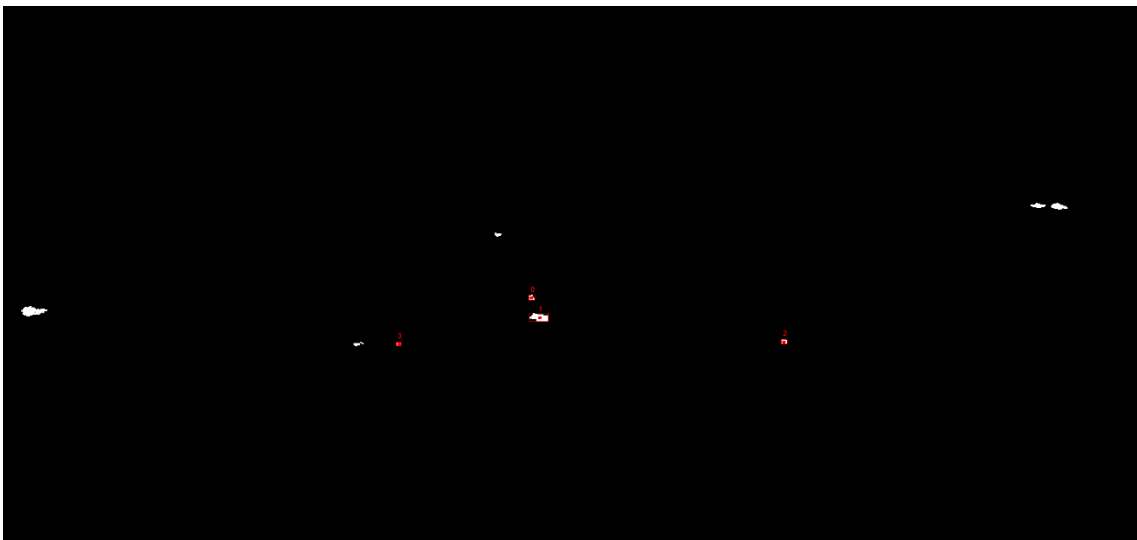
(a) Original image of left



(b) Original image of right



(c) Matching point of left



(d) Matching point of right

Figure 4.10 Image in Singu at 8:50

In Figure 4.10, (a) is the original image of left, (b) is the original image of right, (c) is the image after extracting the sea wave used by our methods from image (a). In addition, (d) is the image after extracting the sea wave from image (b). In image (c), there are many sea waves that are encircled by a rectangle box, which means that the ocean sea waves have been matched with the image (d) in the pair of images. The matched sea waves have serial numbers, which are list by the acquaintance and the size of sea wave. The serial numbers start from zero. The red point in the rectangle box expresses that it is the center of gravity in sea wave, which is the matching point in pair of images. In image (c), we extract 12 sea waves from image (a). In image (d), we extract nine sea waves from image (b). The number of matching points is four. The matching success rate is 33.3% for the left mapping and 44.4% for the right mapping.

In every time, we take 150 pairs of images, so the Figure 4.10 is just one of pairs of images. We extract and match sea wave from 150 pairs of image, then calculate the height of sea level, the result is shown in Figure 4.11

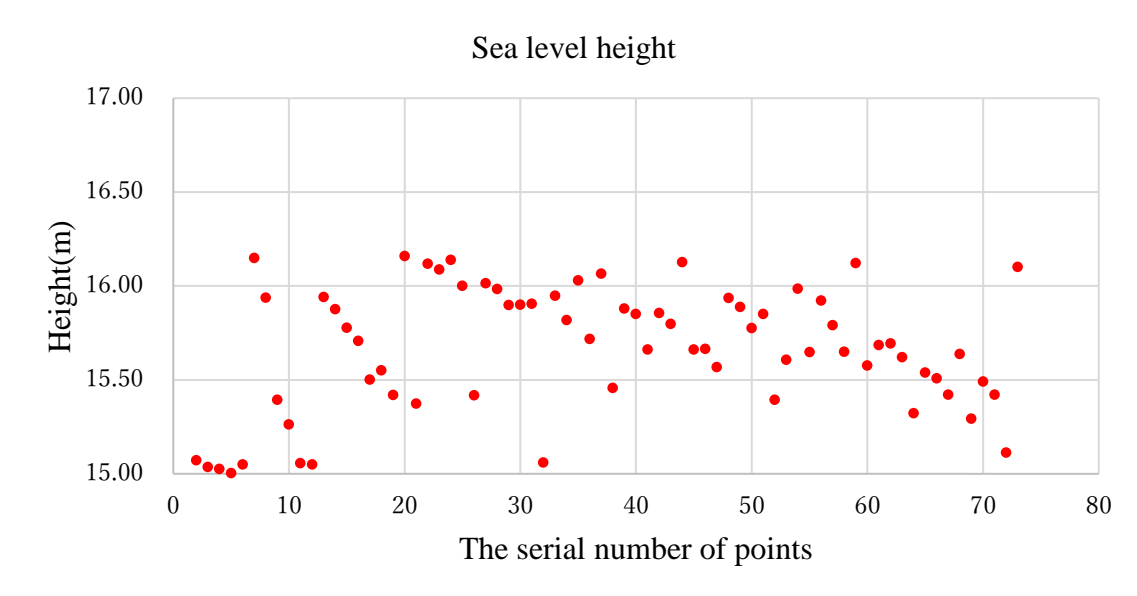


Figure 4.11 Calculation of the height of sea level at 8:50

We successfully match the 72 corresponding points from 150 pairs of images. Through calculation, we could know that the average of sea level height is 15.67(m). The max value is 16.16(m). The min value is 15(m). The standard deviation is 0.33.



(a)Original image of left



(b) Original image of right



(c) Matching point of left



(d) Matching point of right

Figure 4.12 Image in Singu at 9:51

In Figure 4.12, (a) is the original image of left, (b) is the original image of right, and (c) is the image after extracting the sea wave used by our methods from image (a). In addition, (d) is the image after extracting the sea wave from image (b). In image (c), there are many sea waves that are encircled by a rectangle box, which means that the ocean sea waves have been matched with the image (d) in the pair of images. The matched sea waves have serial numbers, which are list by the acquaintance and the size of sea wave. The serial numbers start from zero. The red point in the rectangle box expresses that it is the center of gravity in sea wave, which is the matching point in pair of images. In image (c), we extract 37 sea waves from image (a). In image (d), we extract 25 sea waves from image (b). The number of matching points is nine. The matching success rate is 24.3% for the left mapping and 36% for the right mapping.

In every time, we take 150 pairs of images, so the Figure 4.12 is just one of pairs of images. We extract and match sea wave from 150 pairs of image, then calculate the height of sea level, the result is shown in Figure 4.13

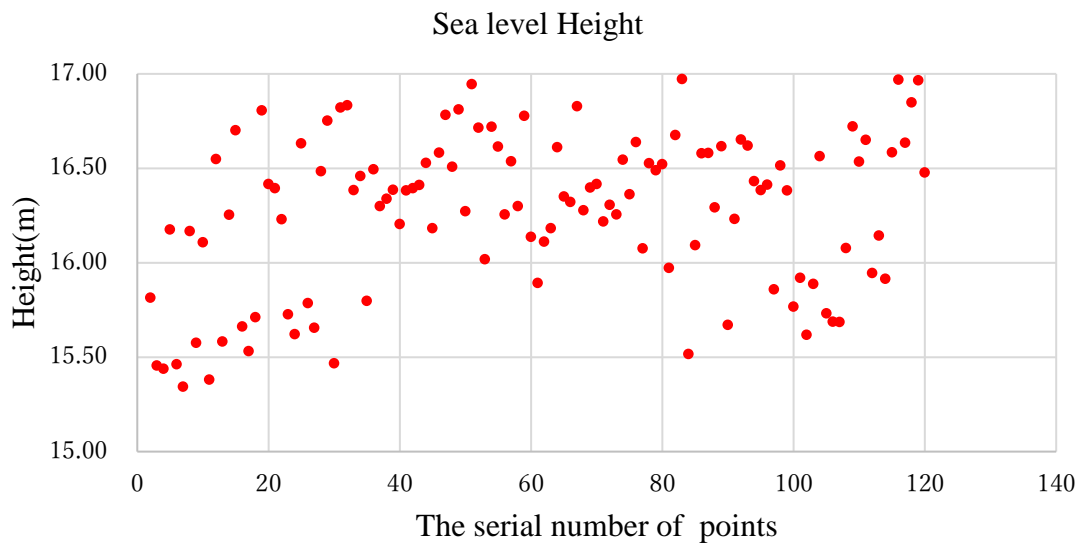


Figure 4.13 Calculation of the height of sea level at 9:51

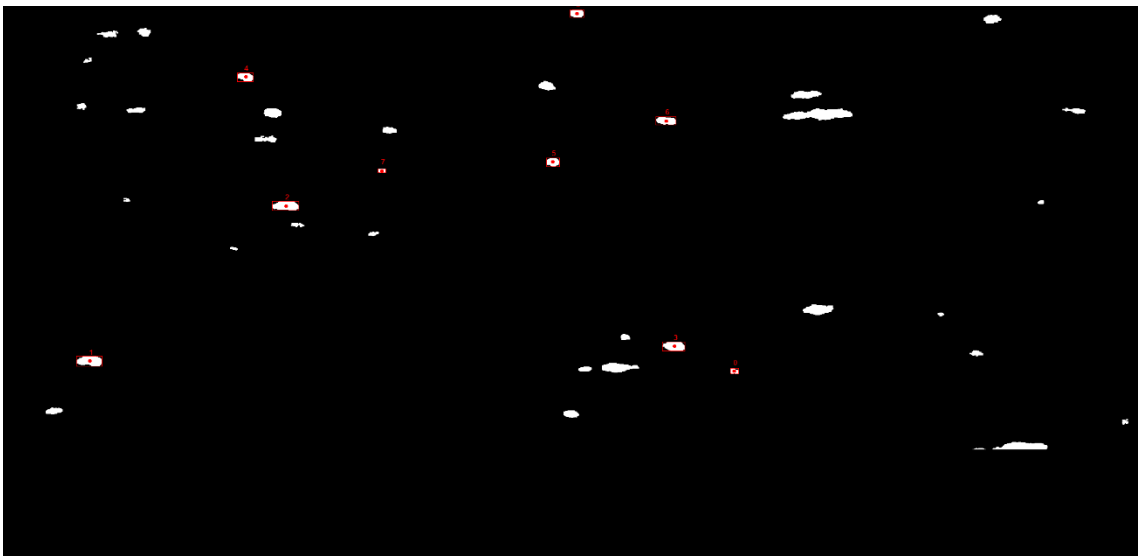
We successfully match the 119 corresponding point from 150 pairs of images. Through calculation, we could know that the average of sea level height is 16.27(m). The max value is 16.97(m). The min value is 15.34(m). The standard deviation is 0.41.



(a)Original image of left



(b) Original image of right



(c) Matching point of left



(d) Matching point of right

Figure 4.14 Image in Singu at 10:52

In Figure 4.14, (a) is the original image of left, (b) is the original image of right, (c) is the image after extracting the sea wave used by our methods from image (a). In addition, (d) is the image after extracting the sea wave from image (b). In image (c), there are many sea waves that are encircled by a rectangle box, which means that the ocean sea waves have been matched with the image (d) in the pair of images. The matched sea waves have serial numbers, which are list by the acquaintance and the size of sea wave. The serial numbers start from zero. The red point in the rectangle box expresses that it is the center of gravity in sea wave, which is the matching point in pair of images. In image (c), we extract 38 sea waves from image (a). In image (d), we extract 40 sea waves from image (b). The number of matching points is nine. The matching success rate is 23.6% for the left mapping and 22.5% for the right mapping.

In every time, we take 150 pairs of images, so the Figure 4.14 is just one of pairs of images. We extract and match sea wave from 150 pairs of image, then calculate the height of sea level, the result is shown in Figure 4.15

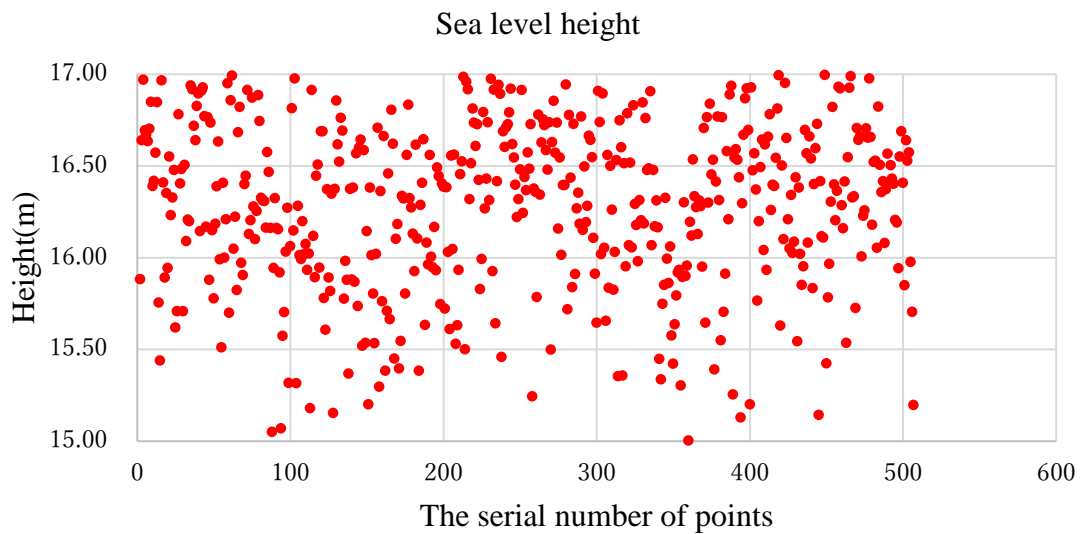


Figure 4.15 Calculation of the height of sea level at 10:52

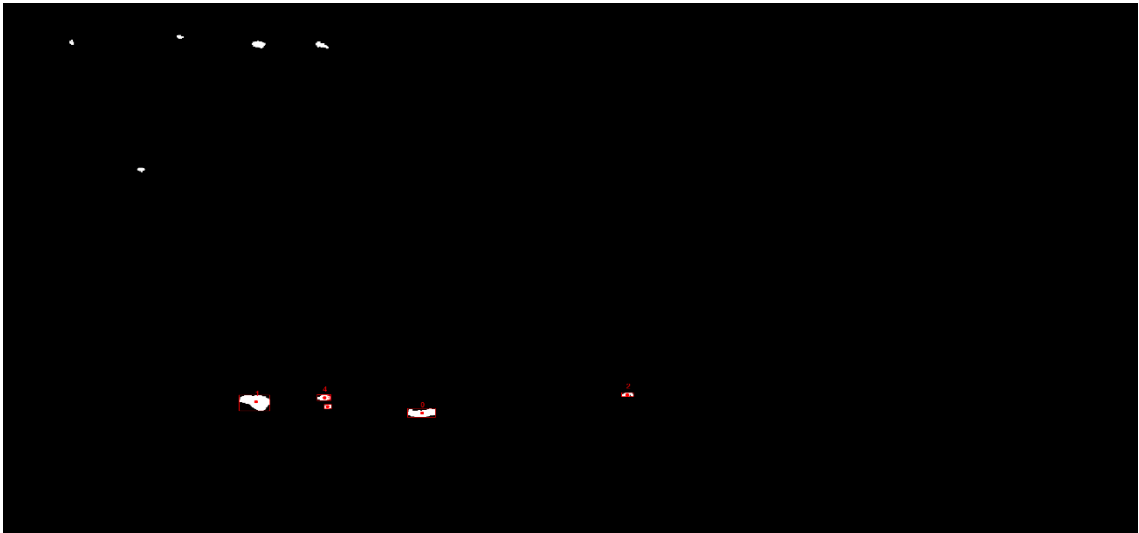
We successfully match the 506 corresponding points from 150 pairs of images. Through calculation, we could know that the average of sea level height is 16.27(m). The max value is 17 (m). The min value is 15 (m). The standard deviation is 0.44.



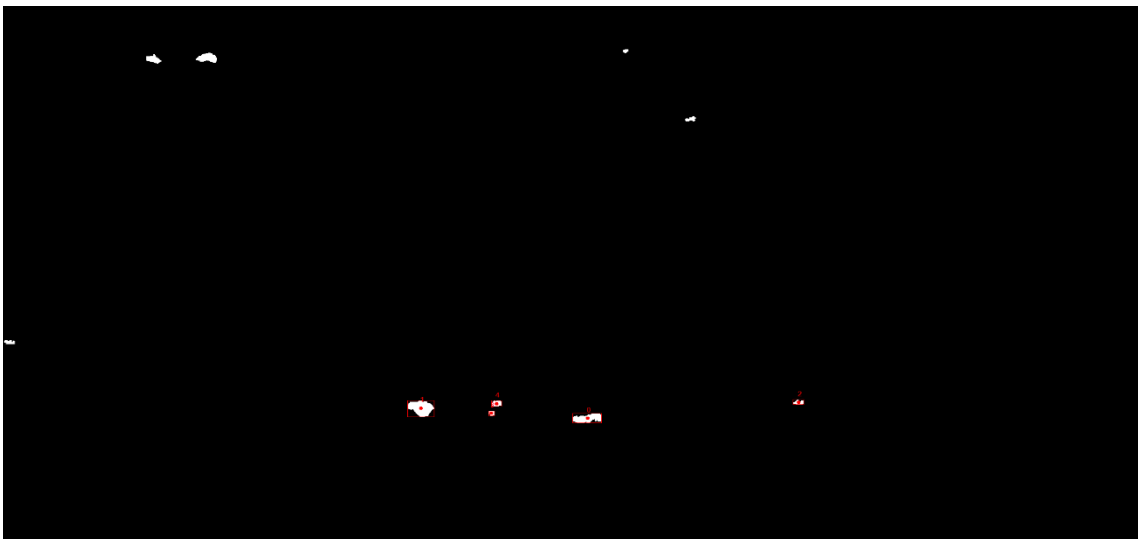
(a)Original image of left



(b) Original image of right



(c) Matching point of left



(d) Matching point of right

Figure 4.16 Image In Singu at 11.53

In Figure 4.16, (a) is the original image of left, (b) is the original image of right, (c) is the image after extracting the sea wave used by our methods from image (a). In addition, (d) is the image after extracting the sea wave from image (b). In image (c), there are many sea waves that are encircled by a rectangle box, which means that the ocean sea waves have been matched with the image (d) in the pair of images. The matched sea waves have serial numbers, which are list by the acquaintance and the size of sea wave. The serial numbers start from zero. The red point in the rectangle box expresses that it is the center of gravity in sea wave, which is the matching point in pair of images. In image (c), we extract 10 sea waves from image (a). In image (d), we extract 10 sea waves from image (b). The number of matching points is five. The matching success rate is 50% for the left mapping and 50% for the right mapping.

In every time, we take 150 pairs of images, so the Figure 4.16 is just one of pairs of images. We extract and match sea wave from 150 pairs of image, then calculate the height of sea level, the result is shown in Figure 4.17

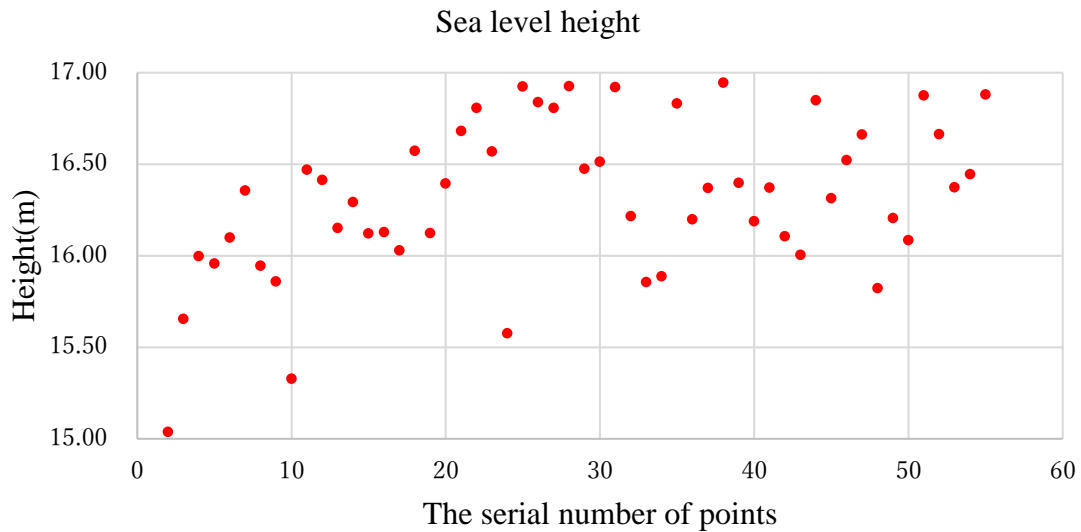


Figure 4.17 Calculation of the height of sea level at 11:53

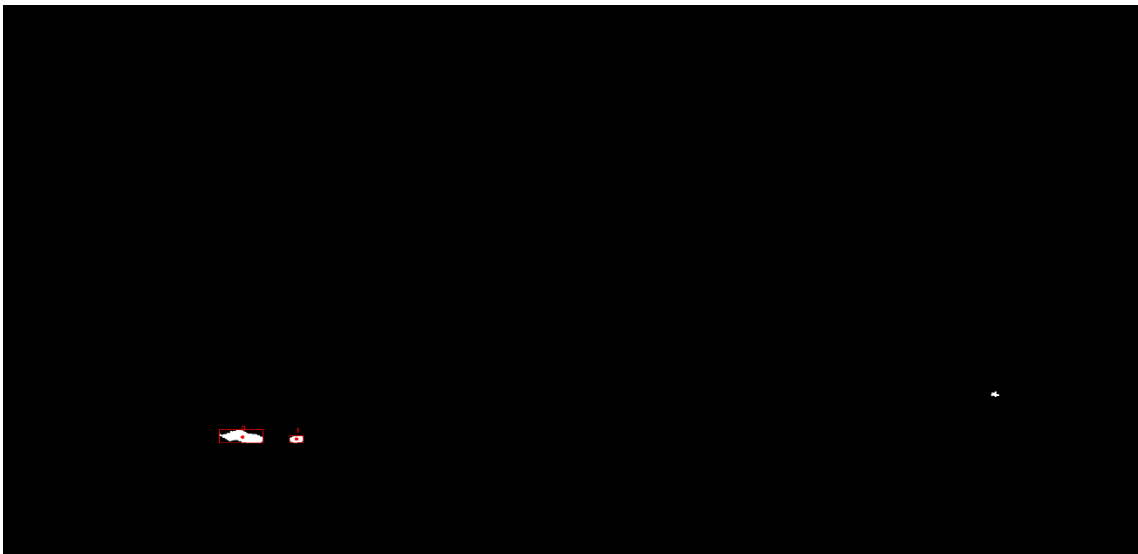
We successfully match the 54 corresponding points from 150 pairs of images. Through calculation, we could know that the average of sea level height is 16.32(m). The max value is 16.95(m). The min value is 15.04 (m). The standard deviation is 0.42.



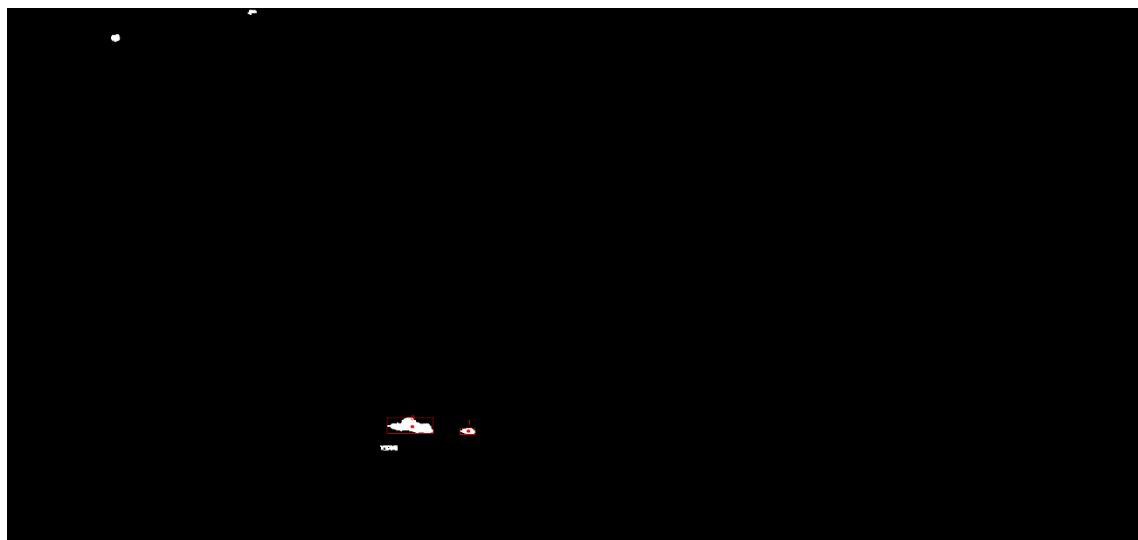
(a)Original image of left



(b) Original image of right



(c) Matching point of left



(d) Matching point of right

Figure 4.18 Image in Singu at 12:53

In Figure 4.18 (a) is the original image of left, (b) is the original image of right, (c) is the image after extracting the sea wave used by our methods from image (a). In addition, (d) is the image after extracting the sea wave from image (b). In image (c), there are many sea waves that are encircled by a rectangle box, which means that the ocean sea waves have been matched with the image (d) in the pair of images. The matched sea waves have serial numbers, which are list by the acquaintance and the size of sea wave. The serial numbers start from zero. The red point in the rectangle box expresses that it is the center of gravity in sea wave, which is the matching point in pair of images. In image (c), we extract 12 sea waves from image (a). In image (d), we extract 18 sea waves from image (b). The number of matching points are seven. The matching success rate is 58.3% for the left mapping and 38.9% for the right mapping.

In every time, we take 150 pairs of images, so the Figure 4.18 is just one of pairs of images. We extract and match sea wave from 150 pairs of image, then calculate the height of sea level, the result is shown in Figure 4.19

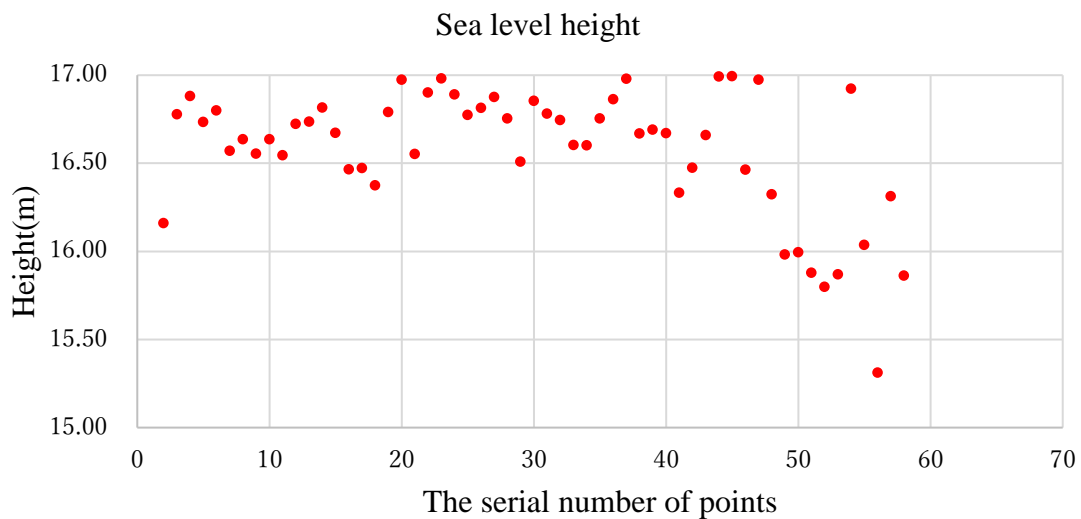


Figure 4.19 Calculation of the height of sea level at 12:53

We successfully match the 57 corresponding points from 150 pairs of images. Through calculation, we could know that the average of sea level height is 16.57(m). The max value is 16.99(m). The min value is 15.31 (m). The standard deviation is 0.36.



(a)Original image of left



(b) Original image of right



(c) Matching point of left



(d) Matching point of right

Figure 4.20 Image in Singu at 13.54

In Figure 4.20 (a) is the original image of left, (b) is the original image of right, (c) is the image after extracting the sea wave used by our methods from image (a). In addition, (d) is the image after extracting the sea wave from image (b). In image (c), there are many sea waves that are encircled by a rectangle box, which means that the ocean sea waves have been matched with the image (d) in the pair of images. The matched sea waves have serial numbers, which are list by the acquaintance and the size of sea wave. The serial numbers start from zero. The red point in the rectangle box expresses that it is the center of gravity in sea wave, which is the matching point in pair of images. In image (c), we extract 12 sea waves from image (a). In image (d), we extract 18 sea waves from image (b). The number of matching points is seven. The matching success rate is 58.3% for the left mapping and 38.9% for the right mapping.

In every time, we take 150 pairs of images, so the Figure 4.20 is just one of pairs of images. We extract and match sea wave from 150 pairs of image, then calculate the height of sea level, the result is shown in Figure 4.21

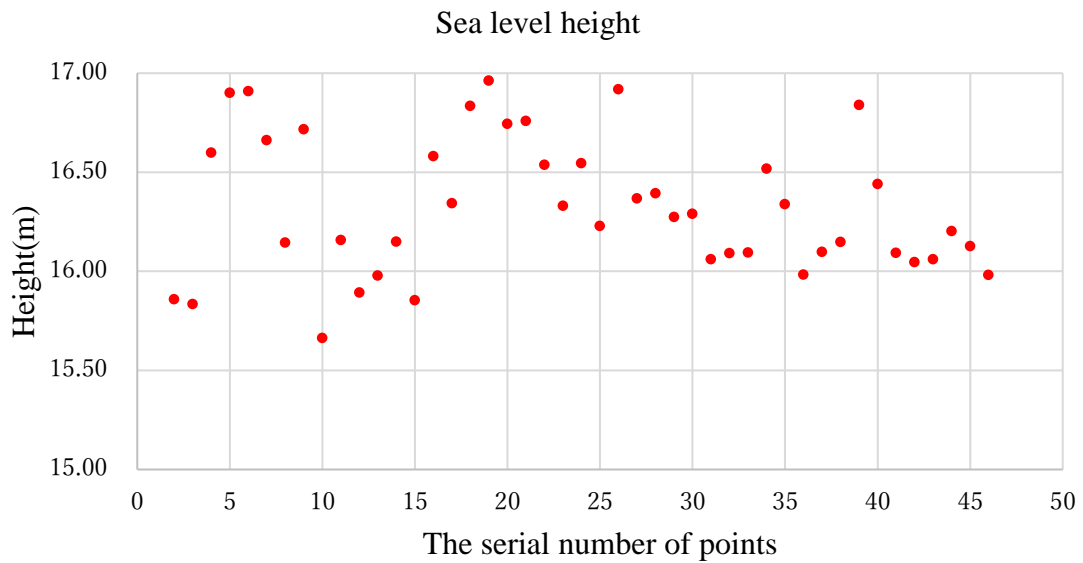


Figure 4.21 Calculation of the height of sea level at 13:54

We successfully match the 45 corresponding points from 150 pairs of images. Through calculation, we could know that the average of sea level height is 16.32(m). The max value is 16.96(m). The min value is 15.66 (m). The standard deviation is 0.34.



(a)Original image of left



(b) Original image of right



(c) Matching point of left



(d) Matching point of right

Figure 4.22 Image In Singu 14:55

In Figure 4.22 (a) is the original image of left, (b) is the original image of right, (c) is the image after extracting the sea wave used by our methods from image (a). In addition, (d) is the image after extracting the sea wave from image (b). In image (c), there are many sea waves that are encircled by a rectangle box, which means that the ocean sea waves have been matched with the image (d) in the pair of images. The matched sea waves have serial numbers, which are list by the acquaintance and the size of sea wave. The serial numbers start from zero. The red point in the rectangle box expresses that it is the center of gravity in sea wave, which is the matching point in pair of images. In image (c), we extract 10 sea waves from image (a). In image (d), we extract eight sea waves from image (b). The number of matching points is five. The matching success rate is 50% for the left mapping and 62.5% for the right mapping.

In every time, we take 150 pairs of images, so the Figure 4.22 is just one of pairs of images. We extract and match sea wave from 150 pairs of image, then calculate the height of sea level, the result is shown in Figure 4.23

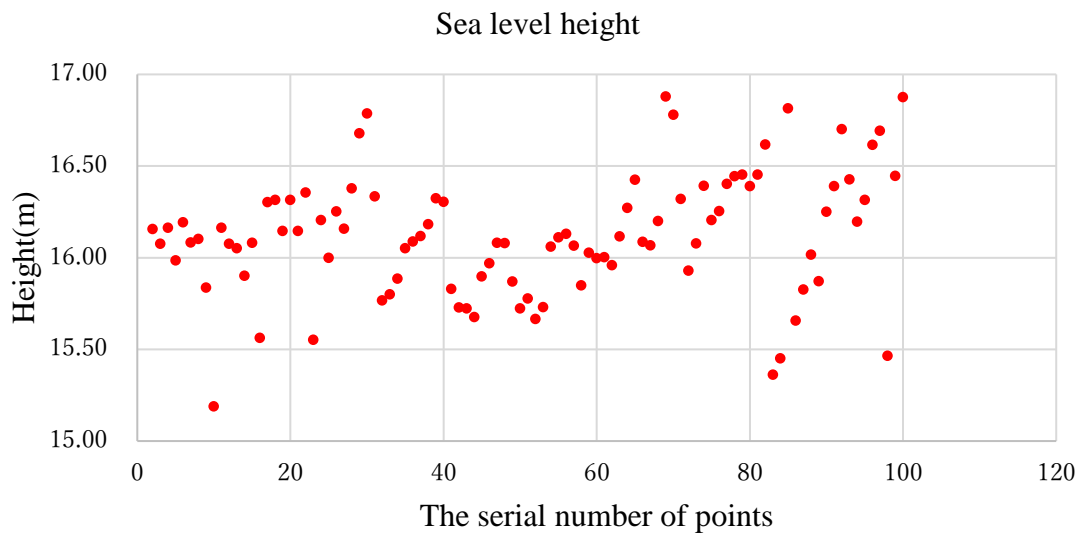


Figure 4.23 Calculation of the height of sea level at 14:55

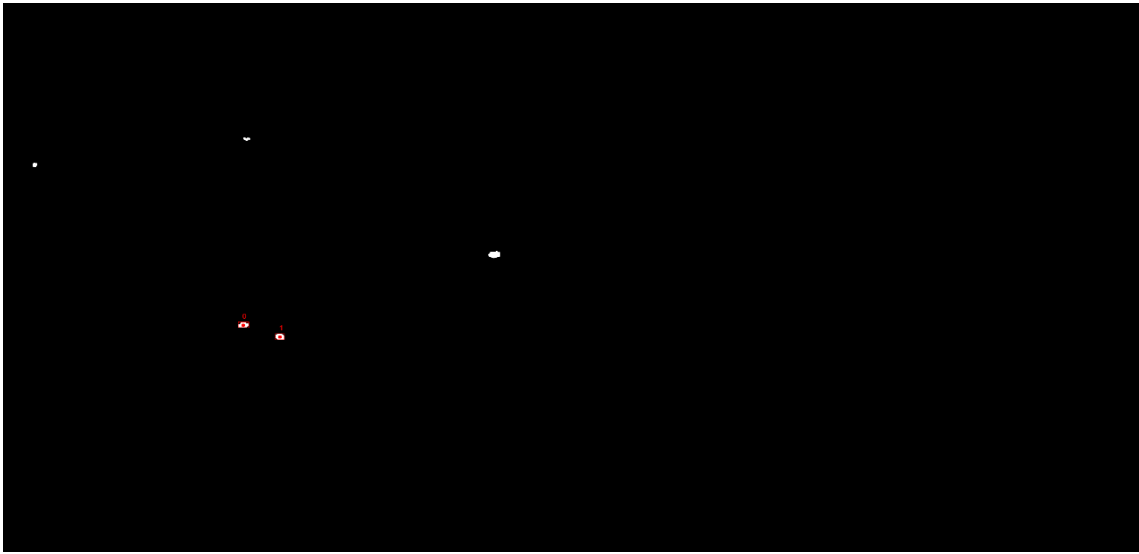
We successfully match the 99 corresponding points from 150 pairs of images. Through calculation, we could know that the average of sea level height is 16.34(m). The max value is 16.88(m). The min value is 15.19 (m). The standard deviation is 0.33.



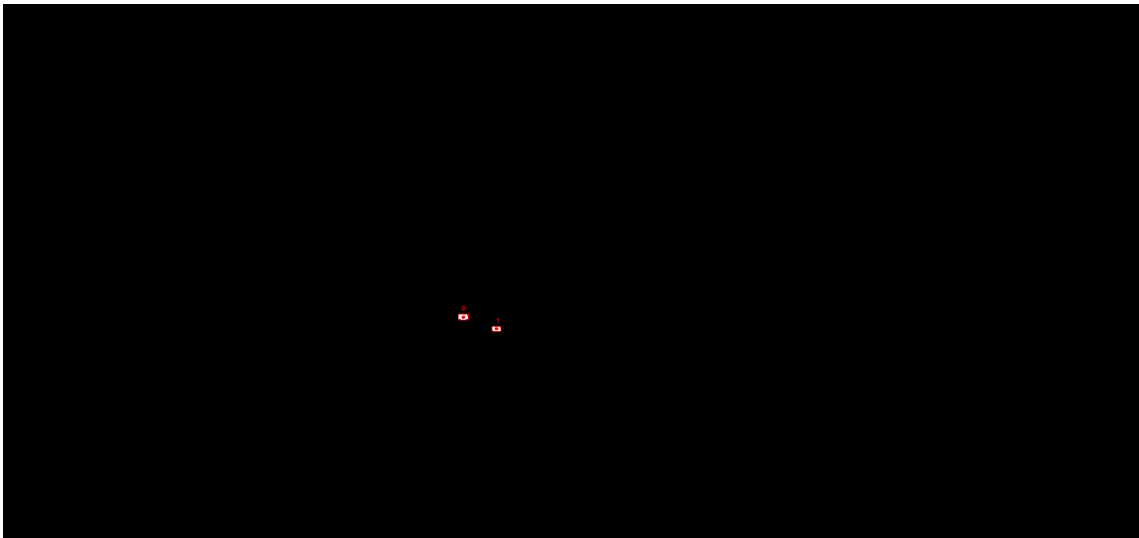
(a)Original image of left



(b) Original image of right



(c) Matching point of left



(d) Matching point of right

Figure 4.24 Image in Singu at 15:56

In Figure 4.24 (a) is the original image of left, (b) is the original image of right, (c) is the image after extracting the sea wave used by our methods from image (a). In addition, (d) is the image after extracting the sea wave from image (b). In image (c), there are many sea waves that are encircled by a rectangle box, which means that the ocean sea waves have been matched with the image (d) in the pair of images. The matched sea waves have serial numbers, which are list by the acquaintance and the size of sea wave. The serial numbers start from zero. The red point in the rectangle box expresses that it is the center of gravity in sea wave, which is the matching point in pair of images. In image (c), we extract five sea waves from image (a). In image (d), we extract two sea waves from image (b). The number of matching points is two. The matching success rate is 40% for the left mapping and 100% for the right mapping.

In every time, we take 150 pairs of images, so the Figure 4.24 is just one of pairs of images. We extract and match sea wave from 150 pairs of image, then calculate the height of sea level, the result is shown in Figure 4.25

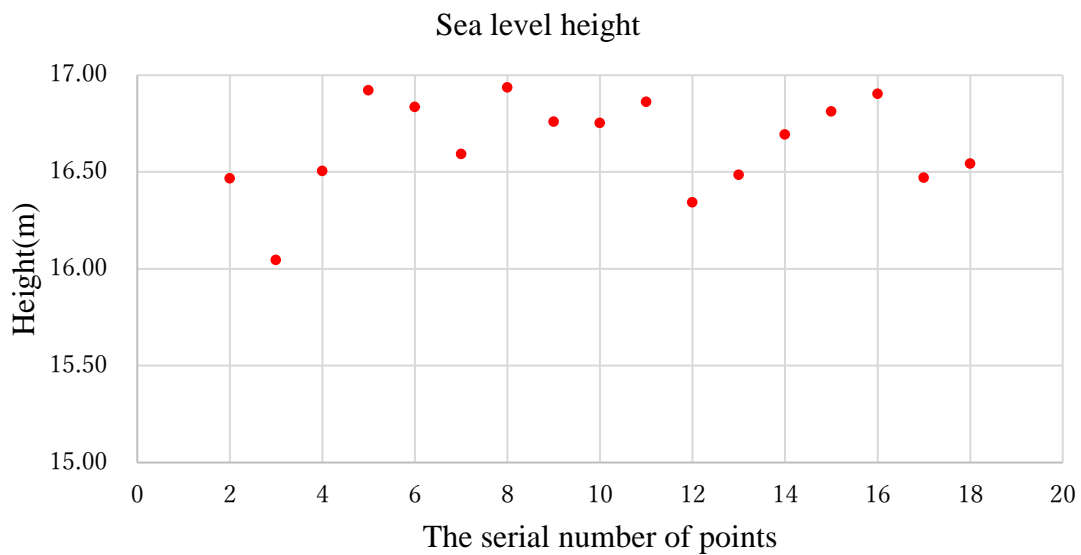


Figure 4.25 Calculation of the height of sea level at 15:56

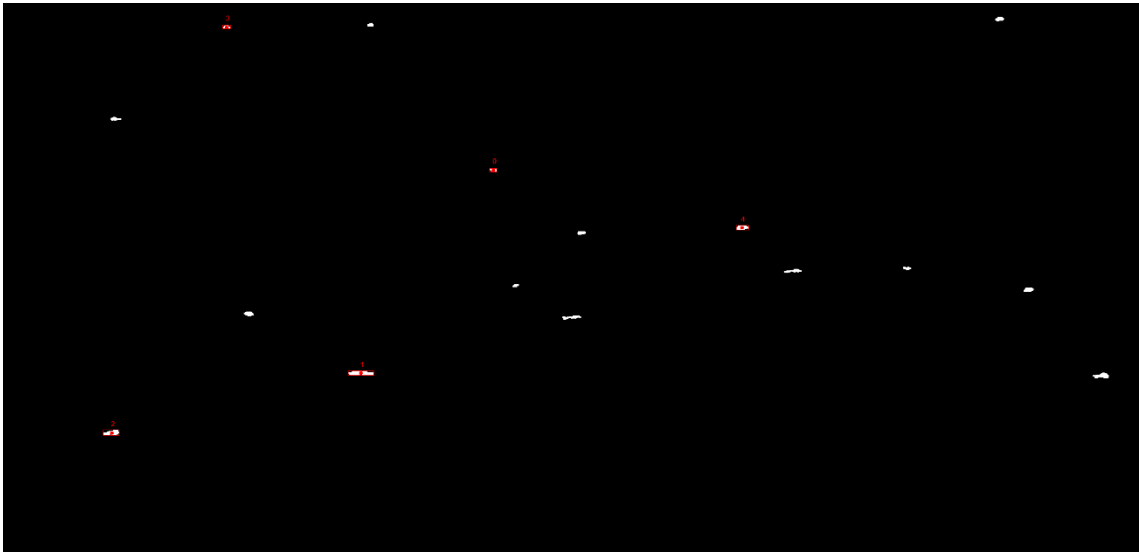
We successfully match the 17 corresponding points from 150 pairs of images. Through calculation, we could know that the average of sea level height is 16.64(m). The max value is 16.94(m). The min value is 16.05(m). The standard deviation is 0.23.



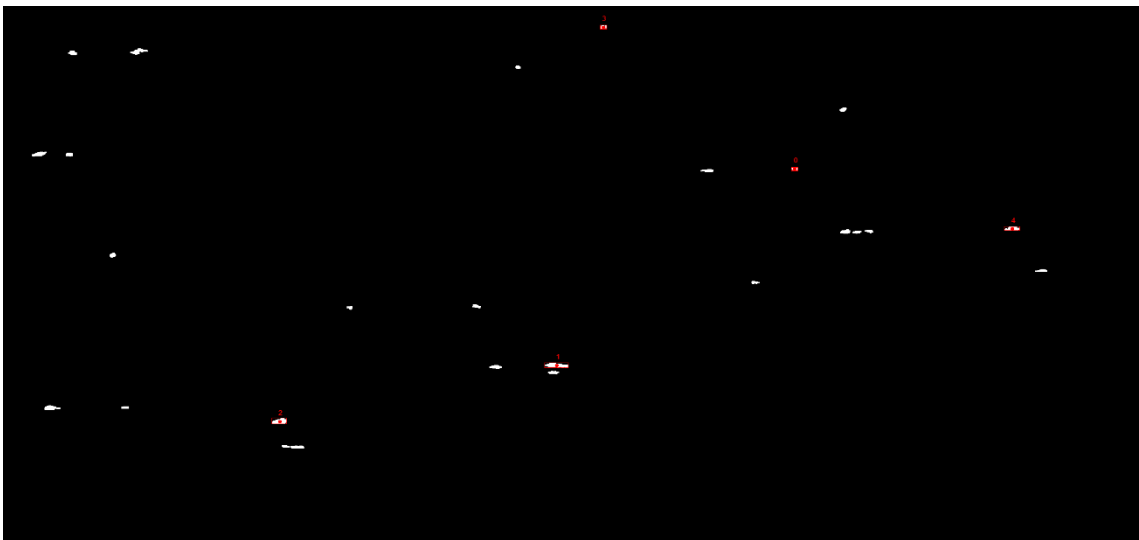
(a)Original image of left



(b) Original image of right



(c) Matching point of left



(d) Matching point of right

Figure 4.26 Image in Singu at 16:57

In Figure 4.26 (a) is the original image of left, (b) is the original image of right, (c) is the image after extracting the sea wave used by our methods from image (a). In addition, (d) is the image after extracting the sea wave from image (b). In image (c), there are many sea waves that are encircled by a rectangle box, which means that the ocean sea waves have been matched with the image (d) in the pair of images. The matched sea waves have serial numbers, which are list by the acquaintance and the size of sea wave. The serial numbers start from zero. The red point in the rectangle box expresses that it is the center of gravity in sea wave, which is the matching point in pair of images. In image (c), we extract 16 sea waves from image (a). In image (d), we extract 25 sea waves from image (b). The number of matching points is five. The matching success rate is 31.25% for the left mapping and 20% for the right mapping.

In every time, we take 150 pairs of images, so the Figure 4.26 is just one of pairs of images. We extract and match sea wave from 150 pairs of image, then calculate the height of sea level, the result is shown in Figure 4.27.

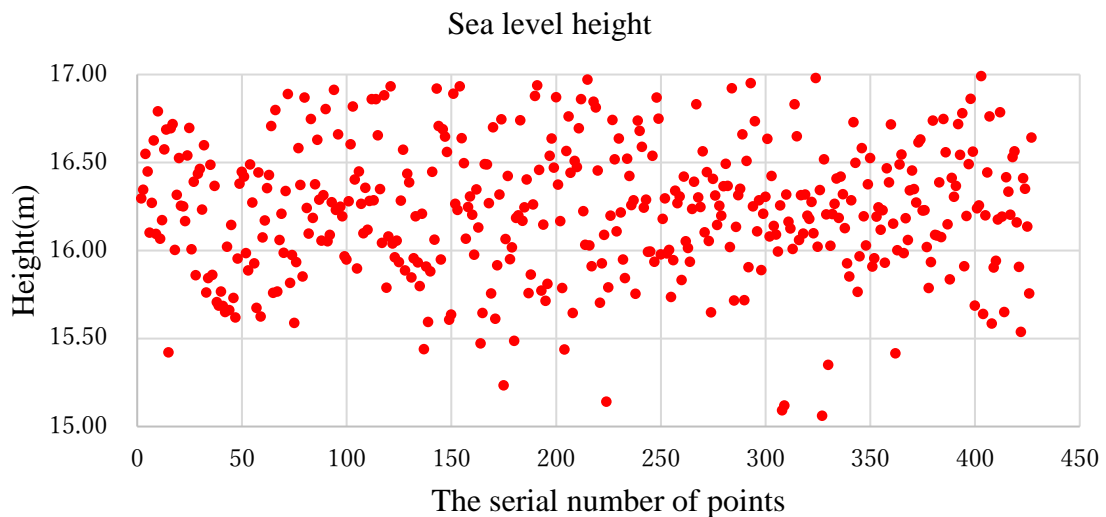


Figure 4.27 Calculation of the height of sea level at 16:57

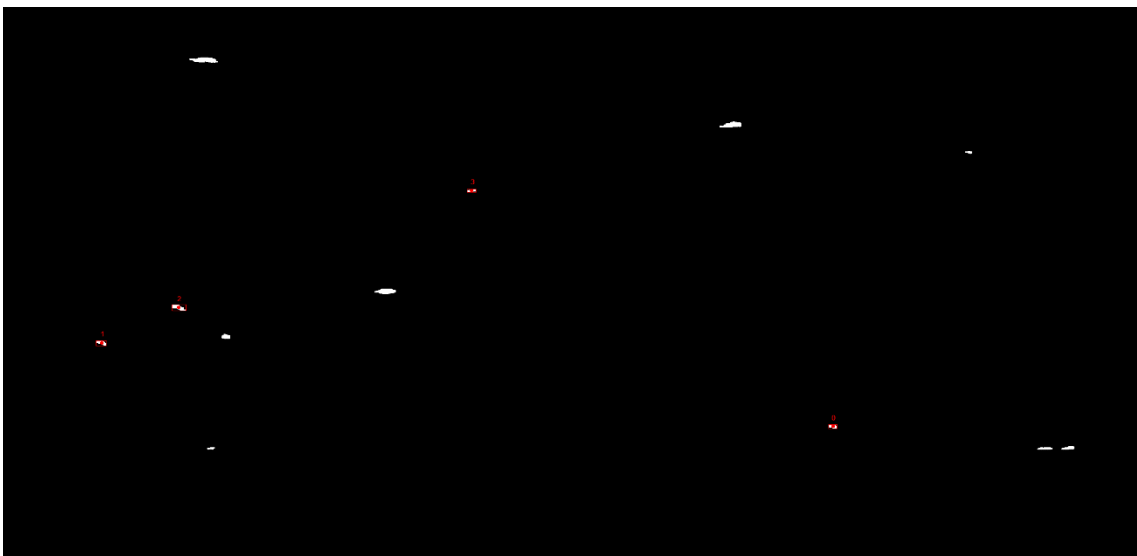
We successfully match the 426 corresponding points from 150 pairs of images. Through calculation, we could know that the average of sea level height is 16.23(m). The max value is 16.99(m). The min value is 15.06(m). The standard deviation is 0.36.



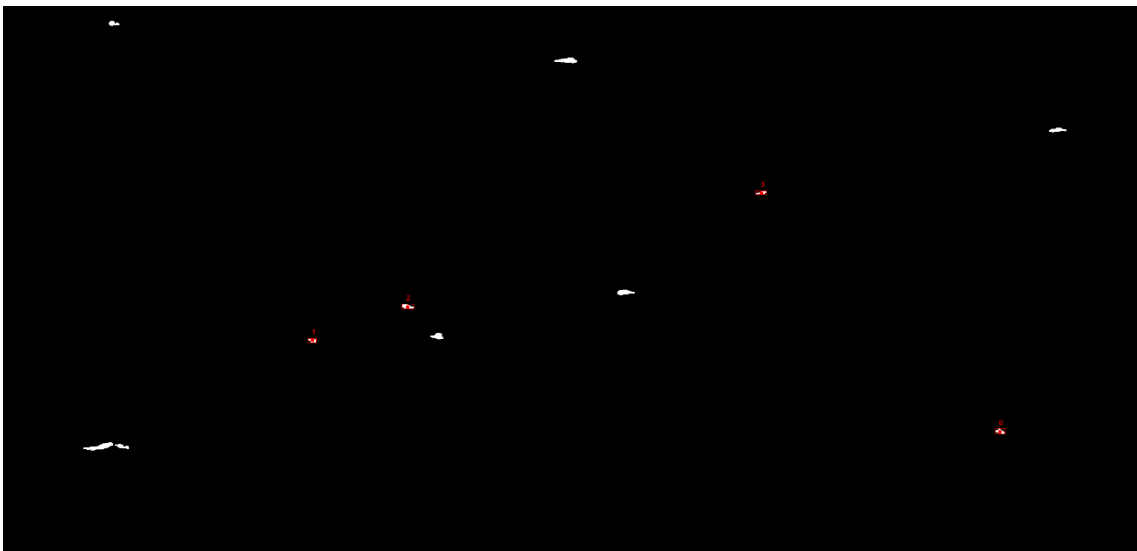
(a)Original image of left



(b) Original image of right



(c) Matching point of left



(d) Matching point of right

Figure 4 .28 Image in Singu at 17:58

In Figure 4.28 (a) is the original image of left, (b) is the original image of right, (c) is the image after extracting the sea wave used by our methods from image (a). In addition, (d) is the image after extracting the sea wave from image (b). In image (c), there are many sea waves that are encircled by a rectangle box, which means that the ocean sea waves have been matched with the image (d) in the pair of images. The matched sea waves have serial numbers, which are list by the acquaintance and the size of sea wave. The serial numbers start from zero. The red point in the rectangle box expresses that it is the center of gravity in sea wave, which is the matching point in pair of images. In image (c), we extract 12 sea waves from image (a). In image (d), we extract 11 sea waves from image (b). The number of matching points is four. The matching success rate is 33.3% for the left mapping and 36.36% for the right mapping.

In every time, we take 150 pairs of images, so the Figure 4.28 is just one of pairs of images. We extract and match sea wave from 150 pairs of image, then calculate the height of sea level, the result is shown in Figure 4.29

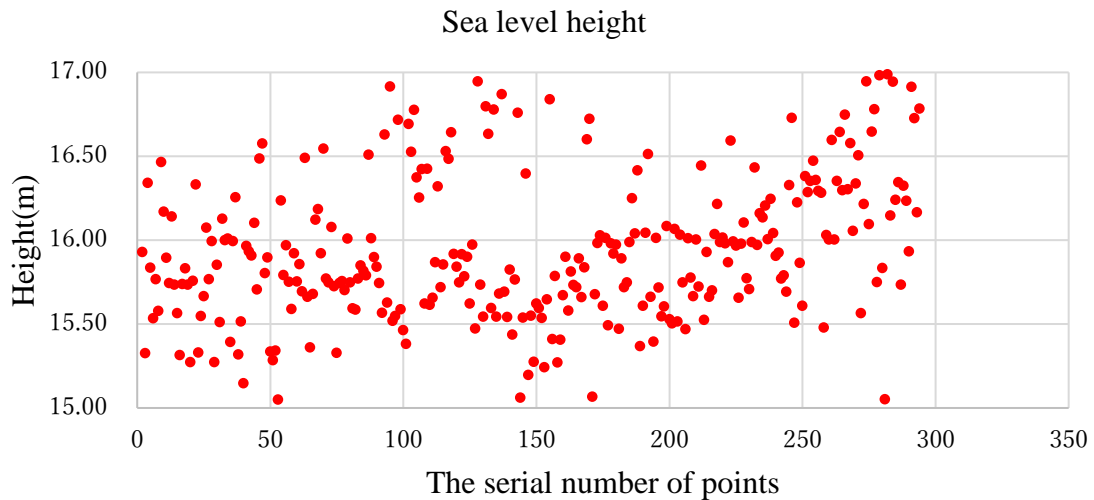


Figure 4.29 Calculation of the height of sea level at 17:58

We successfully match the 293 corresponding points from 150 pairs of images. Through calculation, we could know that the average of sea level height is 15.94(m). The max value is 16.99(m). The min value is 15.05(m). The standard deviation is 0.42.

Finally, replace all the heights with a relative height change and compare with the data provided by the Japanese government. You could see the result in Figure 4.30.

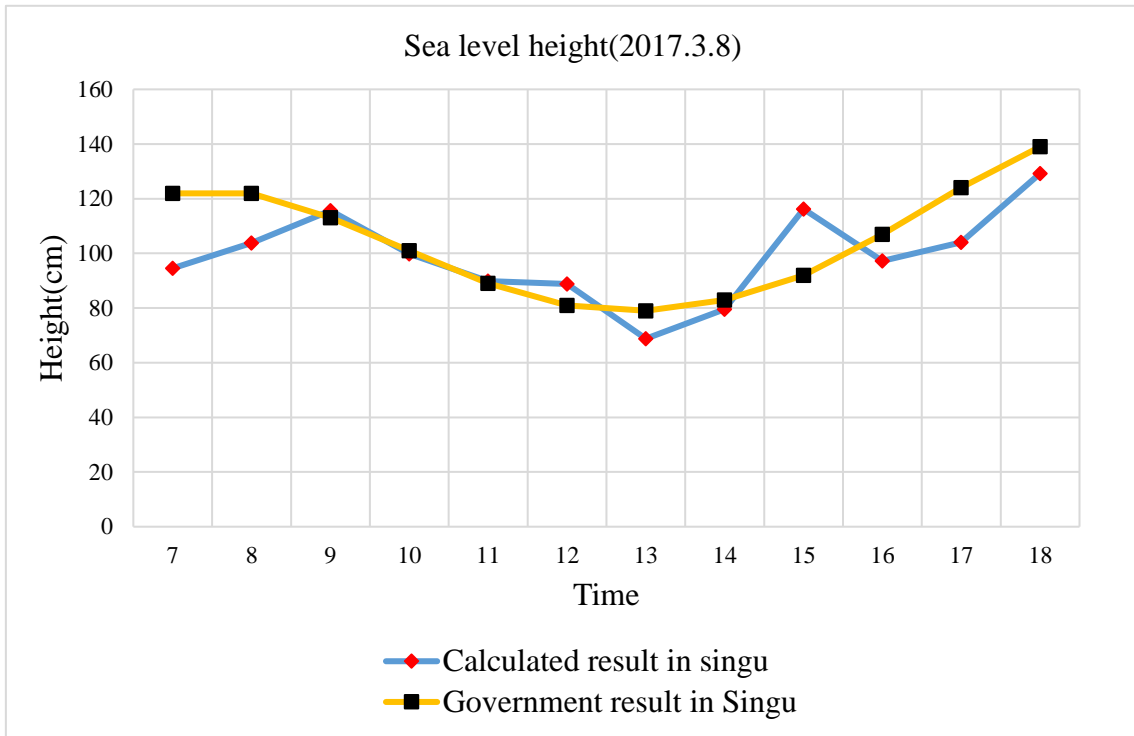


Figure 4.30 Experiment result in Singu on March 8

There are two colors in Figure 4.30. The blue one is the calculated result and the yellow one is provided by Japan Meteorological Agency.

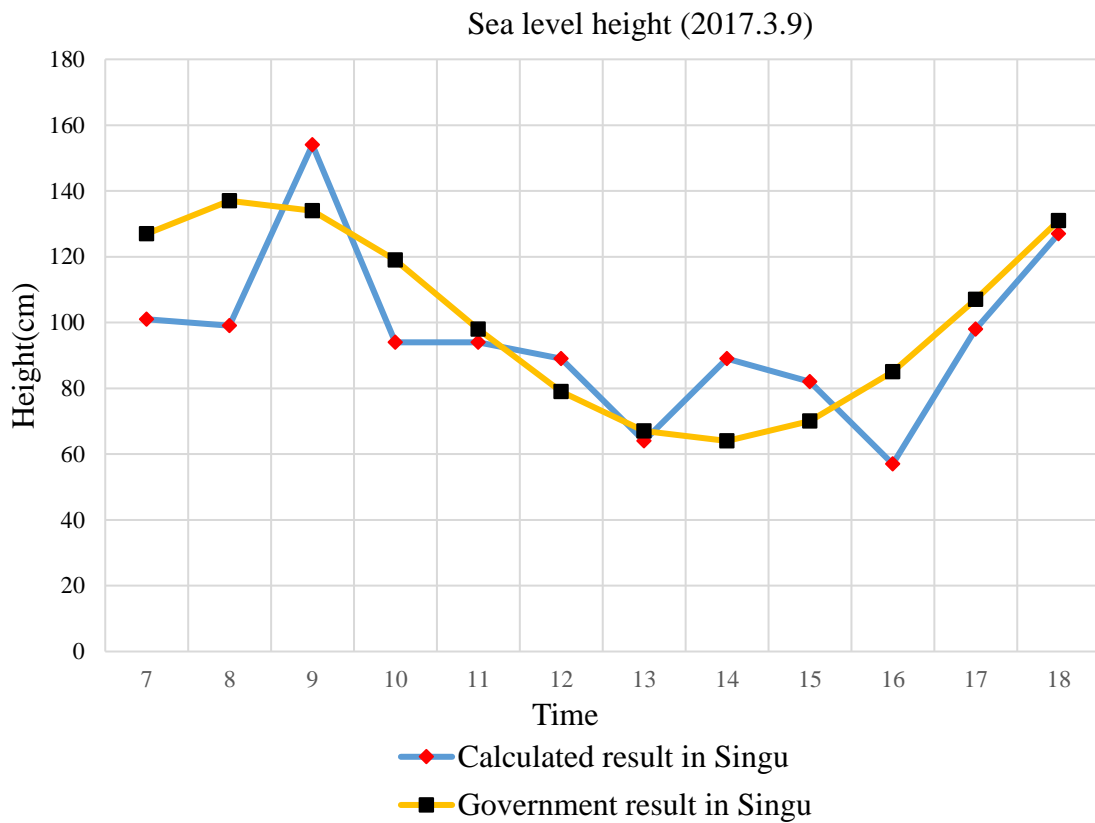


Figure 4.31 Experiment result in Singu on March 9

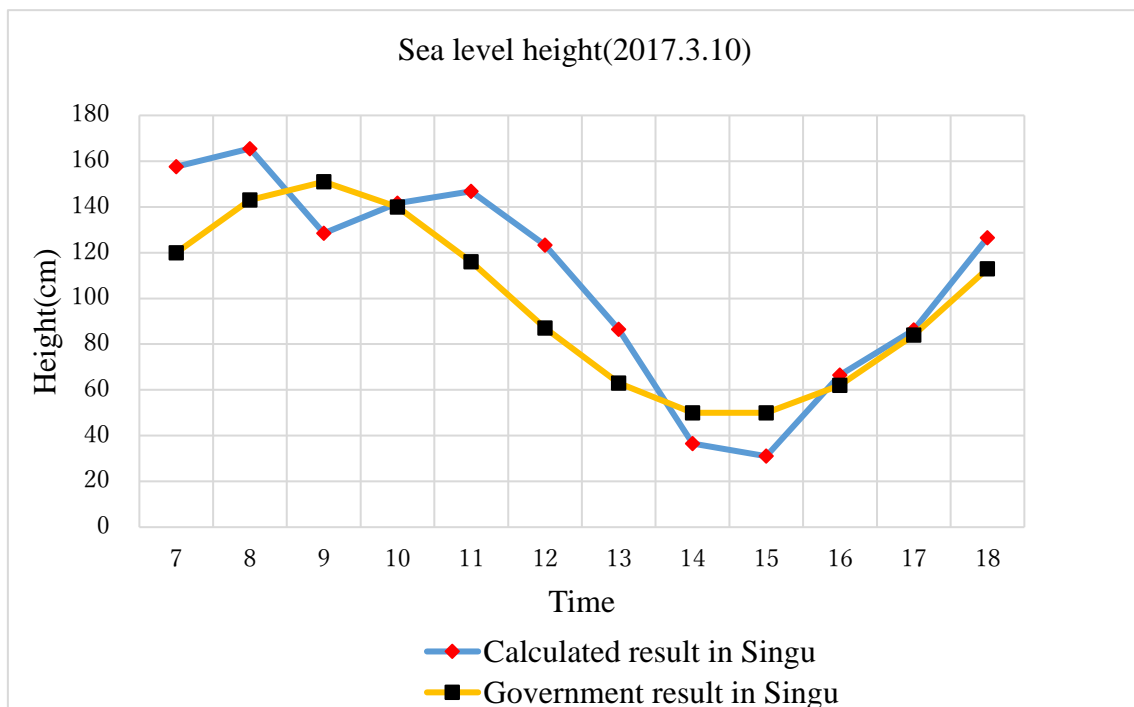


Figure 4.32 Experiment result in Singu on March 10

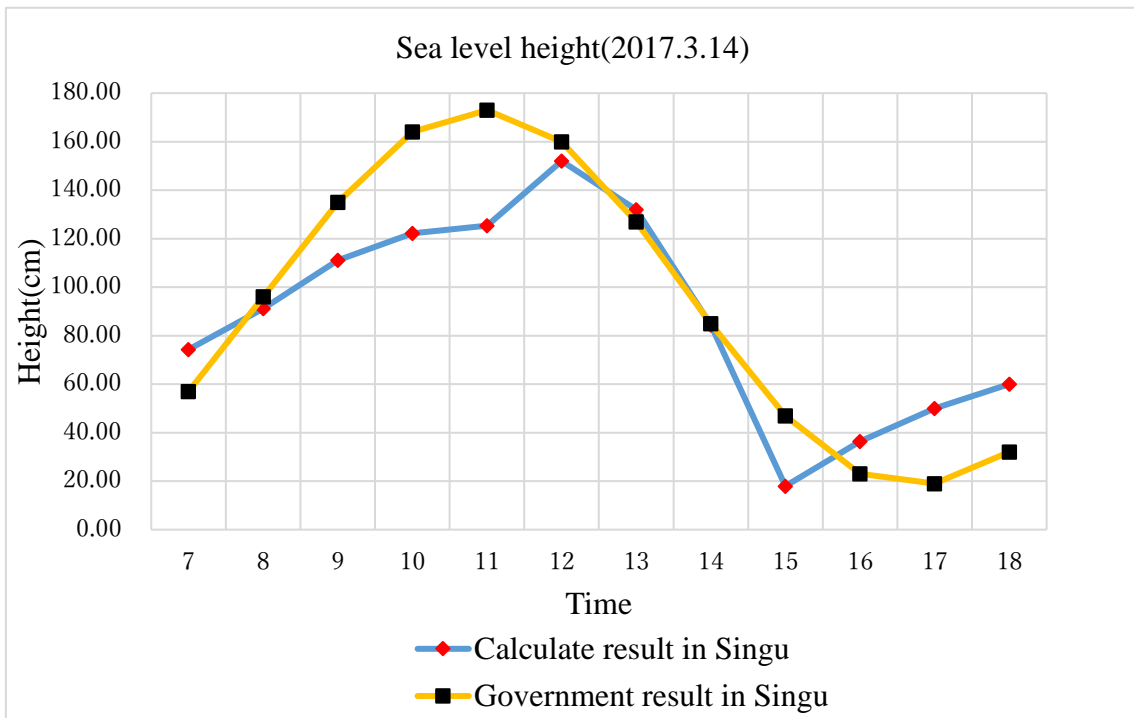


Figure 4.33 Experiment result in Singu on March 14

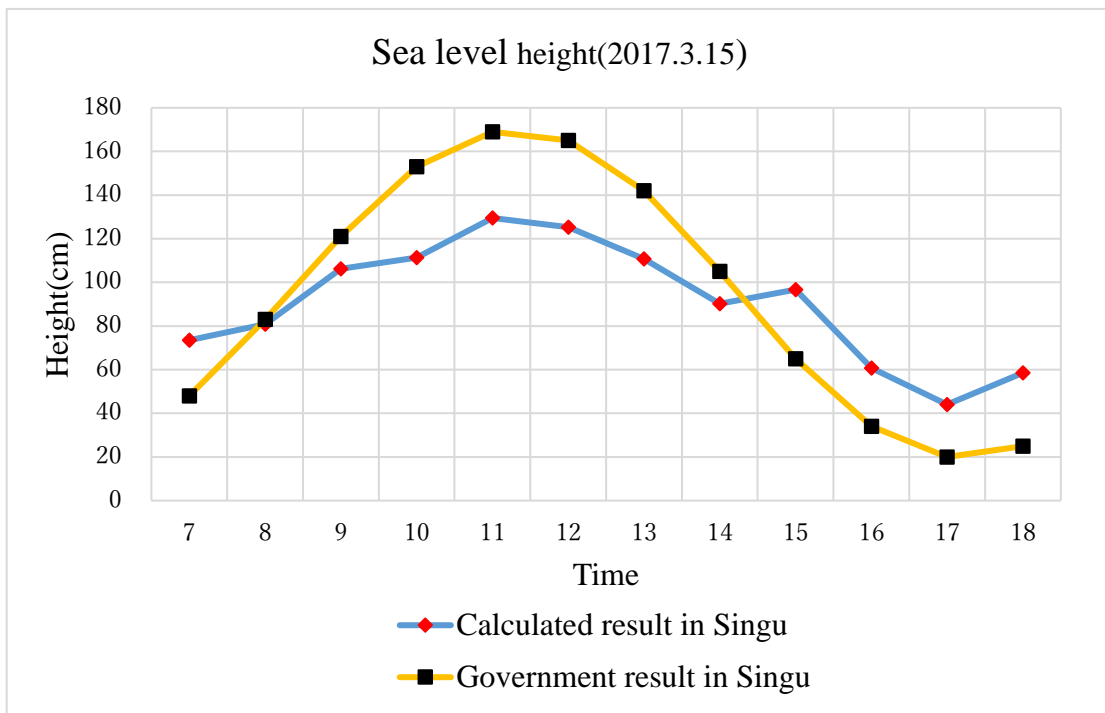


Figure 4.34 Experiment result in Singu on March 15

4.5 Summary

In this chapter, we first introduce the experimental environment and then explain the hardware needed in the system. Then a model for measuring sea level is given. Through this model we can find the change of sea level. Finally, the experimental results are given. It can be seen from the experimental results that the changes of the sea level are consistent with those of the tidal water.

This method can automatically extract the waves and match when the weather is fine. However, when the waves on the sea surface are not obvious, the extraction of the waves is difficult, and it is very influential to the measurement result.

Chapter 5 Conclusions

Tsunami is a great disaster to our life. More damages would be generated when it happens nearby the coast. When the tsunami enters the shallow water, its speed slows down and its amplitude will increase to tens of meters. Therefore, monitoring the state of the tsunami in real-time is very important. To reduce the harm to people's safety, we monitor the distance for more than 20km.

In this paper, we constructed a system of 3-D image measurement of the tsunami for disaster prevention. I mainly do four parts. First, calibrate the camera system in long distance. Second, extract the sea waves. Third, match the corresponding sea waves between the left image and the right image. Forth. Calculate the height of the sea level and compare with the data from Meteorological Agency.

Camera system calibration is an essential part in 3-D image measurement. In order to achieve long distance calibration, we choose a hollow plastic bar as the calibration bar, and paint red and write grid on it. It can be seen clearly from 3km, and it is easy to make and move to experimental place. Another reason is that the central axis of the cylinder remains unchanged when rotating it. No matter what angles you rotated the cylinder, the central axis is always in the middle of the side view of cylinder. We obtain the red and write boundary point on the central axis as the feature point. No matter where you take the picture for cylinder, the location of the feature points will remain unchanged. Through the leveling device, we make sure that the camera is level state. Simplify the process of calibration. First, we take many images to obtain the feature points. Then, we use those feature points to calculate the 3-D coordinate points. Finally, we obtain the unknown parameters using by the Levenberg-Marquardt optimization method.

We proposed the optimum block threshold method to extract the sea waves. This method divide small blocks to solve the problem of uneven brightness. In addition, it associates the thresholds of the surrounding four blocks to extract the complete sea waves. From the experimental result, we could learn that method can extract sea waves from long distance images from 20 to 200 in one image.

We proposed our approach of Feature-matrix method for matching the sea wave. This method defines a feature-matrix to contain all the sea waves. Then, compared with the feature vector directly, the running time is so fast. Finally, through the 2D matching wave, the 3-D verification is performed. It is high accuracy.

In our system, in order to calculate the sea level height, the average value of large number sea wave points are proposed as the sea level height. There are many small waves

on the surface. We can extract many points on the sea surface and some points are located on the top of sea wave. Some points are located on the bottom. We follow the principle that the points are normal distribution. From the experimental result, we can obtain the change of sea level using by this method.

Through the proposed four methods, a stereo vision system is constructed. We use this system to perform actual measurement data in 5km and 10km respectively to verify the proposed methods. Use massive corresponding points to calculate the sea level at daytime. Through comparing with the data from Japan Meteorological Agency, it is concluded that this system can effectively measure the sea level.

For the future work, there are still many works to do. The program now needs about 30 minutes to process 150 photos. This is not possible to perform real-time calculations, and needs to be improved. The number of matching sea wave needs to be increased. Now only horizontal angle is considered, the other two angles will be added later. In addition, the distance of camera calibration is 10km. It will be increased later.

References

- [1] N. Ogawa and F. Yamazaki, “Photo-interpretation of building damage due to earthquakes using aerial photographs”, presented at the 12th World Conf. Earthquake Engineering, vol.3, pp.1906-1918, 2000.
- [2] Lu Xu, “Study of Wave Height Measurement Based on 3-D Image Measurement Technology”, Master degree thesis, The Fukuoka Institute of Technology, 2015.
- [3] C.Potter, “Global assessment of damage to coastal ecosystem vegetation from tropical storms”, Remote Sensing Letter, vol.5, no.4, pp.315-322, 2004.
- [4] Ben-Menahem, A.& M.Nafi Tokssz., “Source-Mechanism from Spectra of Long-Period Seismic Surface-waves”, Journal of geophysical research, vol.67, no.5, pp.1943-1955, 1962.
- [5] Vikas Mendi, Subba Rao, Jaya Kumar Seelam, “Tidal Energy: A Review”, International Journal of Research, vol.2, no.1, pp.55-58, 2015.
- [6] Tolman, H. L, Mahmood, M.F., “CBMS Conference Proceedings on Water Waves: Theory and Experiment”, World Scientific Publications. ISBN 978-981-4304-23-8, pp.1-14, 2008.
- [7] Minoura, K., Imamura F., Sugawara D., Kono Y., Iwashita T, “The 869 Jōgan tsunami deposit and recurrence interval of large-scale tsunami on the Pacific coast of northeast Japan”, Journal of Natural Disaster Science, vol.23, no.2, pp.83–88. 2011.
- [8] J.Wachter, A.Babeyko and M.lendholt, “Development of tsunami early warning systems and future challenges”, Natural Hazards and Earth System Sciences, vol.12, pp.1923-1935, 2012.
- [9] Z. Ezzouine, A. Nakheli, “Conception of water level detector (TIDE-GAUGE) based on a electromagnetic sensor of force”, International Journal of Research in Engineering and Technology, vol.3, no.1, pp.251-260, 2014.

- [10] Sakata, S., A. Araya, and D. Tsuboi, "Development of Laser Tsunami-meter", *Scientific Use of Submarine Cables and Related Technologies*, DoI. 10.1109/SSC.1224113, pp.71-74, 2003.
- [11] Hiroyasu Kawai, Makoto Satoh, Koji Kawaguchi, "Recent tsunamis observed by GPS Buoys off the pacific coast of japan", *coastal engineering*, vol.4, pp.1-15, 2012.
- [12] M. Galletti, G. Krieger, T. Borner, "Concept design of a near-space radar for tsunami detection", *Geoscience and Remote Sensing Symposium*, vol.221, pp.34-37, 2007.
- [13] S. T. Grilli¹, M. Shelby, A. Grilli¹, C. Guerin, S. Grosdidier and T. Insua, "Algorithms for tsunami detection by High Frequency Radar : development and case studies for tsunami impact in British Columbia, Canada", *Proceedings of the Twenty-sixth (2016) International Ocean and Polar Engineering Conference*, Rhodes, Greece, June 26-July 1, pp.807-814, 2016.
- [14] Takao Eguchi, Yukio Fujinawa, Eisuke Fujita, "A real-time observation network of ocean-bottom-seismometers deployed at the Sagami trough subduction zone", *central Japan, Marine Geophysical Researches*, vol.20, pp.73-94, 1998.
- [15] Harold O. Mofjeld, Paul M. Whitmore, M. C. Eble, F. I. Gonzalez and J. C. Newman, "Sensmic-wave Contributions to bottom pressure fluctuations in the North Pacific-Implications for the DART Tsunami Array", vol.5, no.5, pp.468-483, 2001.
- [16] Donald B. Percival, Donald W. Denbo, Marie C. Eble', Edison Gica, Harold O. Mofjeld, Michael C. Spillane, Liujuan Tang, Vasily V. Titov, "Extraction of tsunami source coefficients via inversion of DART buoy data", *Nat Hazards*, vol.58, pp.567-590, 2011,
- [17] Mengqi Ye and Costas P. Grigoropoulos, "Time-of-flight and emission spectroscopy study of femtosecond laser ablation of titanium", *Journal of Applied Physics*, vol.89, no.9, pp.459-478, 2001.
- [18] Cunwei Lu and Limin Xiang, "Optimal intensity-modulation projection technique for three-dimensional shape measurement", *Applied Optics*, vol.42, no.23, pp.342-350, 2003.

- [19] Tsai R., "A versatile camera calibration technique for high-accuracy 3D machine vision metrology using shelf TV cameras and lenses", *Robotics and Automation*, vol.323, no.4, pp.323-344, 1987.
- [20] Bruce D. Lucas, Takeo. Kanade, "An Iterative Image Registration Technique with an Application to Stereo Vision", *Pro 7th Intl Joint Conf on Artificial Intelligence*, vol.3, pp.121-130, 1981.
- [21] Otsu N., "A threshold selection method from gray-level histograms", *IEEE Transactions on system, man, and cybernetics*, vol.9, no.1, pp.376-380, 1979.
- [22] J. M. Foley, "Depth, size and distance in stereoscopic vision", *Perception & Psychophysics*, vol.3, pp.265-274, 1968.
- [23] Lu Xu, Cunwei Lu, "A Height Measurement Method of Sea Wave Based on Stereopsis Technique", *Proceedings of the IEICE General Conference*. DOI. 82.3015-02-24, pp.205-206, 2014.
- [24] Zhang zhengyou, "A flexible new technique for camera calibration," *Pattern Analysis and Machine Intelligence*. vol.22. no.11, pp.1330-1334, 2000.
- [25] Kenichi Kanatani, "Statistical Analysis of Focal-Length Calibration Using Vanishing Points", *IEEE Transactions on Robotics and Automation*, vol.8, no.6, pp.767-775, 1992.
- [26] Peter Sturm, "On focal Length Calibration from Two Views", *Computer Vision and Pattern Recognition*, DOI. 10.1109/CVPR.2001.990940, pp.115-120, 2001.
- [27] Janne H. and Olli S., "Calibration Procedure for Short Focal Length Off-the-shelf CCD Cameras", *Pattern Recognition*, 1996, *Proceedings of the 13th International Conference on*, DOI.10.1109/ICPR.546012, pp.166-171, 1996.
- [28] R. Hayashi, Taro Maeda, S. Shimojo, S. Tachi, "An integrative model of binocular vision: a stereo model utilizing interocularly unpaired points produces both depth and binocular rivalry", vol.44, pp.2367-2380, 2004.

- [29] Deborah Giaschi, S. Narasimhan, Aliya Solski, Emily H., Laurie M. Wilcox, “On the typical development of stereopsis: Fine and coarse processing”, vol.89, pp.65-71, 2013.
- [30] Nicholas j. Wade, “Early of binocular and stereoscopic vision”, Japanese Psychological Research, vol.54, no.1, pp.54-70, 2012.
- [31] Steven D. Cochran, G. Medioni, “3-D Surface Description from Binocular Stereo”, IEEE transactions on pattern analysis and machine intelligence, vol.14, no.10, pp.981-994, 1992.
- [32] Juyang Weng, Paul Cohen, and Marc Herniou, “Camera Calibration with Distortion Models and Accuracy Evaluation”, IEEE transactions on pattern analysis and machine intelligence, vol.14, no.10, pp.965-980, 1992.
- [33] Sutherland, Ivan E, “Three-dimensional data input by tablet”, Proceedings of the IEEE, vol.62, no.4, pp.453–461, 1974,
- [34] Wei Qingchao, Zhou GuoQing, “On DLT Method for CCD Camera Calibration”, Signal Processing, 3rd International Conference on, DOI.10.1109/ICSIGP.566229, pp.883-885, 1996.
- [35] Hao yi, Cunwei Lu, “An improved calibration technique for a long-distance 3-D image measurement system based on stereopsis method”. Kyushu Section, IEICE, pp.784-788, 2015.
- [36] Nobuyuki Otsu. “A threshold selection method from gray-level histograms”, IEEE Trans. Sys., Man., Cyber. vol.9, no.1, pp.62-66. DOI.10.1109/TSMC.1979.4310076, 1979.
- [37] Lei Yan, Hao Yi, and Cunwei Lu, “Overcome the Long Distance: A Universal Method for Sea Wave Matching”, ICISIP2016, pp.341-346, 2016.
- [38] Lei Yan, “Sea Wave Measurement at Long Distance Based on 3-D Image Technique”. Master degree thesis. The Fukuoka Institute of Technology, 2018.
- [39] Cunwei Lu, Yu Wang, Hao Yi, “A Sea Wave Height Measurement Method Based

On 3-D Image Measurement Technique”, International Ocean and Polar Engineering Conference, ISBN 978-1-880653-89-0, Hawaii, USA, June 21-26, 2015.

[40] Hao yi, Yan L, Tsujino K, et al. “A long-distance sea wave height measurement based on 3D image measurement technique”, Progress in Electromagnetic Research Symposium (PIERS), doi.10.1109, pp.4774-4779, 2016.

[41] Hao yi, Kazuhiro tsujino, and Cunwei lu, “3-D image measurement of the sea for disaster prevention”, 22rd International Symposium on Artificial Life and Robotics, pp.643-648, 2017.

Research Published

1. Hao Yi, Kazuhiro Tsujino and Cunwei Lu, “3-D image measurement of the sea for disaster prevention”, *Artificial Life and Robotics*, vol.23 no.3, pp.1-7,2018.
2. Hao Yi, Lei Yan, Kazuhiro Tsujino and Cunwei Lu, “A long-distance sea wave height measurement based on 3D image measurement technique”, *Progress in Electromagnetic Research Symposium (PIERS)*, doi.10.1109, pp.4774-4779, 2016.
3. Hao Yi, Kazuhiro Tsujino, and Cunwei Lu, “3-D image measurement of the sea for disaster prevention”, *22rd International Symposium on Artificial Life and Robotics*, pp.643-648, 2017.
4. Hao Yi , Cunwei Lu, “An improved calibration technique for a long-distance 3-D image measurement system based on stereopsis method”, *Kyushu Section, IEICE*, pp. 500, 2015.
5. Cunwei Lu, Yu Wang, Yaogang Tong, Hao Yi, Lixiang Song, Kazuhiro Tsujino “A Sea Wave Height Measurement Method Based On 3-D Image Measurement Technique”, *International Ocean and Polar Engineering Conference*, ISBN 978-1-880653-89-0, 2015.
6. Lei Yan, Hao Yi, and Cunwei Lu, “Overcome the Long Distance:A Universal Method for Sea Wave Matching”, *ICISIP2016 Kyoto* , pp.341-346, 2016.

Acknowledgement

My PHD study is coming to an end and I will start a new life journey, When I recalling the past four years, I have learned a lot. I am glad to have the chance to take part in the research work of this dissertation.

First, I want to thank my supervisor, Professor Cunwei Lu. Over these four years. He has given not only patient guidance on my study, but also valuable advice when I facing with life choices. He is a good teacher. It is he that led me to a new academic field and helped me finish the research work of this article. He cares about me like my parents and thus I felt enrich and happy during the four years in a foreign country.

I am also very grateful to all the professors who reviewed my thesis, Masao Yokota, Shijie Zhu and Yuuichiro Kogi. They gave me valuable comments.

I want to thank the teacher of graduate school, student department and other staff. I would give my special thanks to doctorate courses teacher Yu Song. I also want to thank the dormitory administrator for takeing care of my daily life.

Thank all the people in the Lu Laboratory of Fukuoka Institute of Technology for their guidance in the academic field. I am grateful to Li xiang Song, Kazuhiro Tsujino, Yonghu Zhu, Ying Kang, Lu Xu, Wei Fan, Yaogang Tong, Yu Wang and Xilei Wang , Ying Yang, Yuqiang Cai, Huan Fan, ChenYu He and Cheng hao Chen. Without their help, I couldn't have completed the work and lived a happy life.

At the same time, I am very grateful to my parents and my wife for their unconditional support and love.